Buku

by Dadan Ramdan

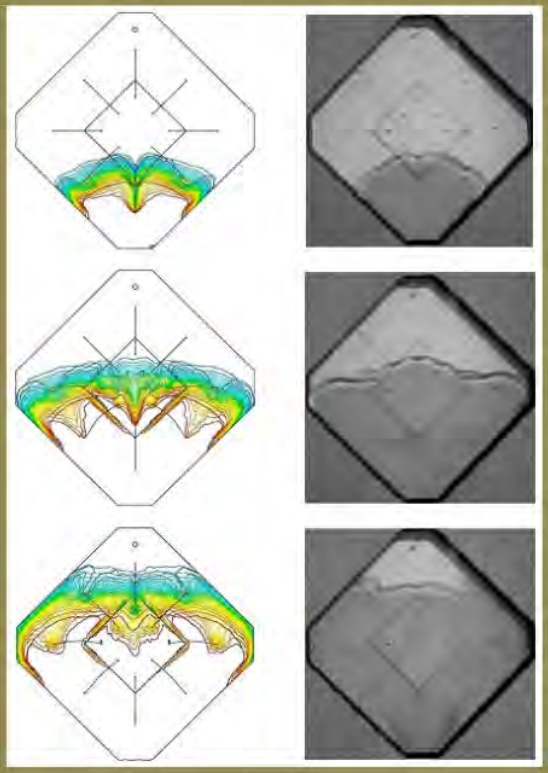

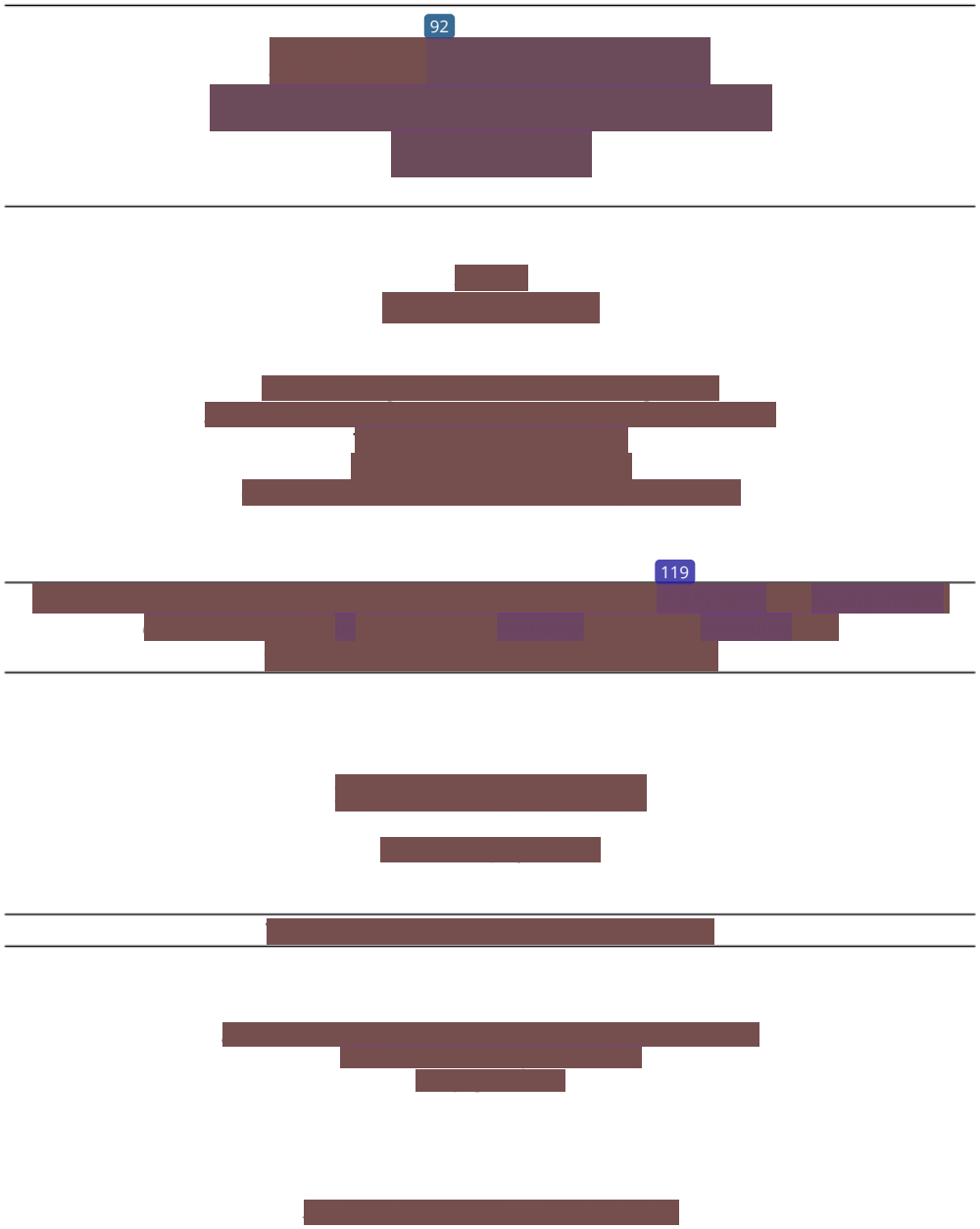

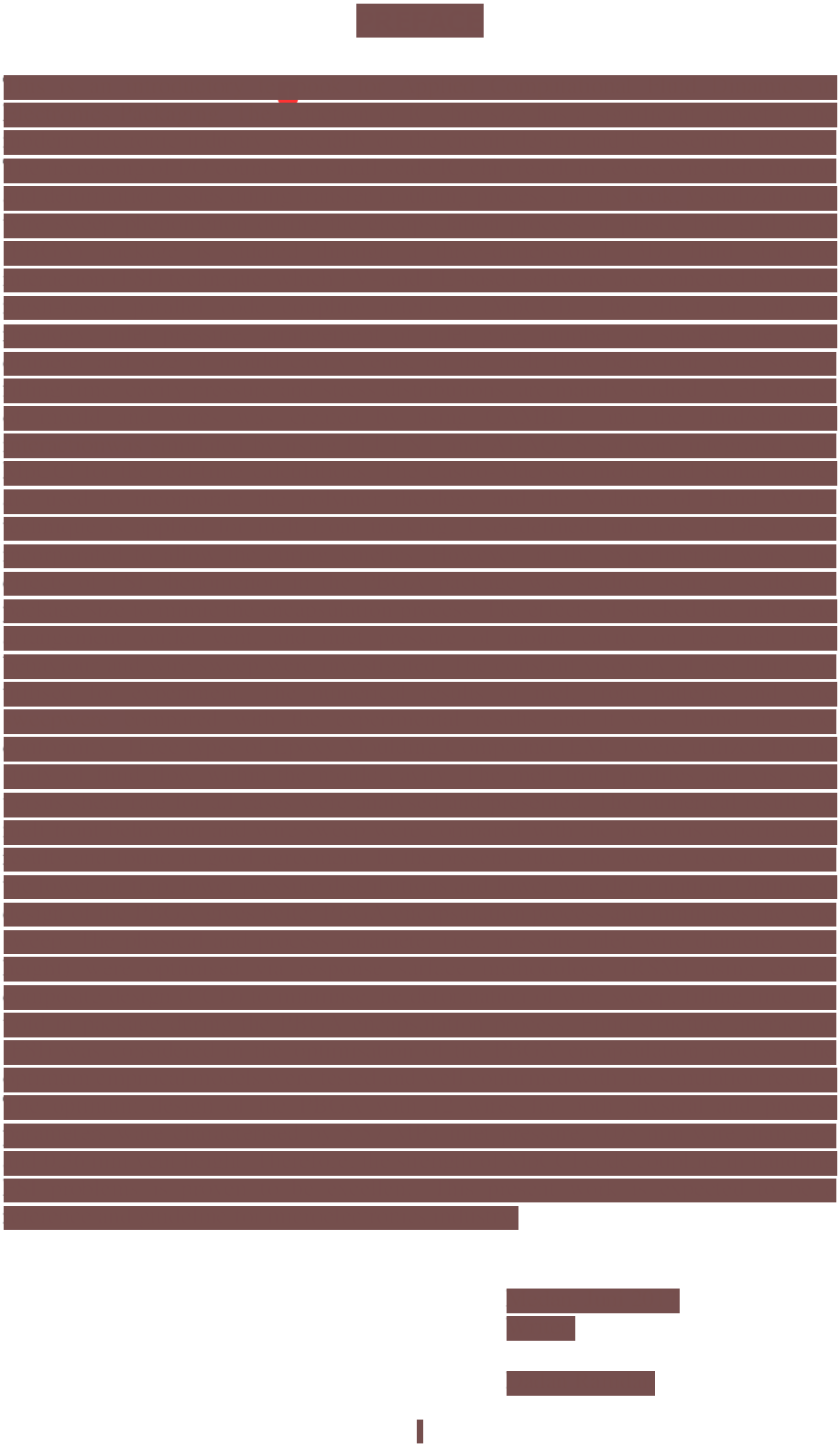

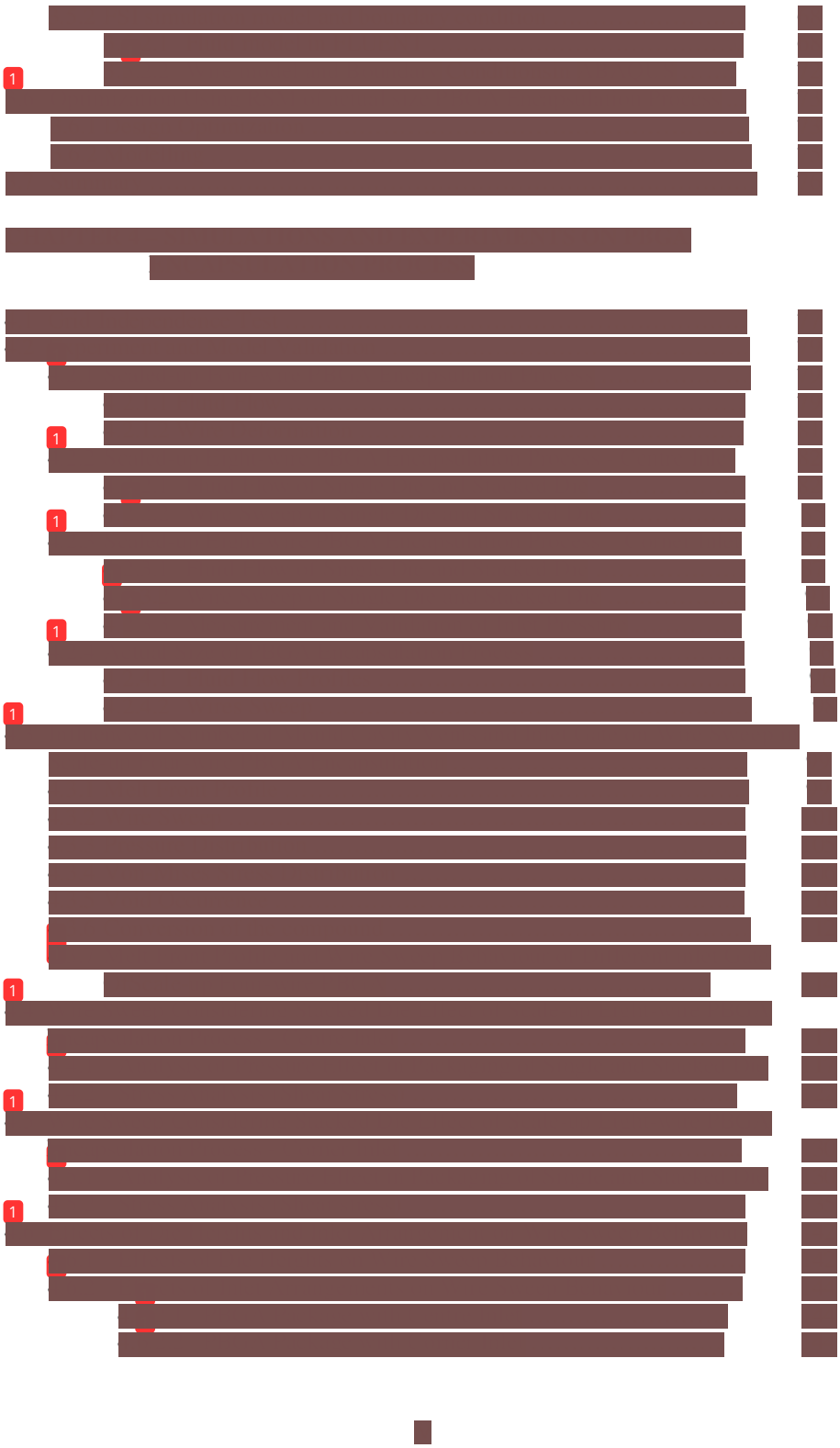

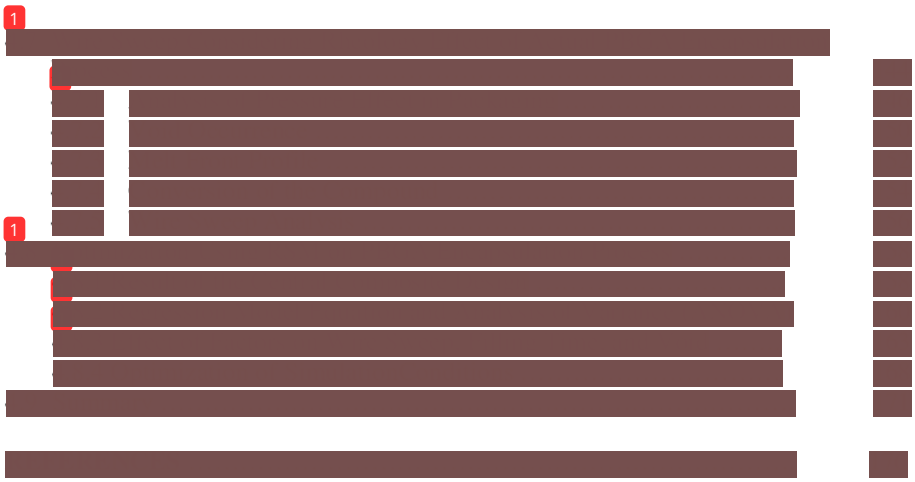

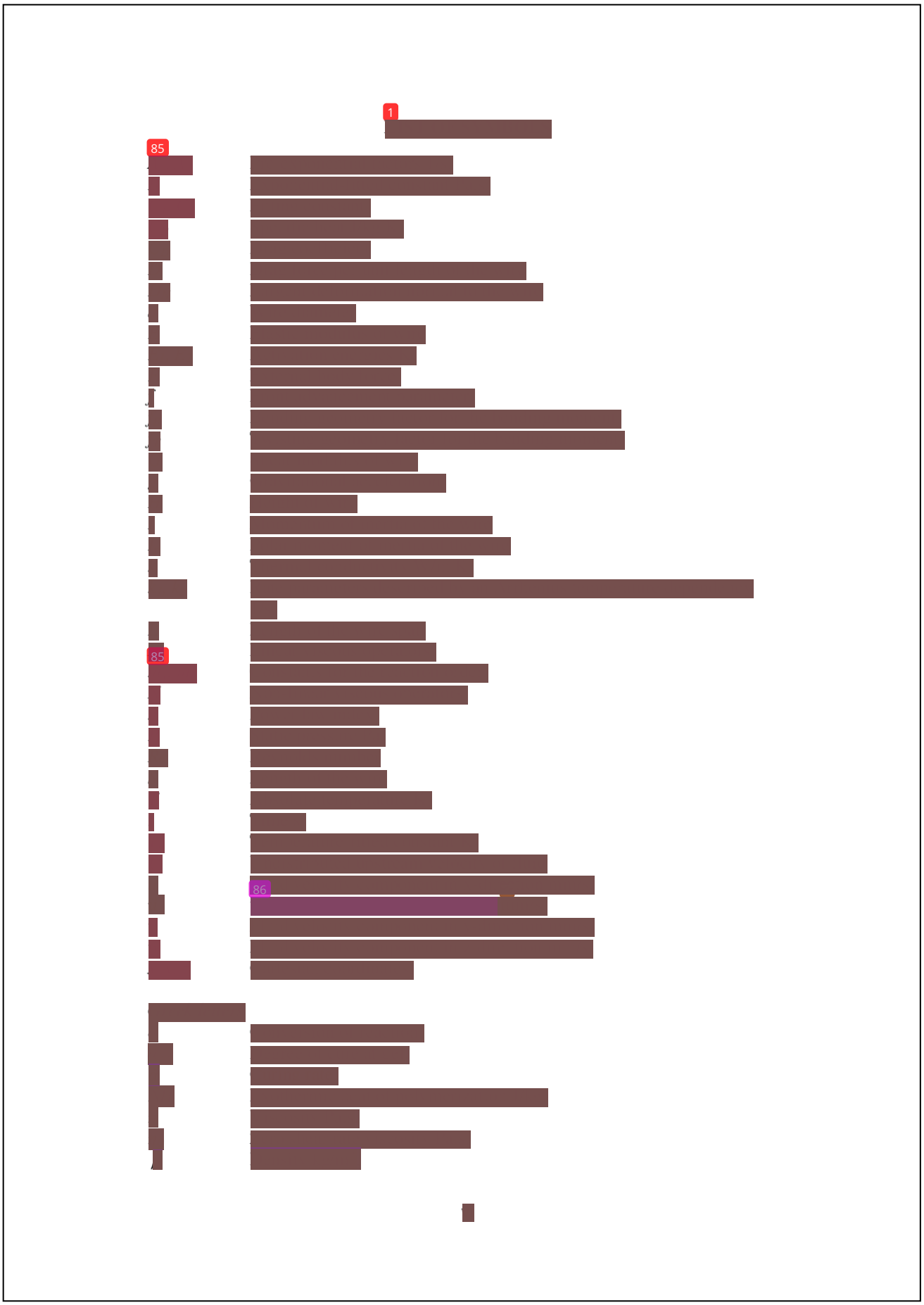

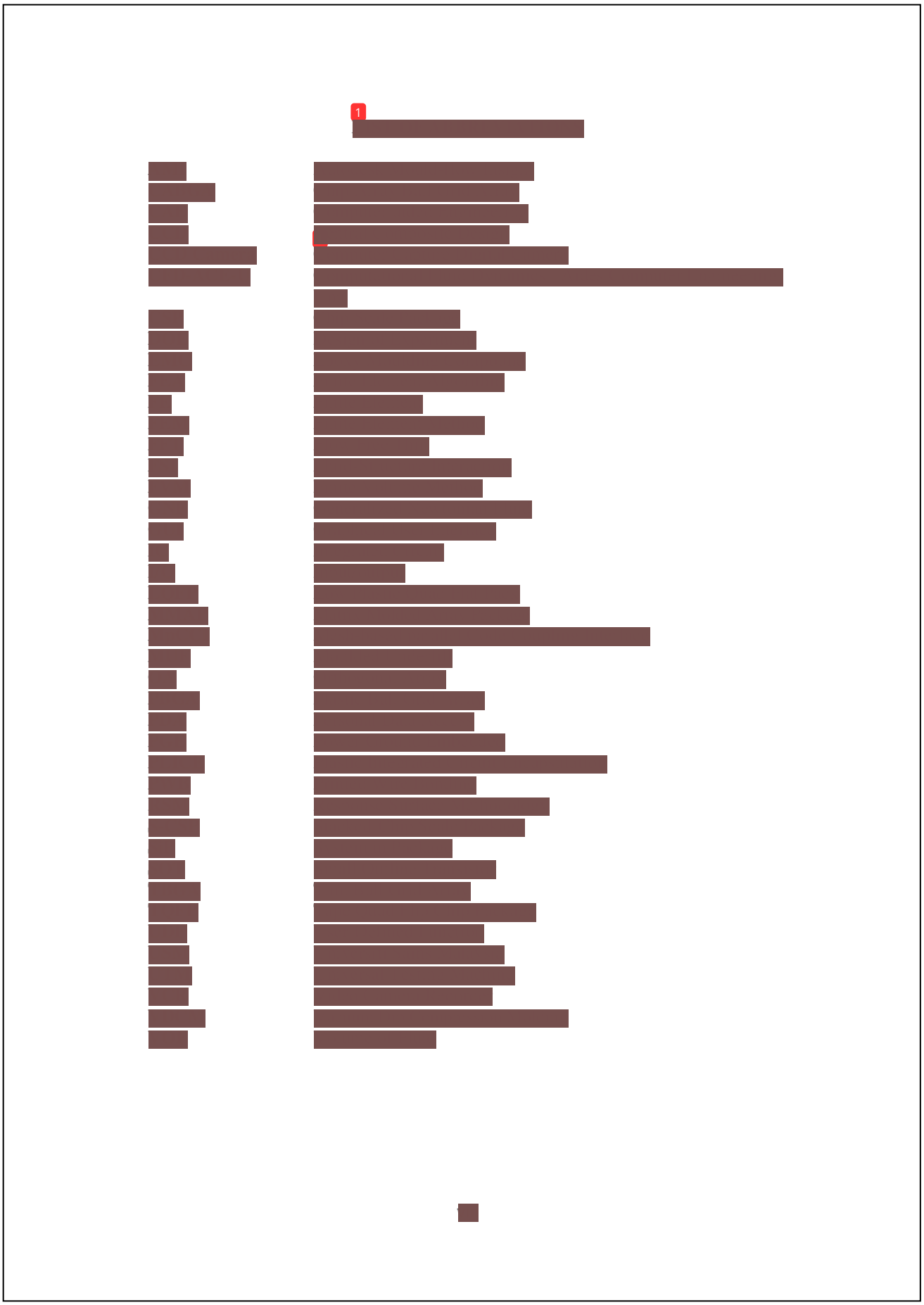

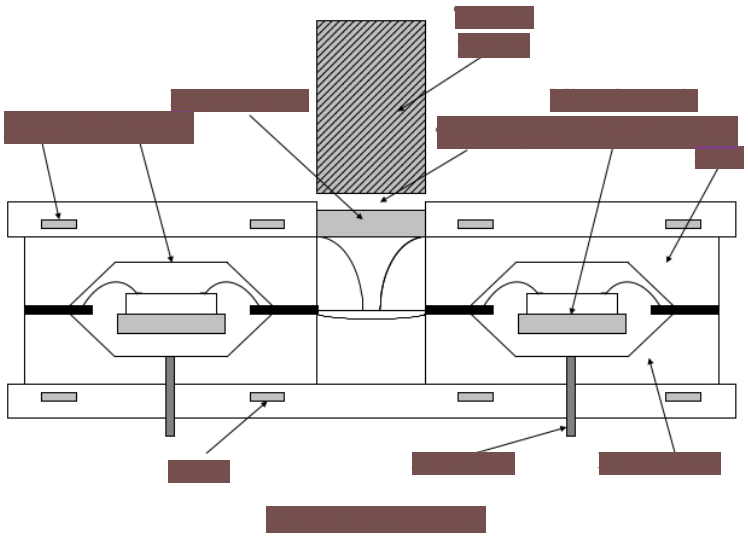

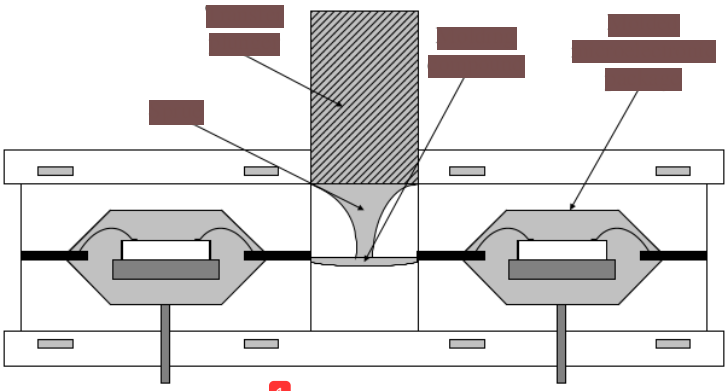

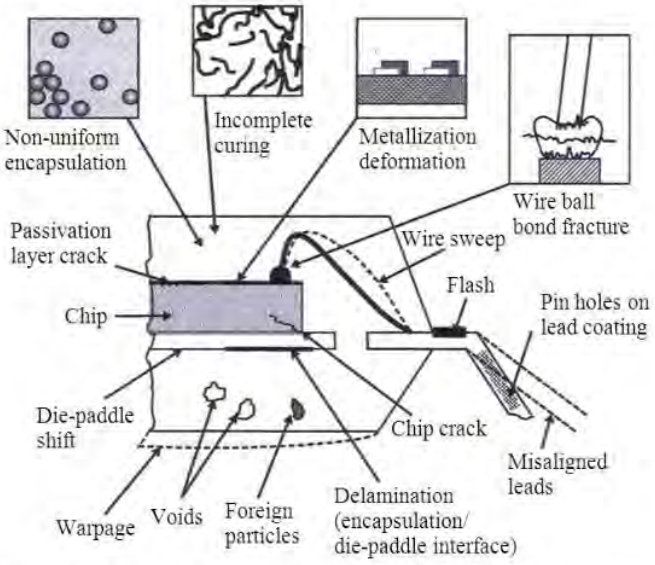

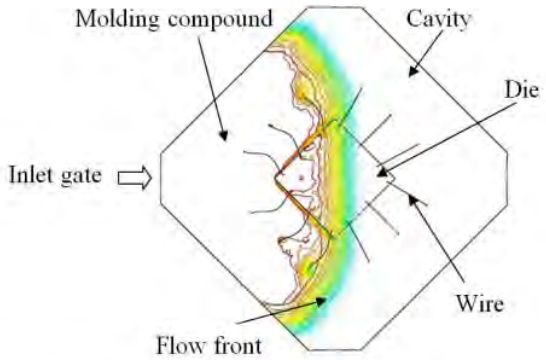

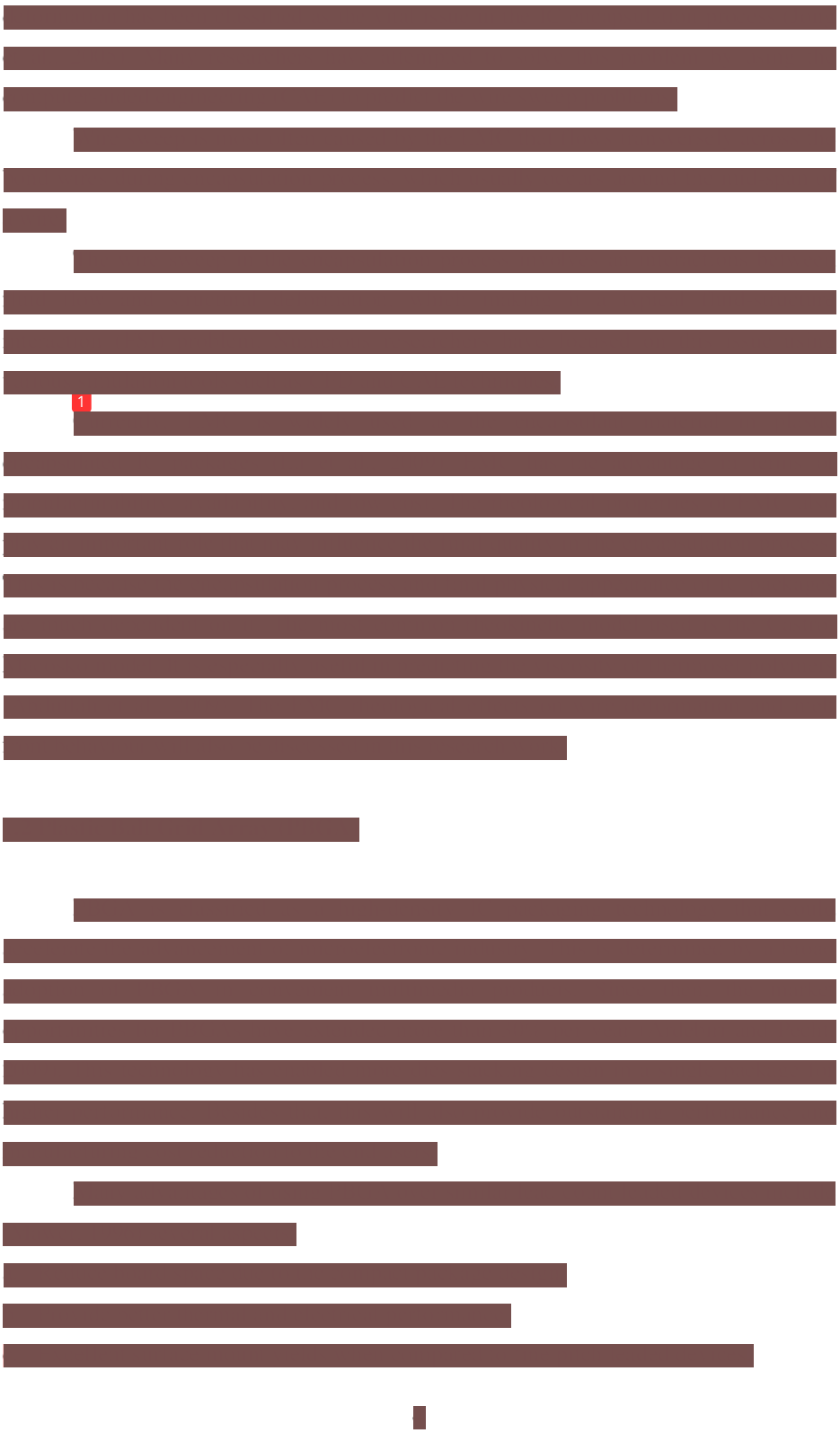

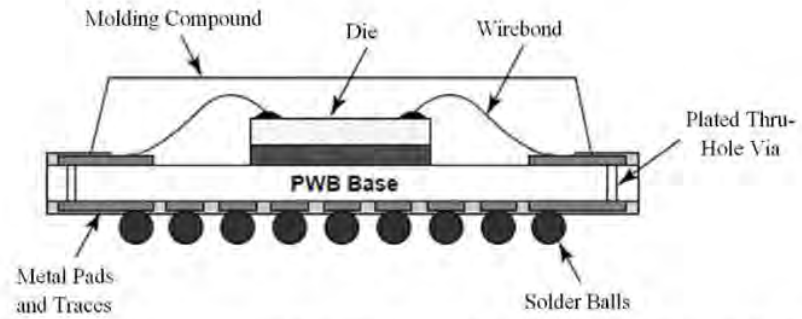

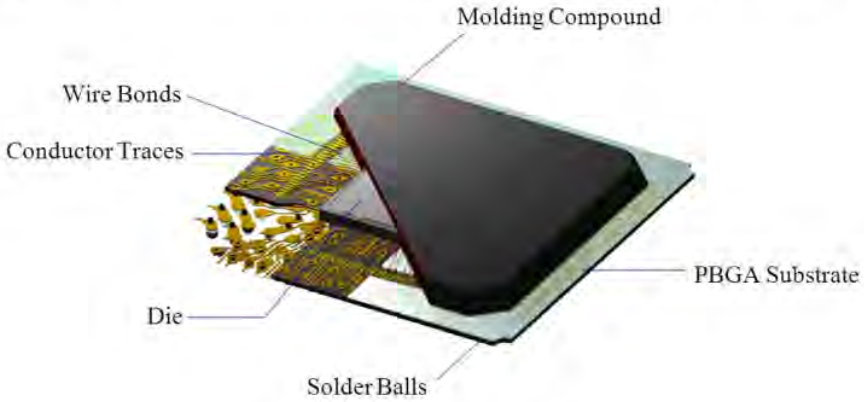

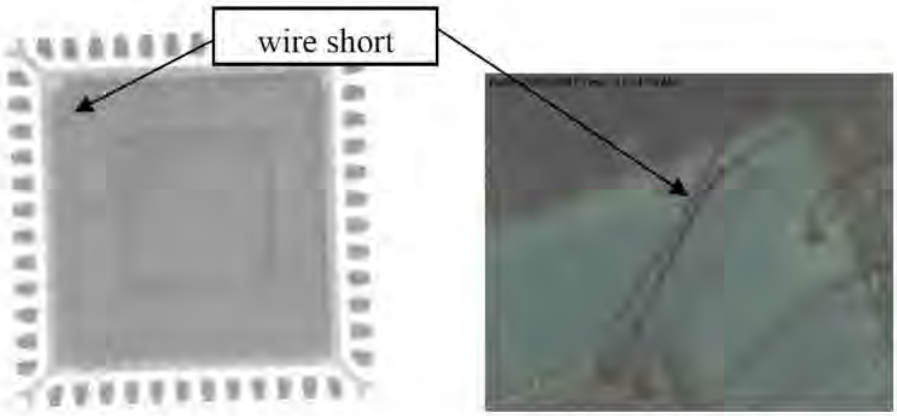

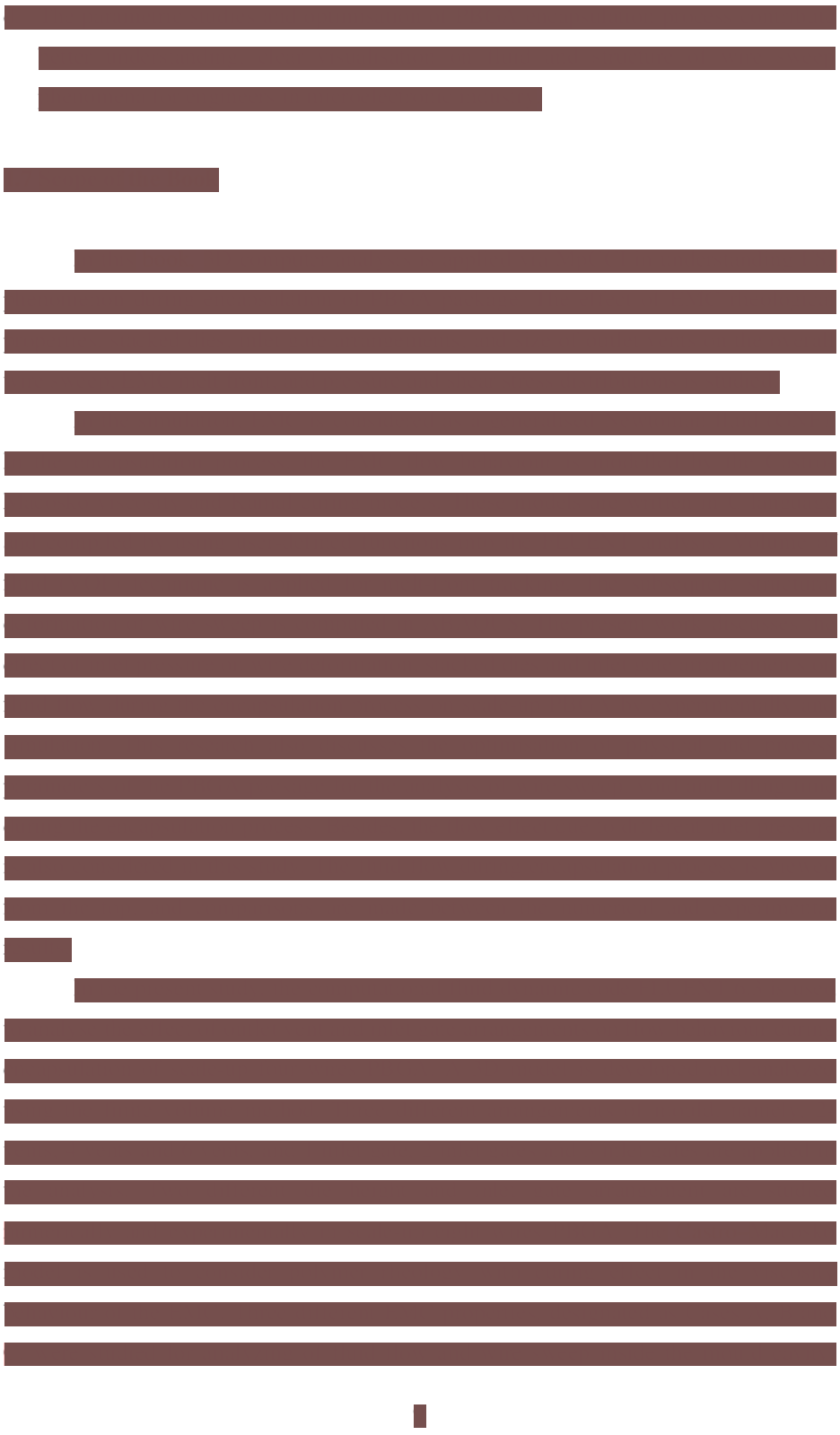

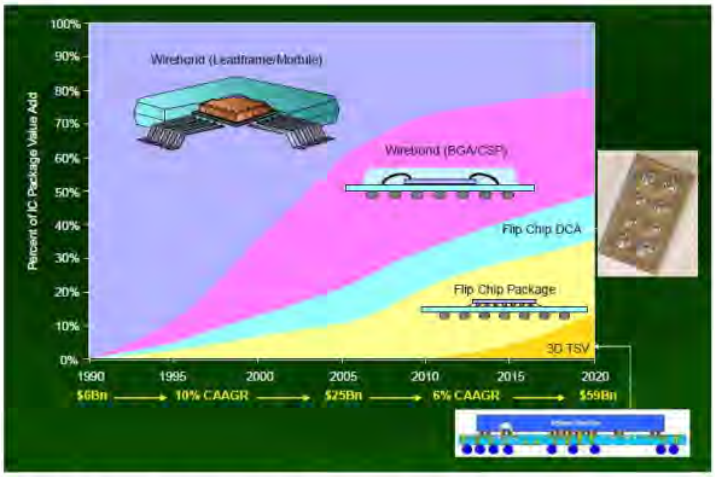

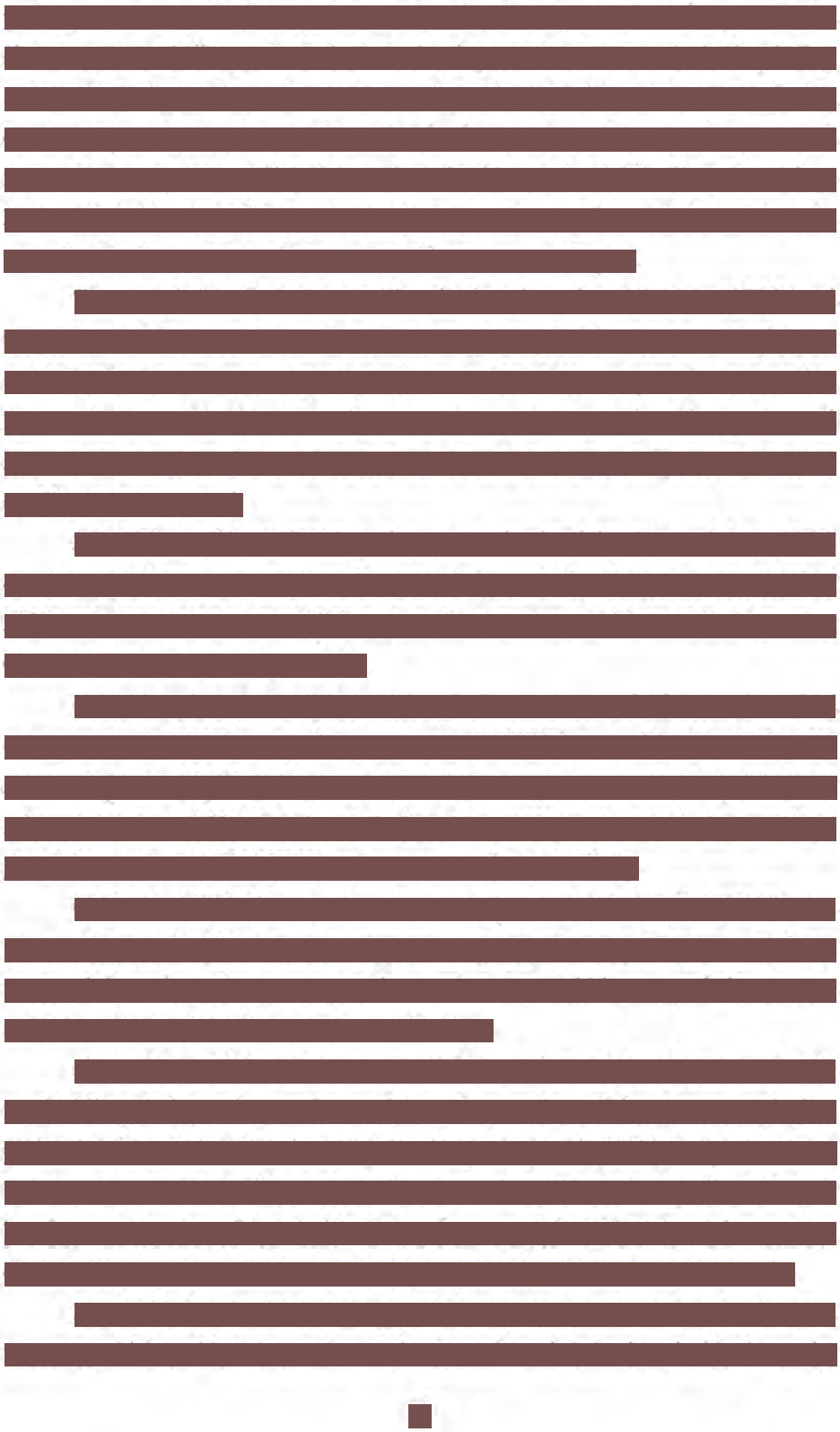

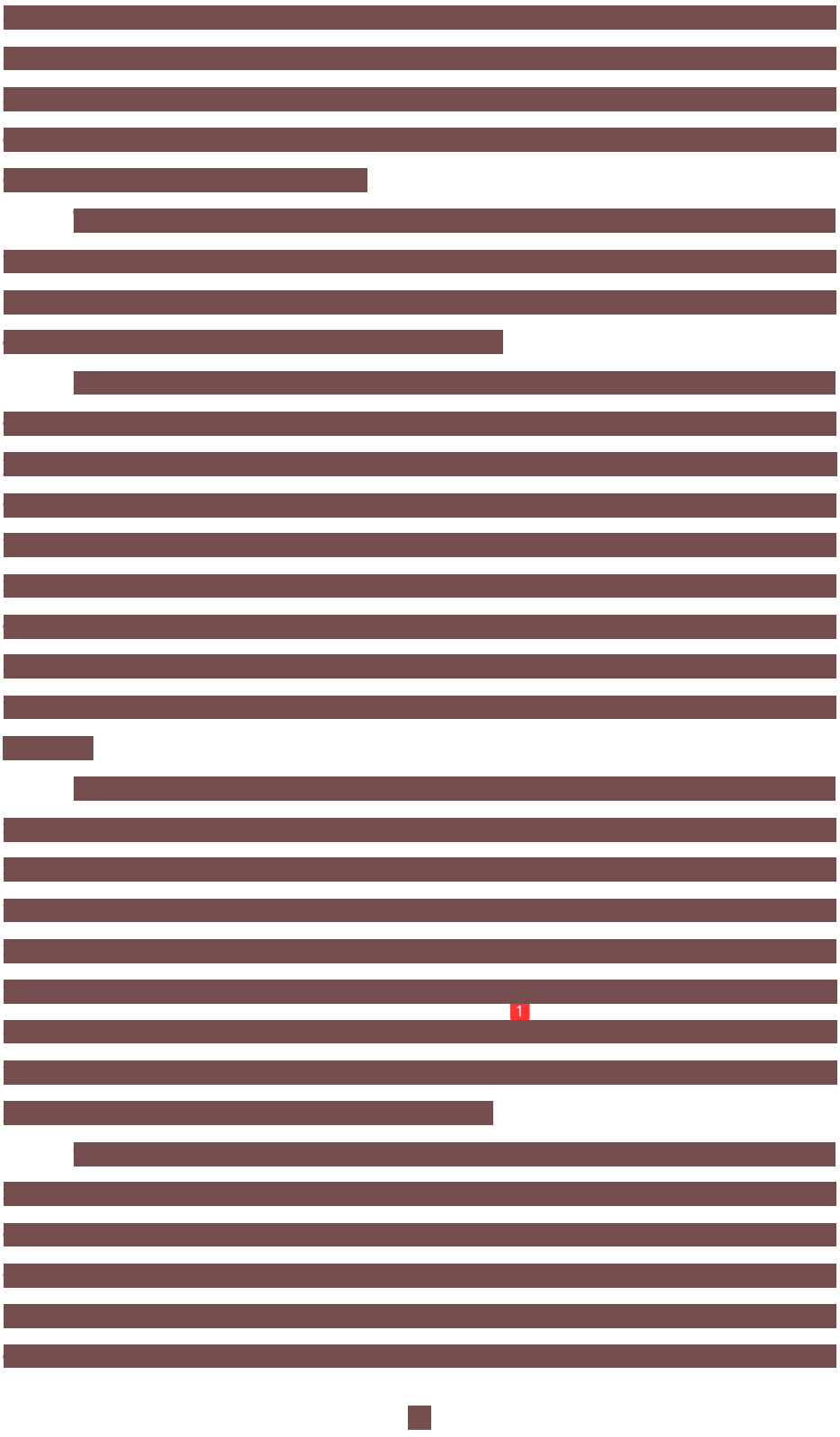

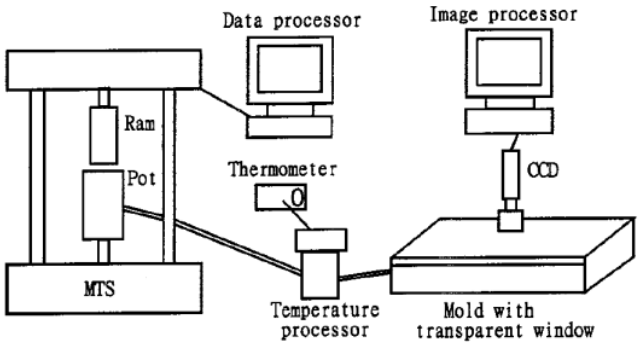

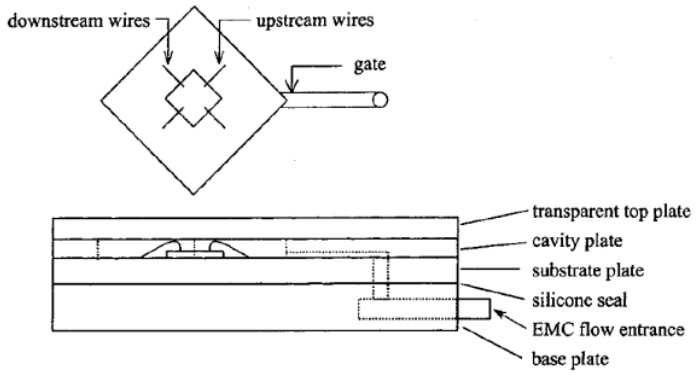

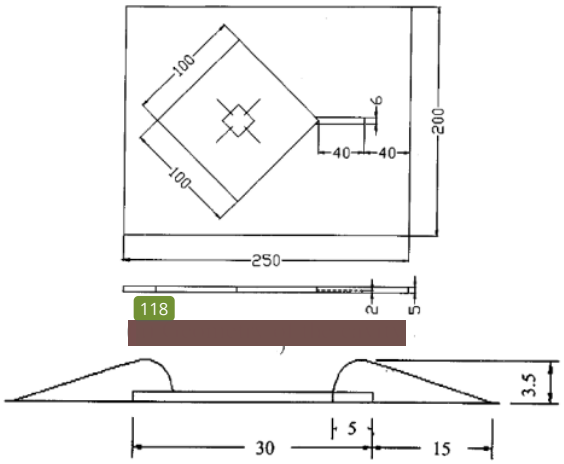

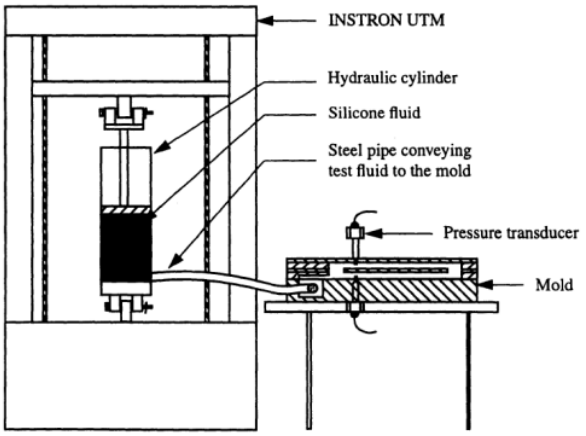

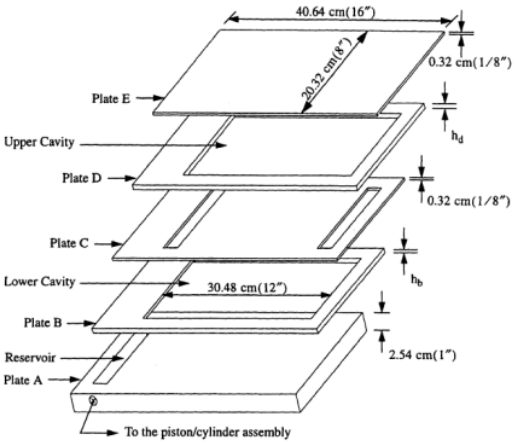

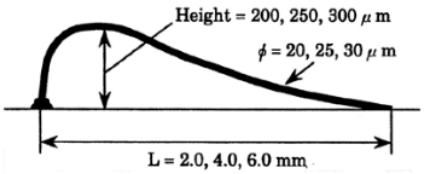

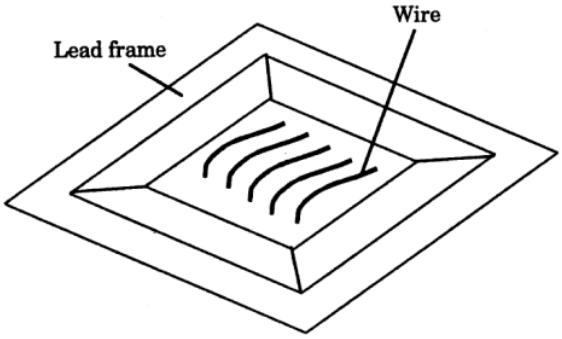

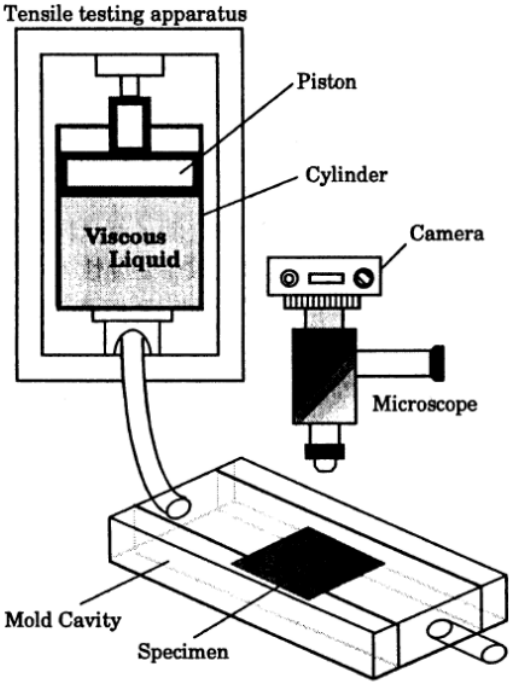

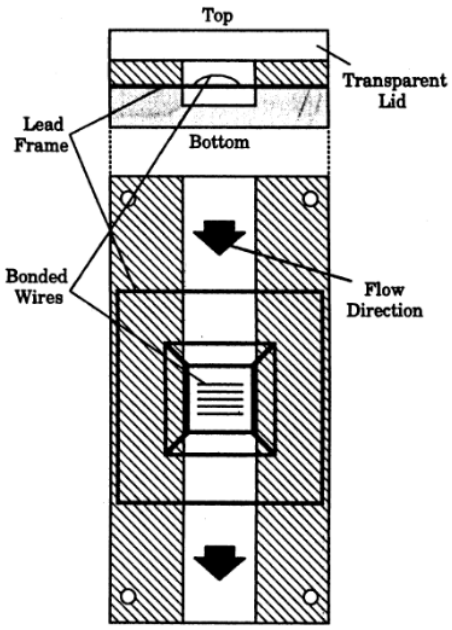

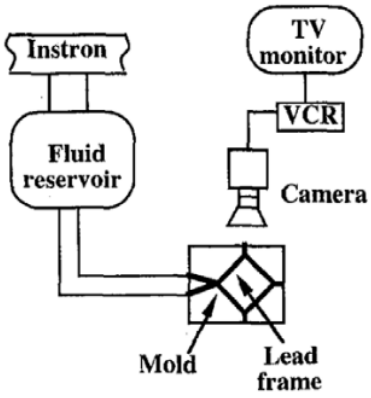

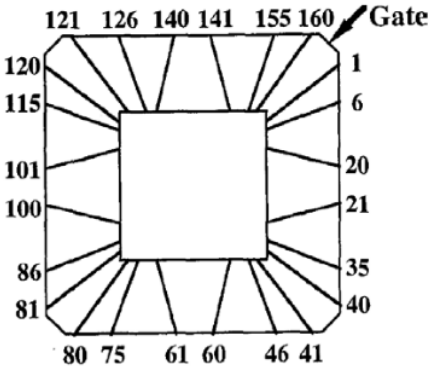

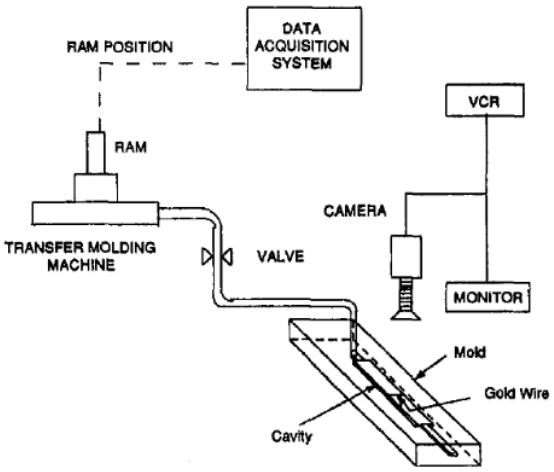

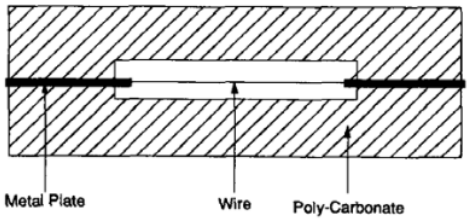

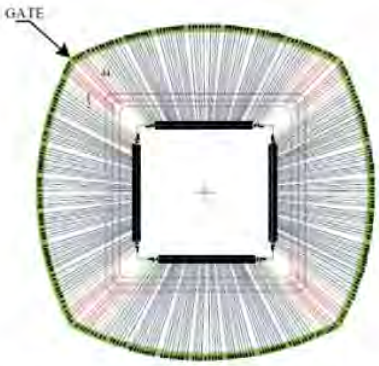

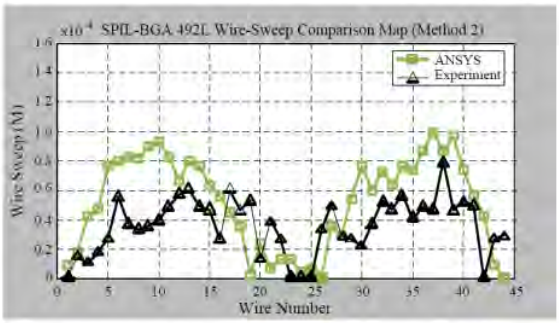

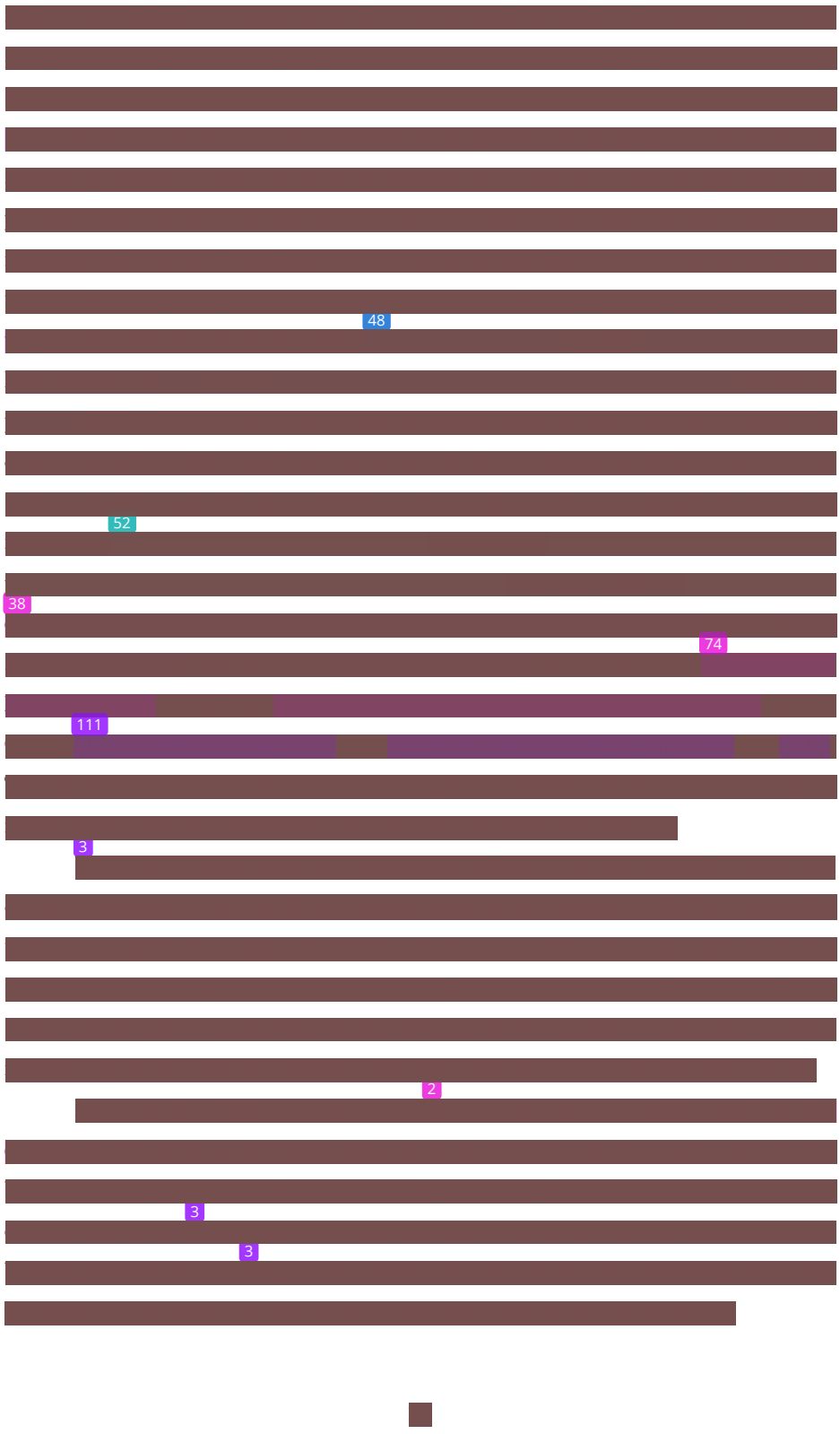

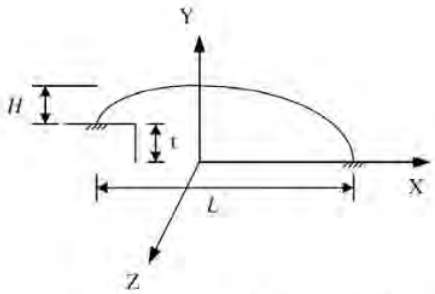

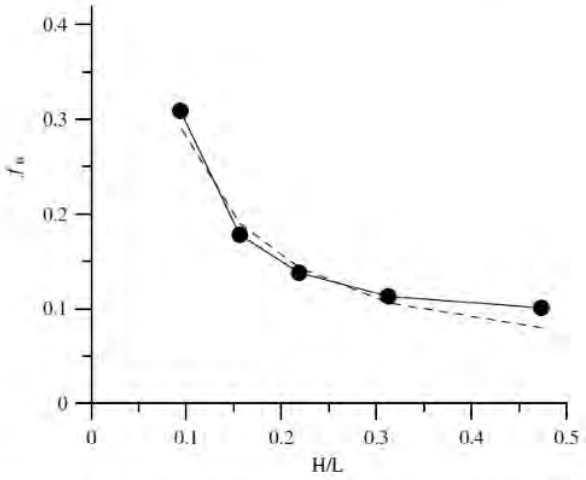

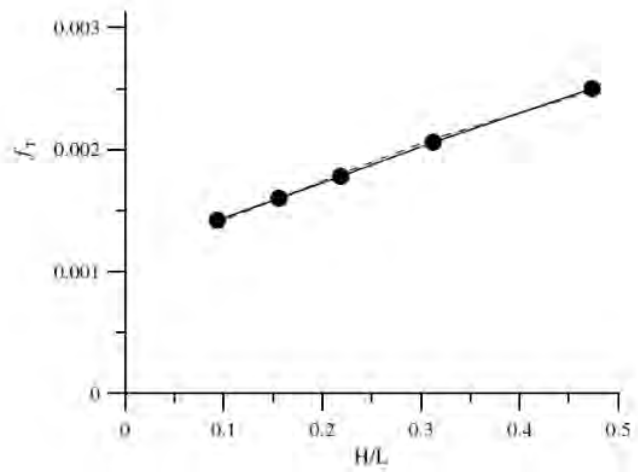

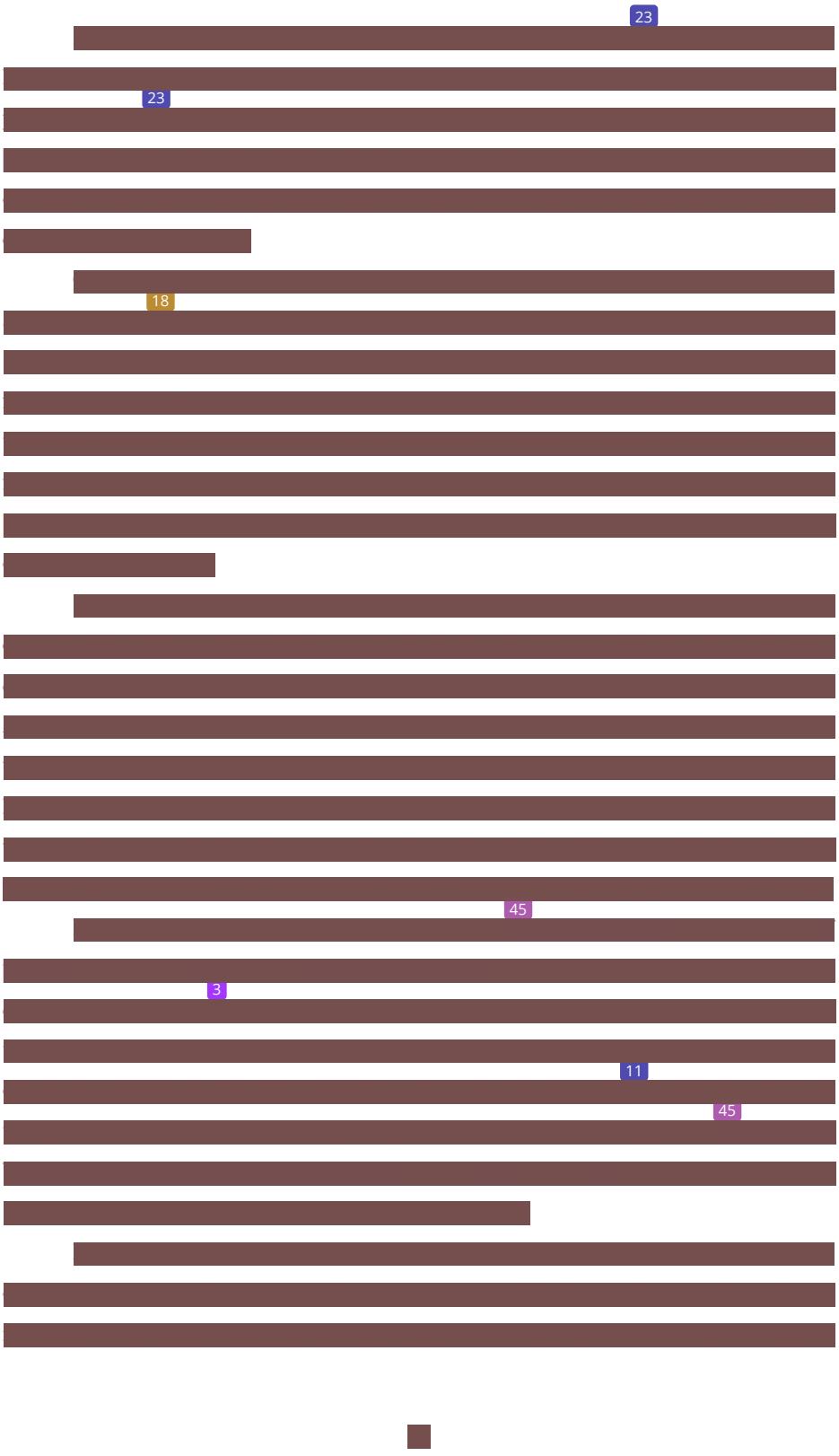

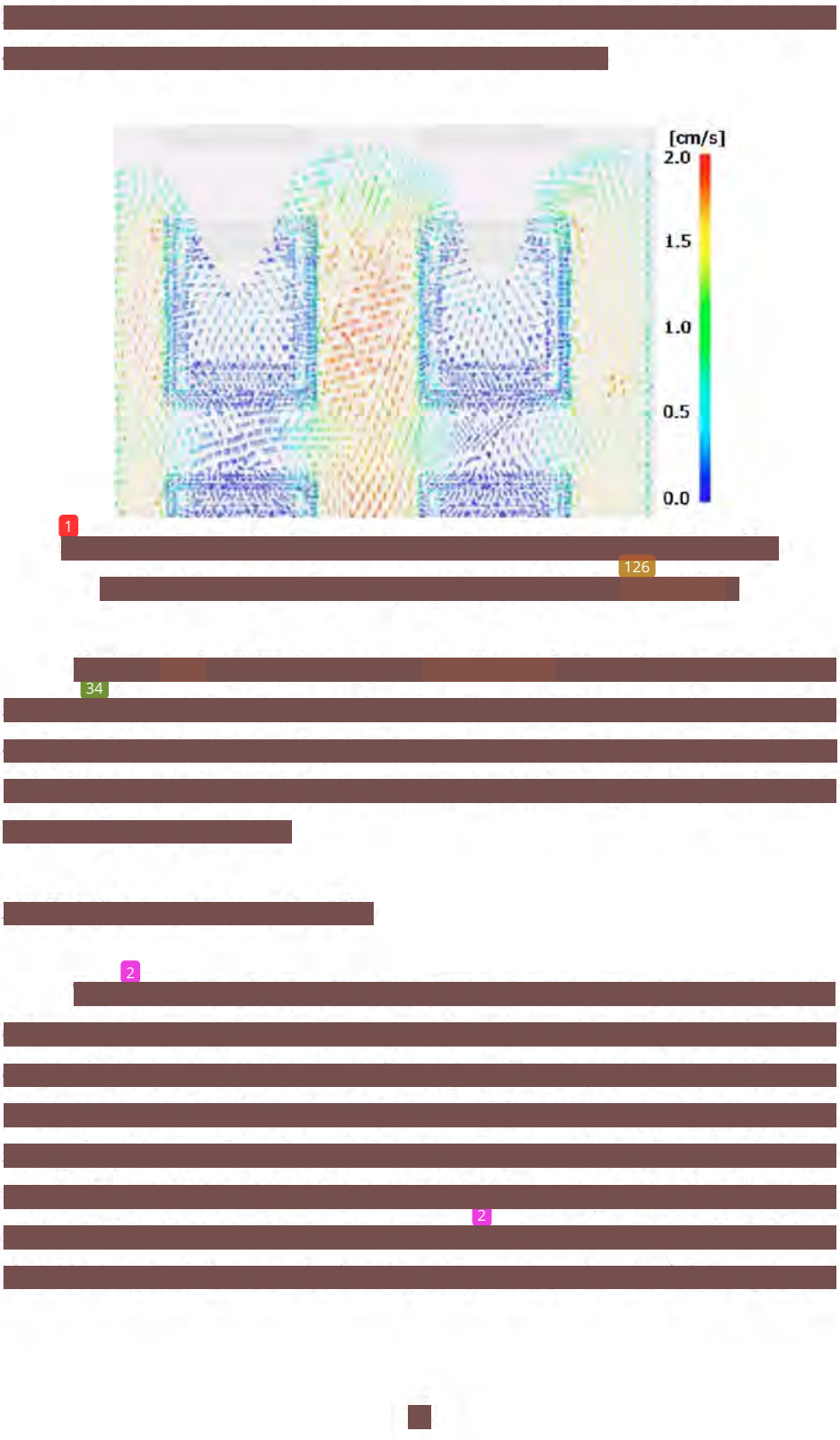

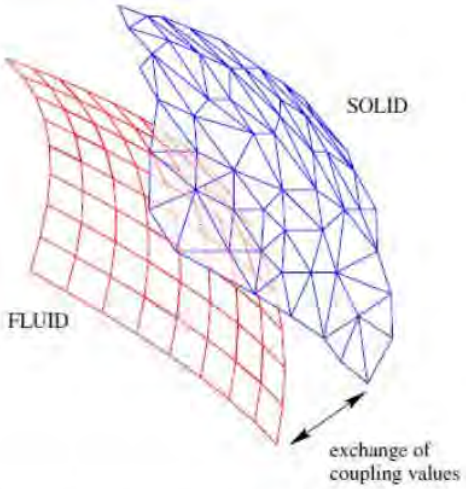

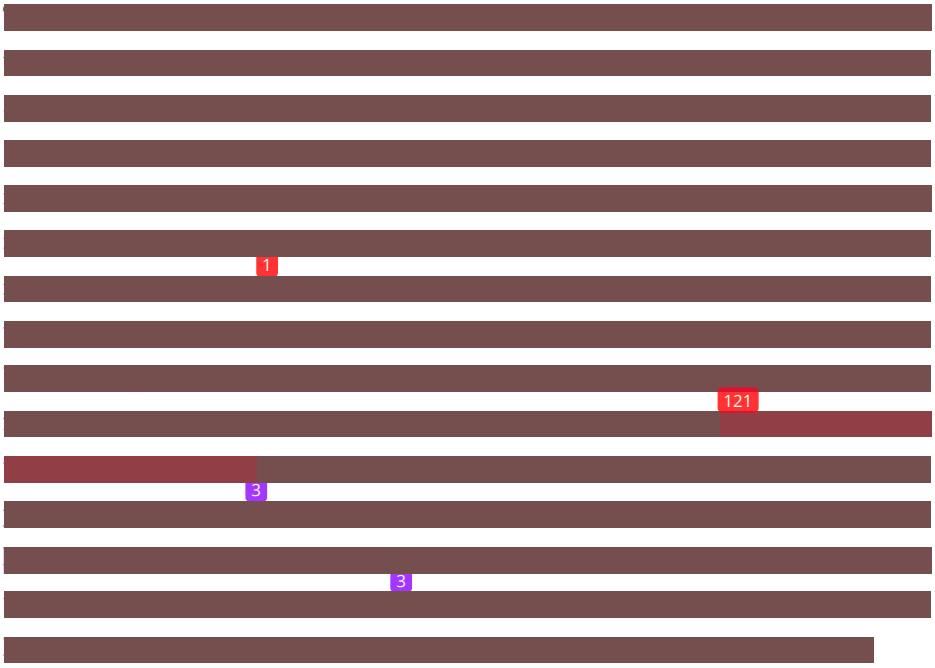

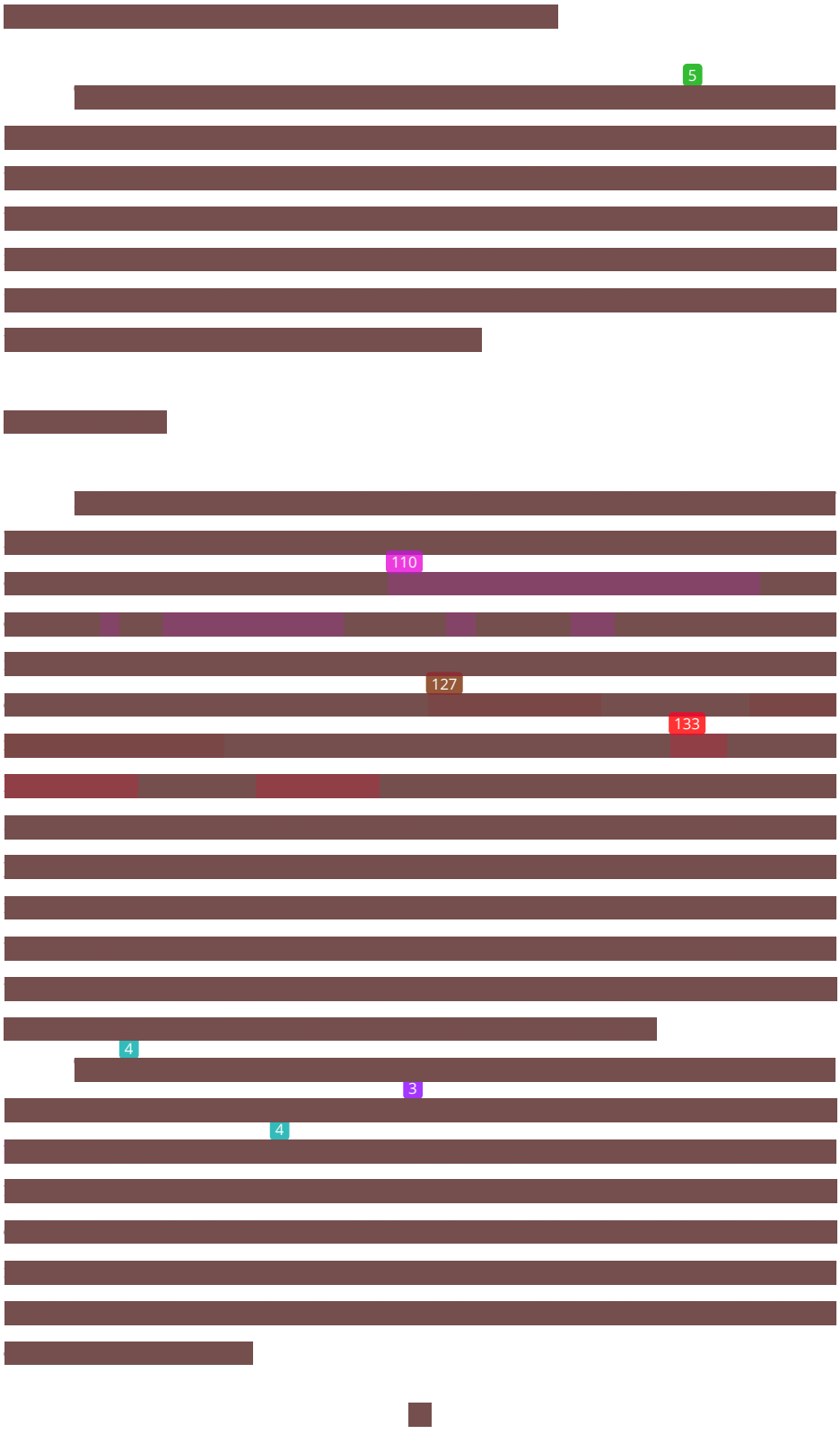

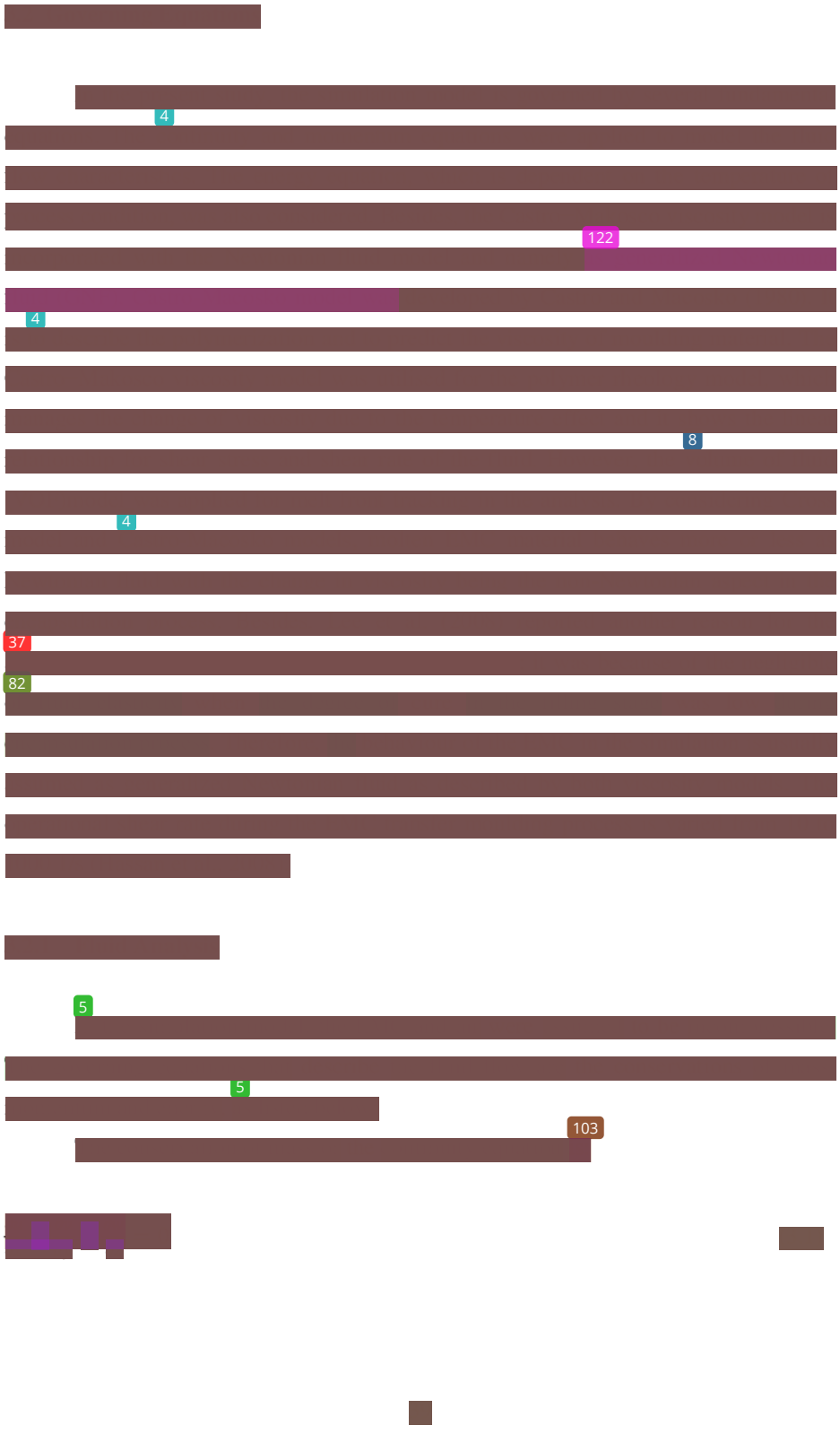

(3.4)

where, ρ is the density, u is the velocity vector, P is the static pressure, and g_i are the gravitational acceleration in the i direction, respectively.

The energy equation in terms of h (static enthalpy) can be written as:

(3.5)

where k is the thermal conductivity, T is the absolute temperature and Φ is the energy source term and it contains two contributions of polymer properties:

$$\Phi = \eta\dot{\gamma}^2 + \dot{\alpha}\Delta H \quad (3.6)$$

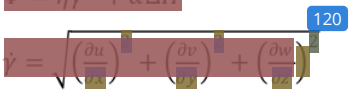

(3.7)

where $\eta$is the viscosity and $\dot{\gamma}$is the shear rate, $\dot{\alpha}$ is the curing rate and ΔH is the reaction heat. The moulding compound was assumed to be a generalised Newtonian fluid (GNF).

Several models have been used to predict the relationship between viscosity (η) and the degree of polymerization. The Castro–Macosko model, as expressed in Eq. (3.6) and (3.7), has been applied by Jong et al.(2005), Nguyen et al. (2000), and Khor et al. (2011)and it is used in this simulation. It is described as follows:

$$\eta(T,\dot{\gamma}) = \frac{\eta_0(T)}{1+\left(\frac{\eta_0(T)\dot{\gamma}}{\tau^*}\right)^{1-n}\left(\frac{\alpha_g}{\alpha_g-\alpha}\right)^{C_1+C_2\alpha}} \quad (3.8)$$

where T is the absolute temperature, n is the power law index, η_o the zero shear rate viscosity, τ^* is the parameter that describes the transition region between zero shear rates and the power law region of the viscosity curve, α is the conversion of reaction, α_g is the conversion at the gel point, and C_1 and C_2 are fitting constants.

$$\eta_o(T) = Bexp\left(\frac{T_b}{T}\right) \quad (3.9)$$

B is an exponential-fitted constant and T_b is a temperature fitted-constant. In addition, the Kamal curing kinetics is coupled together with the Castro–Macosko model. This model predicts the rate of chemical conversion of the compound as follows:

$$\frac{d\alpha}{dt} = (k_1 + k_2\alpha^{m_1})(1-\alpha)^{m_2} \quad (3.10)$$

$$k_1 = A_1 exp\left(-\frac{E_1}{T}\right) \quad (3.11)$$

And

$$k_2 = A_2 exp\left(-\frac{E_2}{T}\right) \quad (3.12)$$

whereA_1 and A_2 are the Arrhenius pre-exponential factors, E_1 and E_2 are the activation energies, and m_1 and m_2 are the reaction orders. The curing degree (α) of the EMC can be defined as a ratio of the heat released to the total heat released at complete conversion (Nguyen et al. 2000, Wang et al. 2010).

$$\alpha(t) = \frac{\Delta H(t)}{\Delta H_{total}} \quad (3.13)$$

The Newtonian fluid equation is as follow:

$$\eta = \frac{\tau}{\dot{\gamma}} \quad (3.14)$$

where, τ is the shear stress and $\dot{\gamma}$ is the strain rate.

The basic idea of VOF scheme is to locate and evolve the distribution of, say, the liquid phase by assigning each cell in the computational grid a scalar f, which specifies the resin proportion in each particular cell. Thus, f takes the value of 1 ($f = 1$) in cell which contains only resin, the value 0 ($f = 0$) in cells which are void of resin, and a value between 0 and 1 ($0 < f < 1$) in "interface" cells or can be referred as the resin melt front. The equation of melt front over time is governed by the following transport equation:

$$\frac{dF}{dt} = \frac{\partial F}{\partial t} + u\frac{\partial F}{\partial t} + v\frac{\partial F}{\partial t} + w\frac{\partial F}{\partial t} - \left(\frac{\partial^2 F}{\partial x^2} + \frac{\partial^2 F}{\partial y^2} + \frac{\partial^2 F}{\partial z^2}\right) = 0 \quad (3.15)$$

3.2.2 Wire Sweep Analysis

To calculate the drag force exerted on the wires by the resin flow, the value of velocities and viscosities have to be determined from the mould filling simulation. Then, the Lamb's model is utilized to calculate the drag force as follows (Su et al., 2003, Pei and Hwang, 2005a, and Han and Huh, 2000):

$$D = \frac{C_D \rho U^2 d}{2} \quad (3.16)$$

where D is the drag force per unit length, ρ is the fluid density, U is the undistributed upstream velocity, d is the wire diameter and C_D is the drag coefficient which can be written as(Su et al., 2003, Pei and Hwang, 2005a, and Han and Huh, 2000):

$$C_D = \frac{8\pi}{Re[2.002 - \ln(Re)]} \quad (3.17)$$

where Re is the Reynold number.

In order to assist the designer of a wire profile to obtain a reasonable allowed sweep, a sweep deformation model based on the contribution of the bending moment and the twisting moment has been proposed by Kung et al. (2006a). According to the model, the sweep deformation of the wire δ can be written as:

$$\delta_{max} = S \times D \left(f_B \left(\frac{H}{L}\right) \frac{H^3}{EI} + f_T \left(\frac{H}{L}\right) \frac{L^3}{G I_p} \right) \quad (3.18)$$

where D is the drag force per unit length of the wire and S is the length of the wire, f_B is the bending geometry factor for the bending moment, f_T is the twisting geometry factor for the twisting moment, H is the height of wire, L is the length of wire span(See Figure 2.18), G is the shear modulus of wire, E is the elastic modulus of wire, I is the moment of inertia of the wire, I_p is the polar moment of inertia of the wire.

In order to make a comparison between the results of simulation and experiment, a dimensionless parameter, wire sweep index (See Figure 3.1), is used. The wire sweep index is calculated from making the largest deformation normal to the wire divided by the projected length of the wire (Nguyen et al., 1997, Pei, 2004, Onodera et al., 2007).

$$\text{Wire Sweep Index } (\%) = D_N/L \quad (3.19)$$

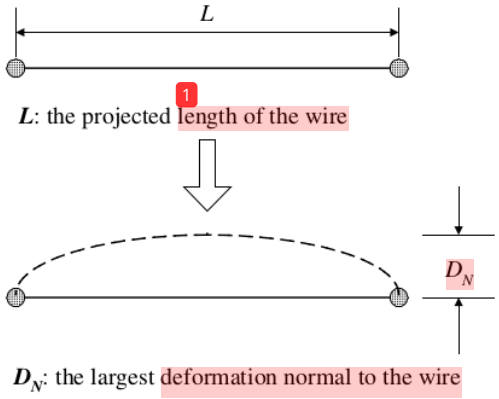

Figure 3.1 Definition of wire sweep

3.2.3 Code Coupling with MpCCI

In the present study, the FSI activity during the encapsulation process is visualized by using the virtual model that is created and simulated in FLUENT and ABAQUS. During the simulation analysis, the two-way coupling method is implemented in parallel for FSI as shown in Figure 3.2. The pressure data generated from the flow (FLUENT) is transferred to ABAQUS for structural analysis by MpCCI. The deformation of the structure in ABAQUS will give the feedback to the flow analysis in the FLUENT in the real time calculations. The deformed wire bonds may cause instability on the flow front profile. The extreme deformation of wire bond during the encapsulation process could cause failure for the package during the process due to short circuit problem. Therefore, the deformation of wire bonds during the encapsulation process is also crucial for the packaging design.

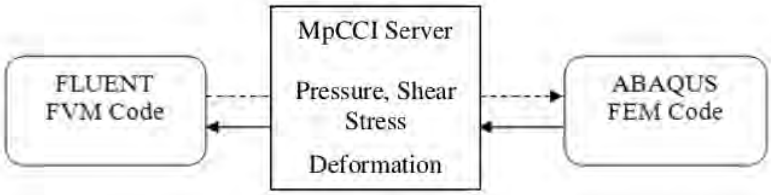

Figure 3.2 Data exchange from FLUENT and ABAQUS by MpCCI.

MpCCI nowadays is the most widely used software for the coupling of several codes. It works quite well for a fixed pair of codes (Wolf, 2007, Yigit et al. 2008). MpCCI is a software library that enables the exchange of data defined on meshes of two or more simulation codes in the coupling region. Since the meshes need not match point by point, MpCCI performs an interpolation and, in the case of parallel codes, keeps track of the distribution of the domains onto different processes (Thirifay and Geuzaine, 2008). In this way, the intricate details of the data exchange are hidden behind the concise interface of MpCCI. Consequently, the simulation codes themselves are changed only moderately when they are prepared for coupling via MpCCI.

For the communication between the involved codes, the message-passing interface is used (Schreiber et al., 2005). At the interface between fluid and structure, there is some mapping of data between two, in general a nonmatching grid. In the MpCCI concept, this mapping is done directly from one solver to the other with the help

of either given library routines. This implies that each solver has to know the grid of the other solver and, thus, inhibits the exchange of one solver without changing the code of the other one.

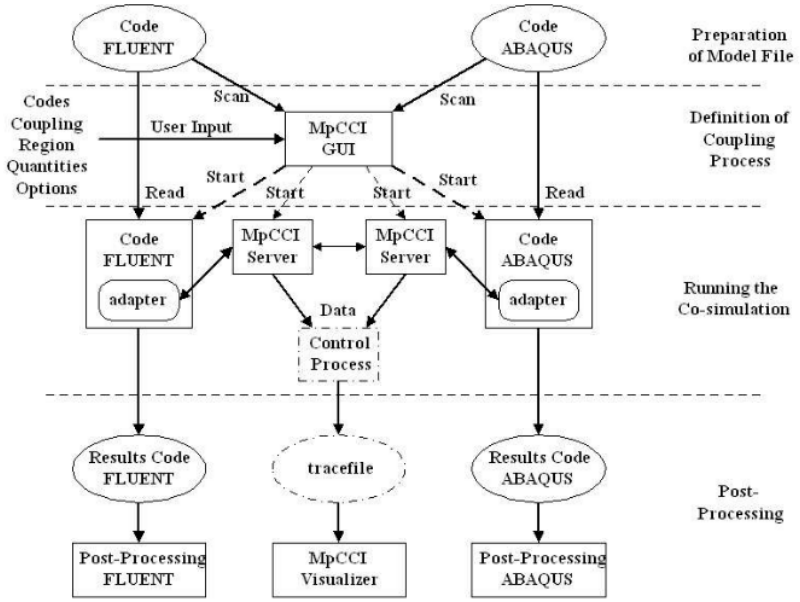

Figure 3.3 FLUENT and ABAQUS coupling simulation process (MpCCI 3.1.0-1 Doc., 2009).

Running a co-simulation with MpCCI require the process given in Figure 3.3.There are four steps of the complete co-simulation with MpCCI: 1) preparation of model files, 2) definition of the coupling process, 3) running the co-simulation; and 4) post processing (MpCCI, 2009). First, each domain is modelled separately and created for each simulation code. The models contain a definition of the coupling region. The interface between solid and fluid depends on the coupling regions, which are the surfaces (wires in the PBGA package) that have been defined in both codes. During the simulation the MpCCI software distributes the data on the surface of wires. Simulation codes, the corresponding model files and the coupled region, quantities, and a coupling algorithm must be selected in the second step. This step is completely supported by the MpCCI GUI. Next, starting with the MpCCI server, both coupled codes are started. Each code computes its part of the problem while MpCCI controls the quantity exchange. Lastly, the results can be analysed with the post-processing tools of each

simulation code, with the FLUENT and ABAQUS visualizer. The sample of coupling process is shown in Appendix A.

For the fluid structure coupling, an implicit portioned approach is employed (Thirifay and Geuzaine, 2008). Figure 3.4 a schematic view of an iteration process, which is performed for each time step, is given. After the initializations the flow field is determined in the actual flow geometry. From this, the friction and pressure forces on the interacting walls are computed, which are then passed to the structural solver as boundary conditions. The structural solver computes the deformations with which the fluid mesh is modified, before the flow solver is started again.

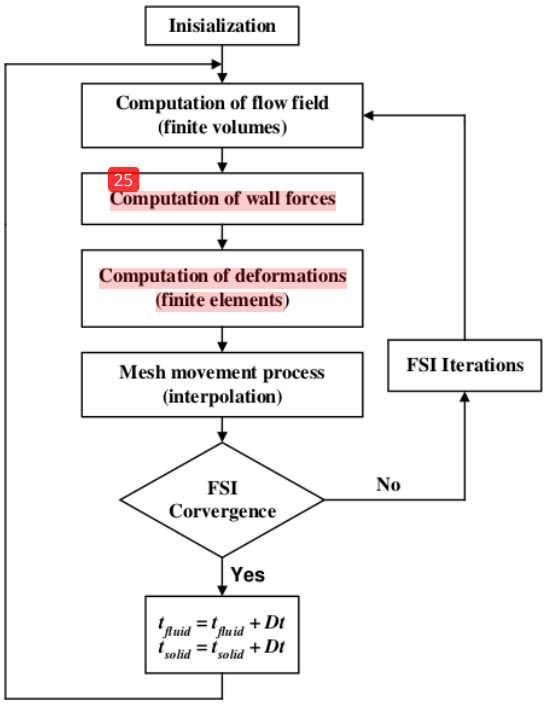

Figure 3.4 Flowchart of couple solution procedure (Michael, 2005, Yigit et al. 2008).

3.3 Influence of Number of Mould Cavity Vents and Inlet Gate on Wire Sweep in Scale-up Four-wire PBGA Encapsulation Process

3.3.1 Problem Description

In all the previous works on wire sweep prediction, the fluid and structural solvers were run separately and coupled manually. As a promising breakthrough in the FSI analysis, MpCCI technique has recently been introduced for the simultaneous real time coupling of fluid and structural solvers. The use of a finite volume flow solver and a finite element structural solver, coupled through MpCCI was reported for variety of engineering problems (Yigitet al., 2008, Thirifay and Geuzaine, 2008, Gatzhammer et al., 2010). However, as far as the authors are aware, the use of MpCCI for wire sweep analysis and the study on the effect of number of vents on wire deformation during the encapsulation of PBGA package have not been reported so far. To address this problem, the finite-volume flow solver FLUENT and the finite-element structural solver ABAQUS are interfaced by MpCCI. Polymer rheology model with curing effect (the Castro–Macosko model) is used in the fluid flow model and the VOF technique is applied for melt front tracking of the EMC. The numerical analysis uses User-defined functions (UDFs) to account for curing kinetics. Keeping one gate, three configurations of mould cavity with 2, 4 and 6 vents are simulated. Melt front profiles, wire sweep, pressure field, and stress distribution on wires, are analysed for each case. The proposed model is well validated by the published experimental results of Yang et al. (2000). Table 3.1 summarises the material properties of the EMC considered in the current simulation.

Table 3.1 Material properties of EMC used in the mould filling analysis (Nguyen et al., 2000).

	Parameter	Value	Unit
Castro–Macosko Model	α_g	0.17	-
	B	0.000381	Kg/m/s
	T_b	5230	K
	n	0.7773	-
	τ	0.0001	N/m^2
	C_1	1.03	-
	C_2	1.50	-
Curing Kinetics	m_1	1.21	-
	m_2	1.57	-
	A_1	33530	1/s
	A_2	30540000	1/s
	E_1	7161	K
	E_2	8589	K
	α	0.05	-
Density	ρ	2000	Kg/m3
Specific Heat	Cp	1079	J/Kg-K
Thermal Conductivity	-	0.97	W/m-K
Reference Temperature	T	298	K

3.3.2 FSI Simulation Model and Boundary Condition

3.3.2.1 Fluid Model in FLUENT

The VOF model in FLUENT 6.3.26 is utilized to simulate the process (Khor et al., 2010a,). In the VOF model, a single set of momentum equations is shared by the fluids, and the volume fraction of each of the fluids in each computational cell is tracked throughout the domain (Khor et al., 2010b). Air and EMC are defined as the phases in the analysis. Implicit solution and time dependent formulation are applied for the volume fraction in every time step. The volume fraction of the encapsulation material is defined as one and zero value for air phase.

The Castro–Macosko viscosity model with curing effect was written into C language using Microsoft VISUAL Studio 2005 and compiled as UDF in FLUENT. The sample of UDF list code of Castro–Macosko viscosity model that refer to Table 3.1 is shown in Appendix B. The mould cavity package models with different number of vents and different inlet gates, and its boundary conditions are shown in Figures 3.5a, 3.5b, 3.6a and 3.6b respectively. The dimension of mould cavity is 10 cm × 10 cm × 0.5cm, die is 3 cm × 3 cm × 0.1 cm and inlet gate is 0.8 cm × 0.8 cm (Han and Huh, 2000). The

flow direction is diagonal of x and z direction to the un-deformed wire axis and the properties are approximately the same as those used in ref. (Han and Huh, 2000). In the current study, the model is created by using GAMBIT software and average 395000 tetrahedral elements are generated for simulation (Figure3.7) in terms of accuracy and computational cost. Besides, time step size is also tested and 0.001 s (Khor et al., 2010a) is found to be the optimum. The governing equations are discretized by the first order upwind scheme, and solved by SIMPLE algorithm.

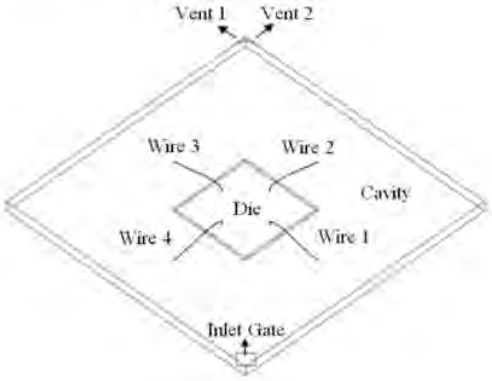

(a) 2 vents

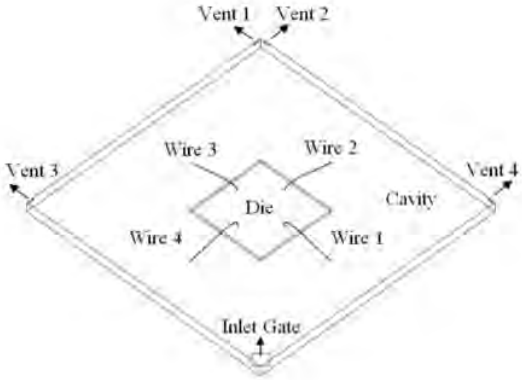

(b) 4 vents

Figure 3.5a Mould cavity models of scale-up four-wire PBGA with different outlet vent: (a) 2 vents, (b) 4 vents

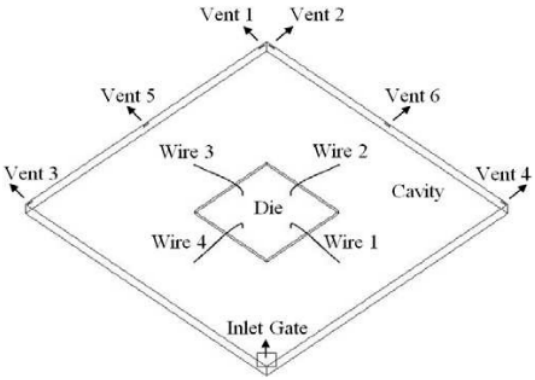

(c) 6 vents

Figure 3.5b Mould cavity models of scale-up four-wire PBGA with different outlet vent: (c) 6 vents (continued).

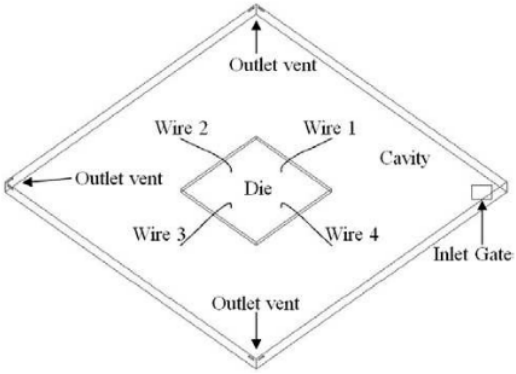

(a) One inlet gate

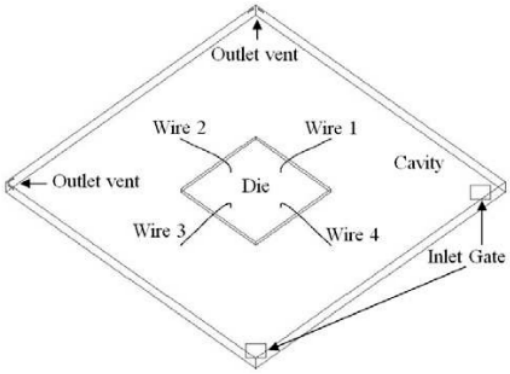

(b)Two inlet gates

Figure 3.6a Mould cavity models of scale-up four-wire PBGA with different inlet gate:
(a) One inlet gate and (b) Two inlet gates.

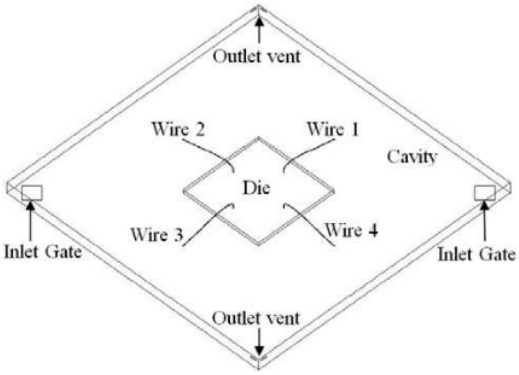

(c)Two inlet gates diagonal

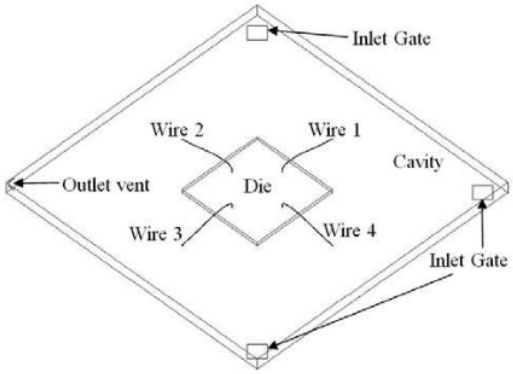

(d)Three inlet gates

Figure 3.6b Mould cavity models of scale-up four-wire PBGA with different inlet gate: (c) Two inlet gates diagonal and (d) Three inlet gates (continued).

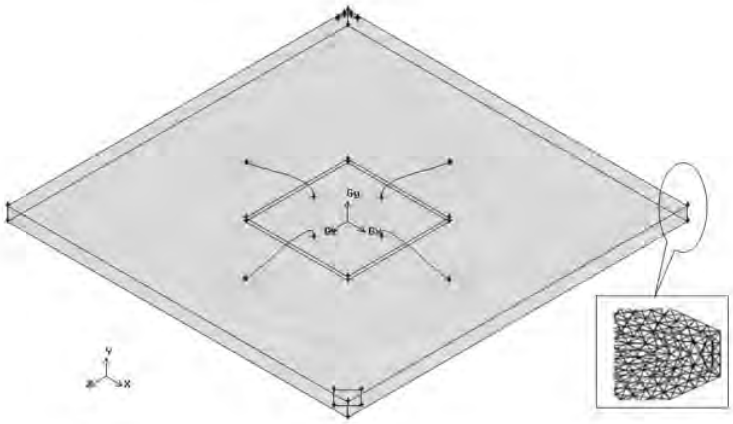

Figure 3.7 Meshed models of scale-up four-wire PBGA with 2 vents for FLUENT analysis.

The boundary and initial conditions used in the calculation are as follows (Khor et al., 2010b):

(a) On the wall: $u_i = 0$; $T = T_w$, $\frac{\partial p}{\partial n} = 0$

(b) On the melt front: $p = 0$ (Gauge pressure)

(c) At the inlet: $u = u_{in}(x,y,z)$; $T = T_{in}$

The mould temperature was considered as 175°C and the package inlet velocity was 0.6 m/s. The simulation is performed on an Intel Core 2 Duo processor E7500, 2.93 GHz with 2 GB of RAM; it took around 74 hours for each case to complete 15000 iterations in time steps of 0.001s.

3.3.2.2 Wire Model in ABAQUS

Commercial FEM based software; ABAQUS has been used in this study to calculate the wire deformation. The structures of the wires are imported from GAMBIT in ACIS '.sat' format. The dimensions of the gold wire used in this study are chosen according to the model of Yang et al. (2000). The wire (Figure 3.8) has a span, L = 20 mm, height H = 3.5 mm and diameter d = 0.14 mm. The wire is divided into 10191 tetrahedral elements (The element is defined by four nodes having three degrees of freedom at each node)as shown in Figure3.9. The shape of the wire is also classified as

typical Q-auto loop wire (Brand et al.,2008). The ball bond boundary conditions of wire were set as fixed in ABAQUS and shown in Figure3.10. The wire mechanical properties are as follows: elastic modulus, E=50 GPa (Yang et al., 2004), density, ρ=19330 kg/m^3, Poisson's ratio, v = 0.42.

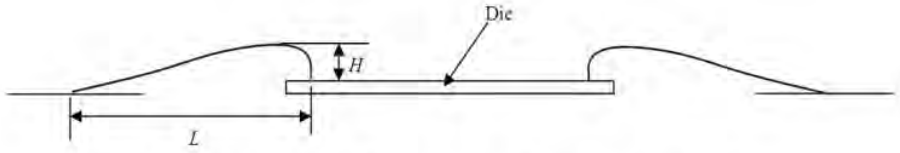

Figure 3.8 Wire specifications of scale-up four-wire PBGA.

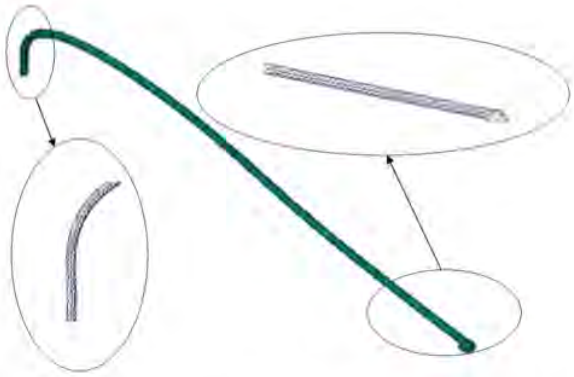

Figure3.9 Meshed wires of scale-up four-wire PBGA for ABAQUS analysis.

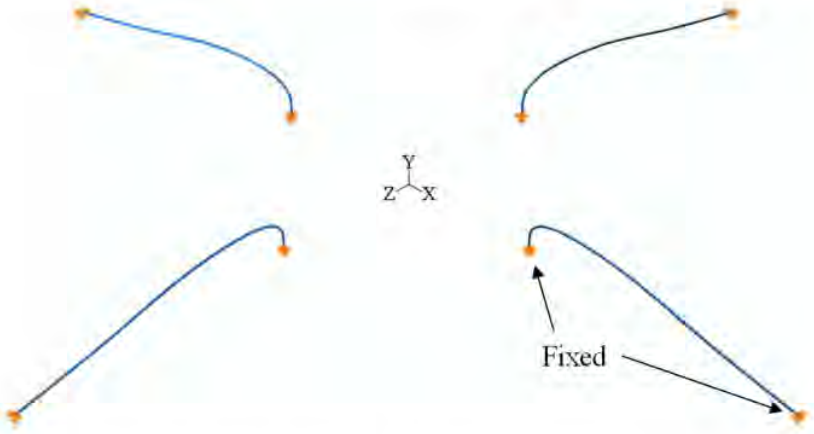

Figure 3.10 Boundary conditions of wires of scale-up four-wire PBGA in ABAQUS.

3.4 Wire Sweep Analysis Considering Stacked Die Effect and Arrangement of Inlet Gate of Scale-up Eight-wire PBGA Encapsulation Process

3.4.1 Problem Description

The small PBGA and non-transparent packaging mould used in the actual encapsulation process causes difficulties in visualisation of the FSI phenomenon. The deformation of the wire bond is normally observed from the top view of the package using x-ray. It is the best method for visualising FSI through vertical and top views of the mould for better understanding of FSI. Investigation can also be conducted using simulation tools. However, the visualisation of FSI during the encapsulation of PBGA is complicated. Therefore, a transparent and scaled-up mould was fabricated to emulate the package with single and stacked die with copper wires for the encapsulation process, as illustrated in Figure3.11 and 3.12 for PBGA with centre inlet and corner inlet respectively. Two different packages (single die and stacked die) were considered to provide the better visualisation of FSI on the interaction phenomenon between fluid and wires in the experimental work. The virtual modelling technique using finite volume (FV) and finite element (FE) codes was applied for the FSI analysis.

The inlet gates in the moulding equipment are located as depicted in Figure 3.11, which can be easily removed and polished if necessary. Properly designed inlet gates should allow proper flow of material as it enters the mould cavity. Inlet gates should be located at points away from the functioning parts of the moulded component.

Outlet vents are provided in all transfer moulds to facilitate the escape of trapped air. The locations of these outlet vents depend on the part design, and locations of pins and inserts. The outlet vent is sufficiently small so that it allows the air but not the moulding compound to pass through. Outlet vents are often placed at the far corners of the cavity, near inserts where a knit line will be formed, or at the point where the cavity fills last.

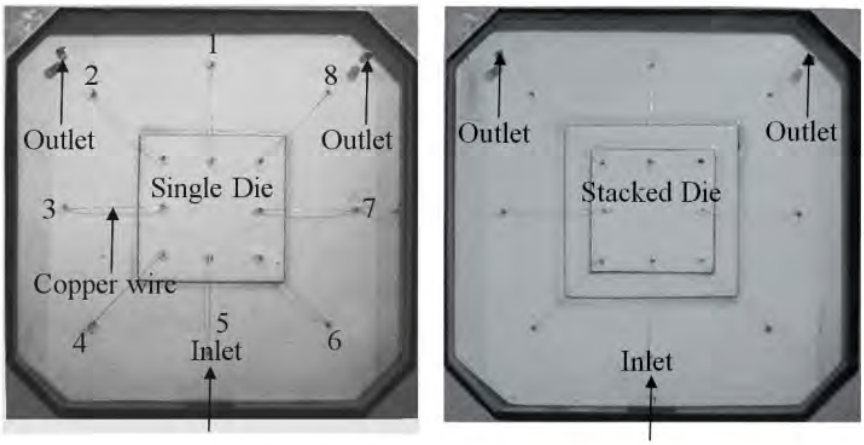

(a) Single die. (b) Stacked die.

Figure 3.11 Scale-up of eight-wire PBGA model with centre inlet: (a) Single die and (b) Stacked die.

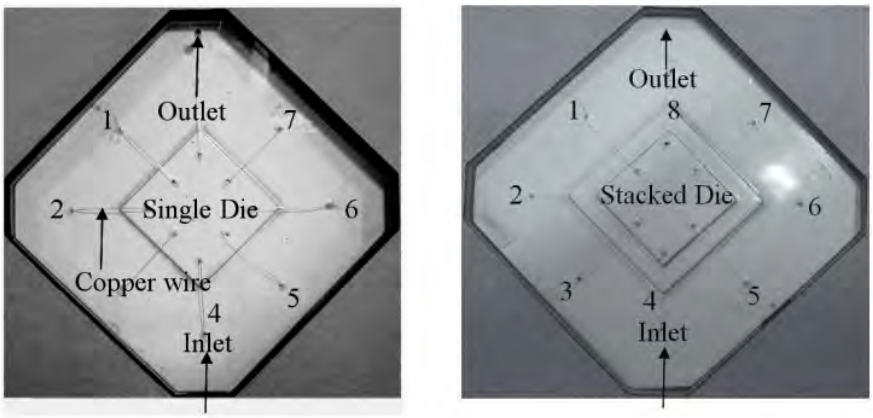

(a) Single die. (b) Stacked die.

Figure 3.12 Scale-up of eight-wire PBGA model with corner inlet: (a) Single die and (b) Stacked die.

3.4.2 Experimental Setup

In the present study, the experiment of scaled-up PBGA encapsulation process was carried out using the system depicted in Figures 3.13 and 3.14.The actual diagram and the schematic of experimental setup are illustrated in Figures3.13 and 3.14 respectively. The dimension of the wire was built as presented in Figure 3.15.The wire bond span has a length L = 2cm, height of wire H = 0.15 cm, and diameter of wire d = 0.01cm.The elastic modulus (E) of copper wire is 47.296GPa that measure by using tensile test. The graph of tensile test result is presented in Appendix C.

A test fluid with a constant viscosity of 4Pa·sthat measured by using viscometer (Appendix D) and a density of 1067 kg/m^3 was utilised as the fluid medium. The servomotor illustrated in Figure3.13 controlled the system delivery of the test fluid into the mould.

The system was tested to obtain a constant voltage for the experiment. The FSI process during encapsulation was recorded using a camera and processed by computer. The detailed and exploded views of the mould of scale-up eight-wire PBGA with centre and corner inlet are presented in Figure3.16–3.19 respectively. The mould was fabricated from transparent perspex for better visualization. The material used for the imitated die was a thin layer of acrylic. Scale-up eight-wire models of the PBGA package with different heights of die and inlet arrangement were built and sized, as shown in Figure3.20 and 3.21 respectively. The dimensions of the cavity were 8 cm × 8 cm × 0.5cm. The total thickness of the imitated dies was 0.11 cm for a single die package and 0.22 cm for a stacked die package. The dimensions of the imitated die were 3cm × 3cm ×0.11cm for the single die and 2.5 cm × 2.5 cm × 0.11 cm (top die) and 3.5 cm × 3.5 cm × 0.11 cm (bottom die) for the stacked die. The experiment presented here is focused on the interaction between the test fluid and the wire. Therefore, the effect of temperature is not considered in this experiment.

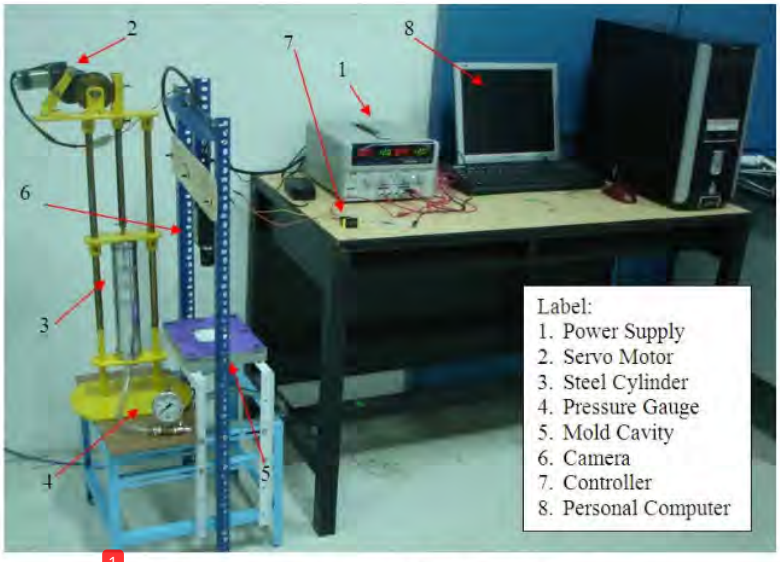

Figure 3.13 Actual diagram of the experimental setup.

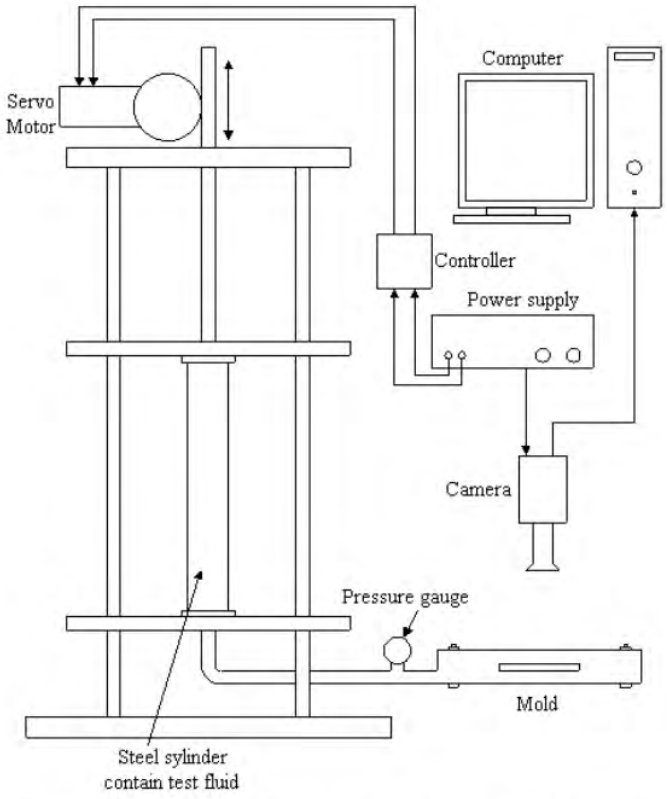

Figure 3.14 Schematics diagram of the experimental setup.

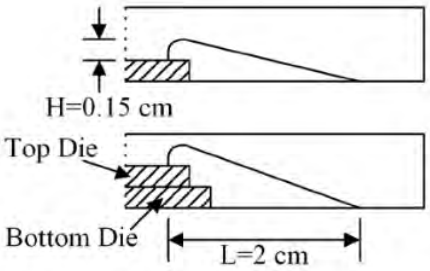

Figure 3.15 Dimension of the wire of scale-up eight-wire PBGA model.

Figure 3.16 Detailed construction of mould of scale-up eight-wire PBGA model with centre inlet.

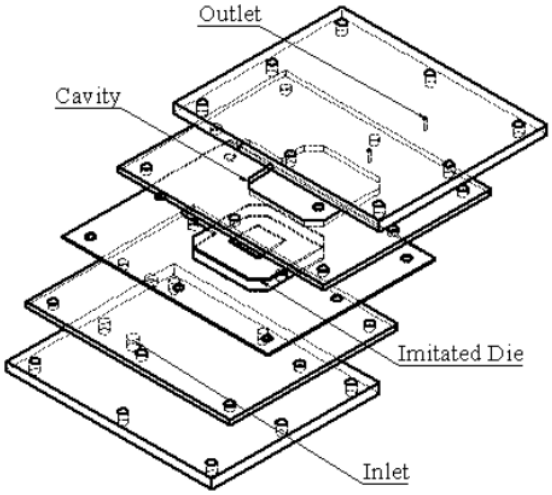

Figure 3.17 Exploded views of the mould of scale-up eight-wire PBGA model with centre inlet (Layer 1: top plate, Layer 2: cavity plate, Layer 3 - 5 base plates with inlet).

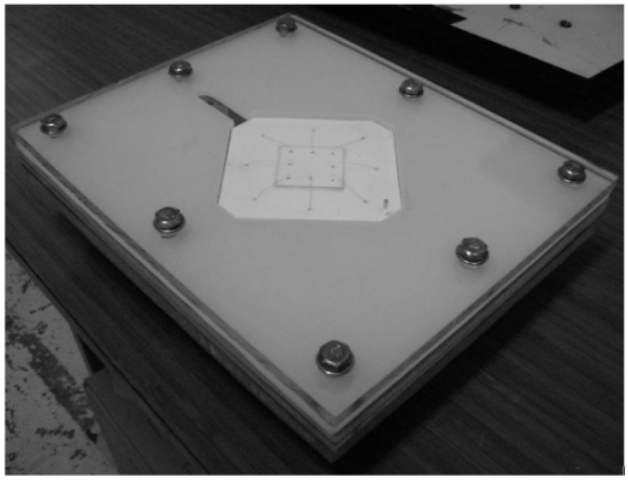

Figure 3.18 Detailed construction of mould of scale-up eight-wire PBGA model with corner inlet.

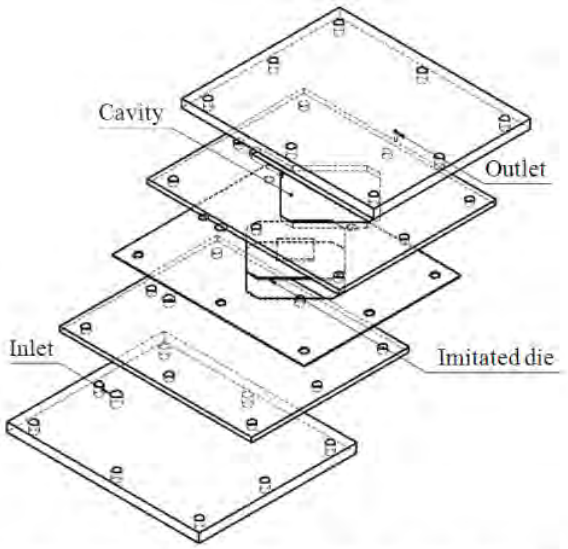

Figure 3.19Exploded views of the mould of scale-up eight-wire PBGA model with corner inlet.(Layer 1: top plate, Layer 2: cavity plate, Layer 3 - 5 base plates with inlet).

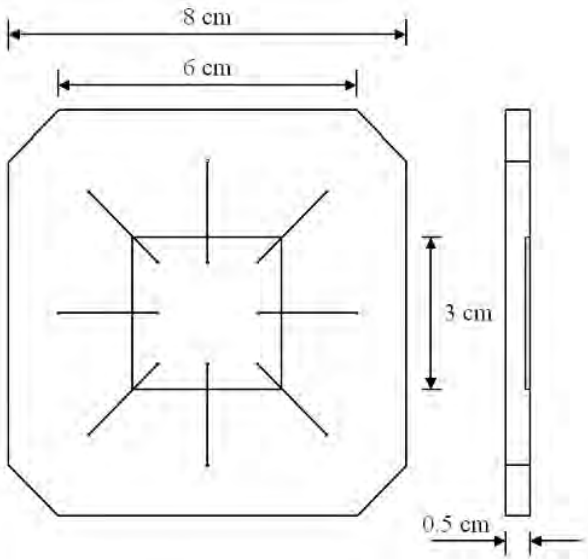

Figure 3.20 Dimension of scale-up eight-wire PBGA model of single die.

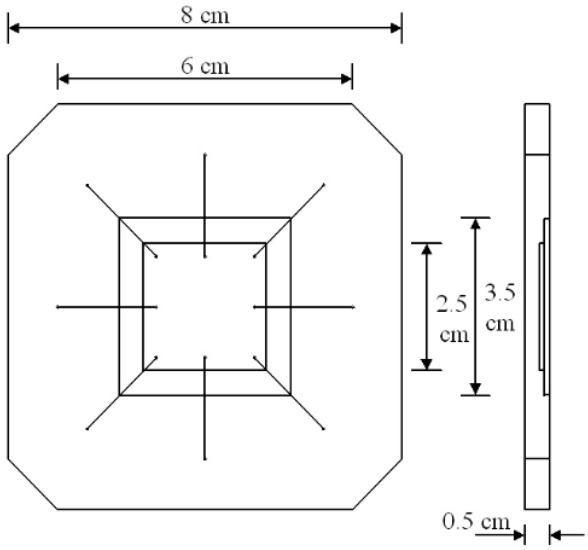

Figure 3.21 Dimension of scale-up eight-wire PBGA model of stacked die.

3.4.3 FSI Simulation Model and Boundary Condition

The concept of the FSI modelling is the coupling of FVM- and FEM-based software in conducting fluid and structural analysis. During FSI analysis, the transformation of analysis generated from the FLUENT 6.3.26 to ABAQUS 6.9 was performed using MpCCI (Khor et al., 2012a). Real-time data were transferred from one program to another. During the interaction, the forces induced from the fluid acting on the wires were directly solved by ABAQUS. Thus, the deformations of the wires were calculated simultaneously. The wires were defined as the coupled regions in FSI simulation. FLUENT was used to analyse the fluid flow modelling by simulating the physic of the flow front that fed into the cavity. ABAQUS was used to calculate the displacement, von Mises stress, and shear stress of wires during the encapsulation process.

3.4.3.1 Fluid Model in FLUENT

In the FLUENT analysis, the 3-D model was built according to the dimensions of the package that was fabricated in the experimental work. The model was meshed

with a total of 457424 and 481919 tetrahedral elements for scale-up eight-wire PBGA with centre inlet of single and stacked die respectively. The total meshes for scaled-up eight-wire PBGA with corner inlet of single and stacked die are 459889 and 497986 tetrahedral elements. Figure 3.22 illustrates the boundary conditions for single and stacked die and Figure 3.23 illustrates the meshed model of the imitated scale-up eight-wire PBGA package for single and stacked die. The surfaces of the mould, die, and wire were defined as wall boundaries with no-slip condition. Temperature effects were not considered in the experiment. Therefore, this process was assumed to be isothermal during the simulation and was set at room temperature. The FSI phenomenon focused on the fluid feeding into the cavity until the "final" stage, which is before the plunger is retracted from the fluid cylinder.

Air and test fluid are defined as the phases in the analysis. The implicit solution and the time-dependent formulation are applied for the volume fraction in every time step. The volume fraction of the encapsulation material is defined as 1 and 0 value for the air phase. The boundary and initial conditions that are used in the calculation are as follows (Khor et al., 2012a):

(a) On the wall: $u = v = w = 0$; $T=T_w$, $\frac{\partial p}{\partial n} = 0$.

(b) On the melt front: $p = 0$. (Gauge pressure)

(c) At the inlet: $p=p_{in}(x,y,z)$; $T=T_{in}$.

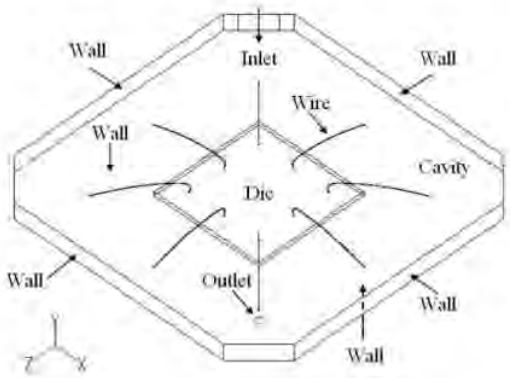

(a) Single die.

Figure 3.22 Boundary conditions of scale-up eight-wire PBGA model: (a) Single die

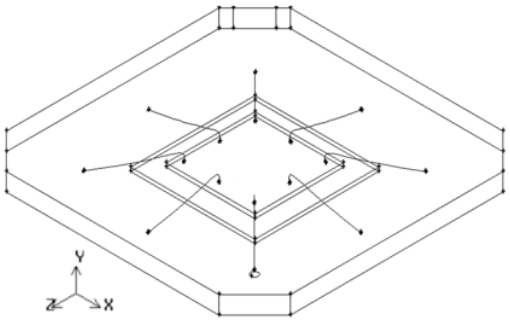

(b) Stacked die.

Figure 3.22b Boundary conditions of scale-up eight-wire PBGA model:

(c) Stacked die.

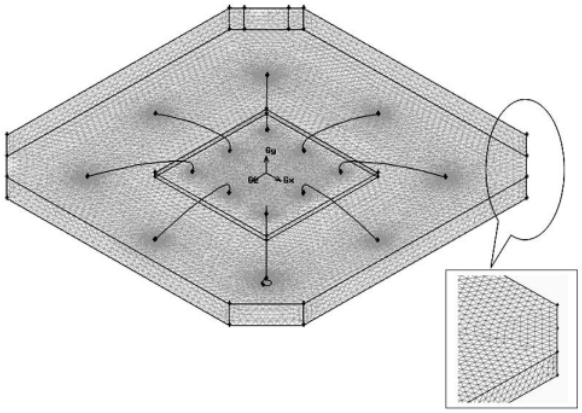

(a) Single die.

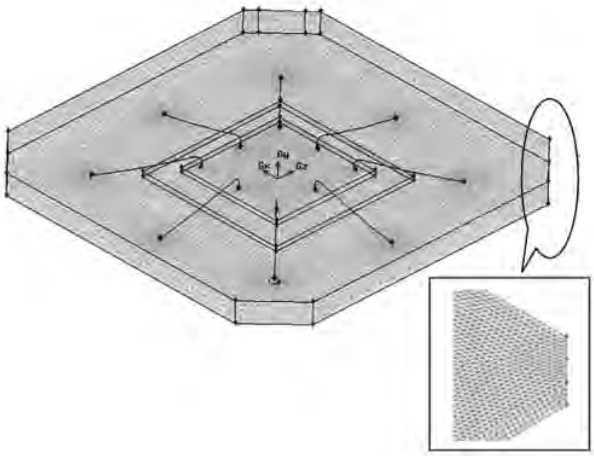

(b) Stacked die.

Figure 3.23 Meshed model of scale-up eight-wire PBGA package: (a) Single die and (b) Stacked die.

In the present study, the geometry of the scaled-up eight-wire PBGA is modelledusing3-D finite volume grid. The dimensions of the mould model were 8 cm × 8 cm × 0.5cm and the analysis was performed on two different types of package (Single dies and stacked die). The outlet vent position of the mould cavity is opposite to the inlet gate, as shown in Figure 3.22, and considered the boundary conditions in the present investigation. Only eight wires were considered in the wire region of the package in the simulation and experiment.

In the encapsulation process, test fluid was used as the moulding compound. The test fluid density and viscosity were 1067 kg/m^3 and 4 Pa.s respectively. The voltage was set as 6 Volt (70.7 kPa) as Case 1, 9 Volt (113.3 kPa) as Case 2, and 12 Volt (161.4 k.Pa) as Case 3 during the process. The inlet pressure was measured by fluid Pressure Gauge. The simulation was performed on an Intel Core 2 Duo processor E7500, 2.93 GHz with 2 GB of RAM; it took around 4hours for each case to complete 4000 iterations for optimum time steps of 0.001s (Khor et al., 2010a).

3.4.3.2 Simulation Model and Boundary Conditions in ABAQUS

Figure 3.15 shows the model of wire dimension for structural analysis. The 3-D meshed model was generated using tetrahedral elements with the sweep method by

ABAQUS 6.9 (Khor et al., 2012a). The mechanical aspects were considered. Thus, the structures of the coupled regions were defined as deformable in the analysis.

The commercial FEM-based software ABAQUS is employed in this study to calculate the wire deformation. The structures of the wires are imported from GAMBIT in ACIS '.sat' format in order to get the identical coordinate. The wire bond span has a length L = 2cm, height of wire H = 0.15 cm, and diameter of wire d = 0.01cm. The wire bond is divided into 3087(single die) and 3675 (stacked die) tetrahedral elements as shown in Figure3.24. The shape of the wire is classified as typical Q-auto loop wire bond (Brand et al., 2008). The ball bond boundary conditions of the wire were set as fixed in ABAQUS and shown in Figure3.25. The mechanical properties of wire are as follows: elastic modulus E= 47.296GPa, density ρ = 8960 kg/m^3, and Poisson's ratio v = 0.355.

In the experiment, the structures of wires were properly positioned on the die in the cavity. In addition, some basic assumptions were considered in the FEM analyses for simplification purpose. The elastic behaviour was taken as homogeneous and isotropic in the structures of wire(Khor et al., 2012a). The solder bond was neglected where the solder pad was not considered in the scaled-up PBGA model. The temperature effect on the structures was not considered in the experimental work. Therefore, no thermal effect on the creep and fracture behaviour was considered in the present modelling. In reality there are some residual stresses in the wirebond due to the wire looping process, especially at the neck of the wirebond adjacent to the ball bond. However, in the finite element simulation of the structural deformation of the wirebonds, the wirebonds were assumed to have no initial stress before the action of the flow-induced forces (Tay and Lee, 2002).

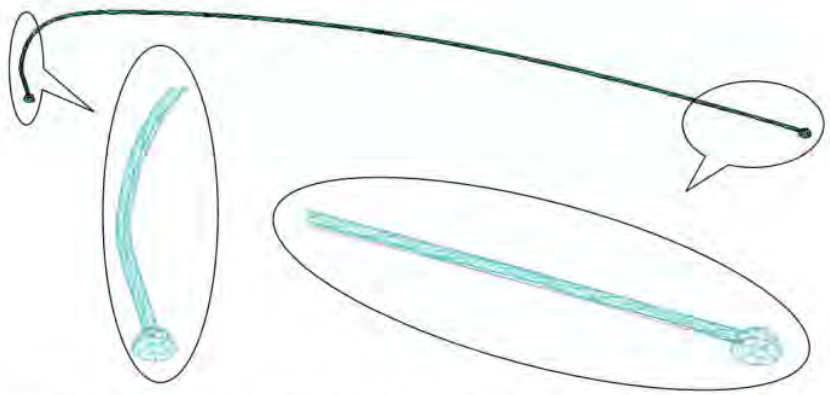

Figure 3.24 Meshed wire for ABAQUS analysis for Single Die of scale-up eight-wire PBGA model.

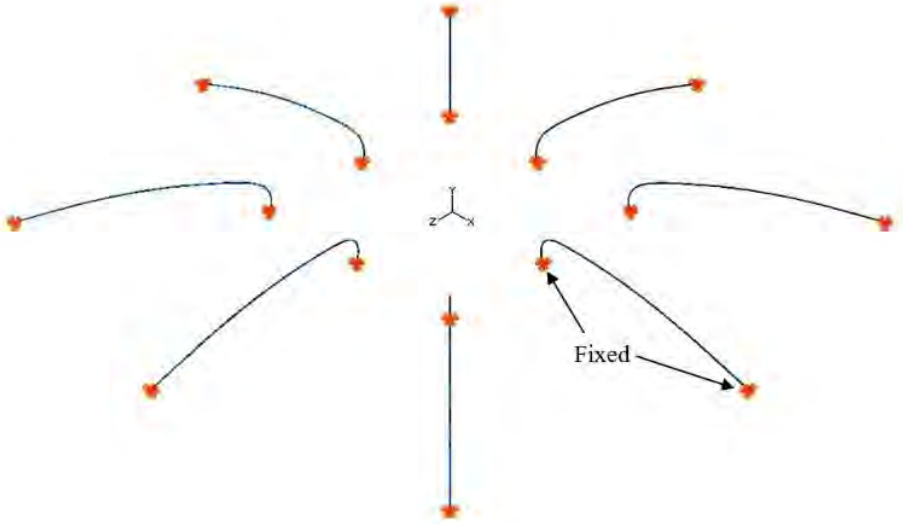

Figure 3.25 Boundary conditions of wires in ABAQUS for Single Die of scale-up eight-wire PBGA model.

3.5 Wire Sweep Analysis Considering Rheology Effect of actual size PBGA Encapsulation Process

3.5.1 Problem Description

In fact, wire sweep during encapsulation is a typical FSI problem, which is normally handled by a coupled analysis of fluid flow and structural deformation. The

use of a finite-volume flow solver and a finite-element structural solver, coupled through MpCCI has been reported for a variety of engineering problems (Yigit et al., 2008; Thirifay and Geuzaine, 2011; Gatzhammer,2010).However, the use of MpCCI has not been reported so far for wire sweep analysis. Accordingly, a novel 3-D computational technique using the MpCCI method is introduced on the PBGA encapsulation process for the prediction of wire sweep. This method utilizes the finite-volume flow solver FLUENT and the finite-element structural solver ABAQUS, interfaced by MpCCI. Polymer rheology model with curing effect (the Castro–Macosko model) is used in the fluid flow model, and the volume of fluid (VOF) technique is applied for melt-front tracking of the EMC. The numerical analysis uses UDFs to account for the curing kinetics. In the present study, the computational fluid dynamic code FLUENT 6.3 (Khor et al., 2010a) is used to analyze the effect of rheology on the flow behaviour and wire sweep of the encapsulation process of PBGAs. The 3-D models are developed and analyzed by using finite volume method. Three different EMC properties, designated as Case A, Case B, and Case C,were studied for analyzing of fluid flow and wire sweep inside the mould cavity. Numerical results of flow patterns and percentage of the void of the three arrangements of EMC properties are compared. Wire sweep profiles and pressure field are analyzed and presented. The simulation results are compared with the previous experimental result available in literature.

3.5.2 FSI Simulation Model and Boundary Condition

3.5.2.1 Fluid Model in FLUENT

The VOF model in FLUENT 6.3.26 is utilised to simulate the process (Khor et al., 2010b). EMC types are set at different parameters, as shown in Table 3.2.Table 3.2 summarizes the material properties of the EMC considered in the current simulation (Jong et al., 2005; Nguyen et al., 2000; Wu at al., 1998).Air and EMC are defined as the phases in the analysis. Implicit solution and time dependent formulation are applied for the volume fraction in each time step. The volume fraction of the encapsulation material is defined as 1 and that of the air phase as 0. Besides, the viscosity Castro–Macosko model and VOF techniques are applied to track the melt front. The PBGA chip package model used in the present study and its dimensions and boundary condition are shown

in Figure3.26 and 3.27 respectively. The boundary and initial conditions used in the calculation are as follows (Khor et al. 2011a):

(a) Onthe wall: $u = v = w = 0$; $T=T_w$, $\frac{\partial p}{\partial n} = 0$.

(b) Onthe melt front: $p = 0$. (Pressure gauge)

(c) Atthe inlet: $u=u_{in}(x,y,z)$; $T=T_{in}$.

Table 3.2 EMC material properties used in rheology effect.

			Value		
		Unit	CaseA (Jong et al., 2005)	Case B(Nguyen et al., 2000)	Case C (Wu et al., 1998)
Density	ρ	kg/m^3	1578	2000	1820
Tabulated Thermal Conductivity	T	°C	66.95	175	75
	k	W/m.K	0.74	0.97	0.669
Tabulated Specific Heat	T	°C	169.95	175	169.95
	C_p	J/kg.K	1078	1079	1205
Reactive I Viscosity	N	-	0.7773	0.7773	0.28
	τ*	Pa	0.0001	0.0001	2361
	B	Pa.s	0.04219	3.81E-04	0.416
	Tb	K	4810	5.230E+03	2.091E+03
	C_1	-	10.96	1.03	3.496
	C_2	-	0.00626	1.50	8.503
	α_g	-	0.6946	0.17	0.17
Reaction Kinetics	H	J/kg	3.91E+04	4.01E+04	4.585E+04
	m_1	-	0.4766	1.21	0.7241
	m_2	-	1.08	1.57	1.234
	A_1	1/s	0.1	33.53E+03	8475
	A_2	1/s	5.926E+05	30.54E+06	9.715E+06
	E_1	K	2E+004	7161	7216
	E_2	K	7501	8589	8585

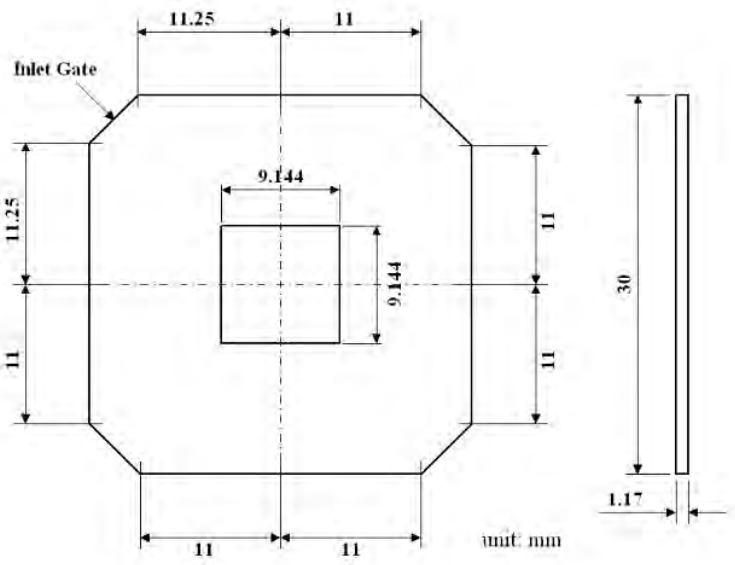

Figure3.26 Dimension of actual size PBGA model package (Chen, 1990).

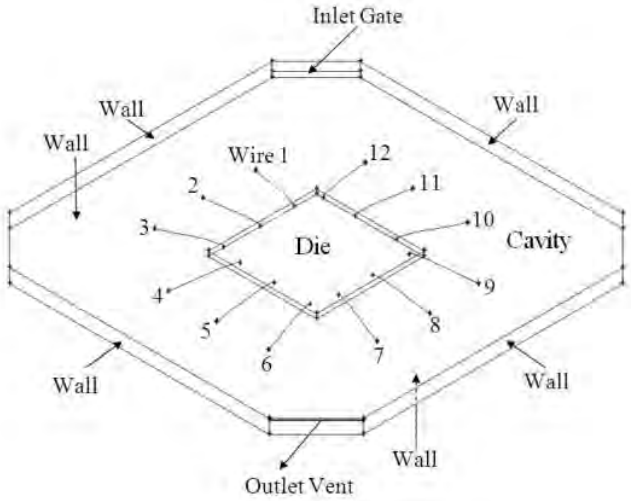

Figure3.27 Boundary conditions of actual size PBGA model.

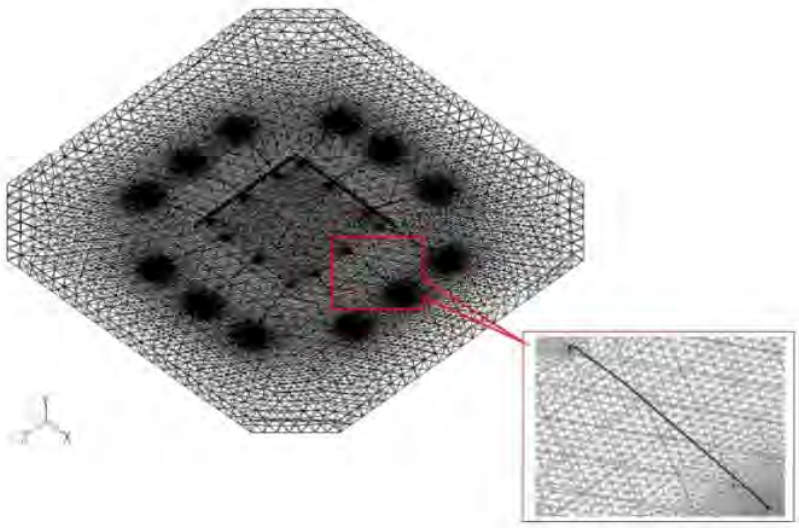

Figure3.28 Meshed model of actual size PBGA package.

In the present study, geometry of the PBGA is modelled as a 3-D finite volume grid. The dimension of the mould model is 30 mm × 30 mm × 1.17 mm and the mould entrance is oppositely located to the outlet vent of the mould cavity as shown in Figure 3.27, and is considered the boundary conditions in the present investigation, and only 12 wires bonding are considered as the reference wires in the wire region of the package in the simulation refer to Chen (1990). In the present modelling, the walls boundaries are as shown in Figure 3.27 are defined as non-slip wall in the FLUENT. The meshed model is created by using the GAMBIT software, and an average 480000 tetrahedral elements of the package volume are generated for simulation (Figure 3.28). The wire consists of surfaces of the ball bond and wire body. The total meshing of wire surface is 1626 triangles and for ball bond40 triangles.

In the encapsulation process, EMC is used as the moulding compound. The mould temperature is set as 175 °C, and 0.3 m/s of inlet velocity is applied during the process. The simulation is performed on an Intel Core 2 Duo processor E7500, 2.93 GHz with 2 GB of RAM; it took around 12 hours for each case to complete the 14000 iterations in time steps of 0.001s (Khor, 2010a).

3.5.2.2 Wire Model and Boundary Conditions in ABAQUS

The commercial FEM based software ABAQUS is used in this study to calculate the wire deformation. The structures of the wires are imported from GAMBIT in ACIS ".sat" format. The dimension of the wire is built according to Chen (1990)model. The wire bond span length L = 4.875 mm, height of wire H = 1.75 mm and diameter of wire d = 0.032 mm. The wire bond is divided into 6240 tetrahedral elements as shown in Figure 3.29. The shape of the wire as also classified as typical Q-auto loop wire bond (Brand, 2008). The ball bond boundary conditions of wire are set as fixed in ABAQUS and shown in Figure3.30. The wire mechanical properties are as follows: elastic modulus, E=34 GPa(Chen, 1990), density, ρ=19330 kg/m^3, Poisson's ratio, v = 0.42 and reference temperature, T=175°C.

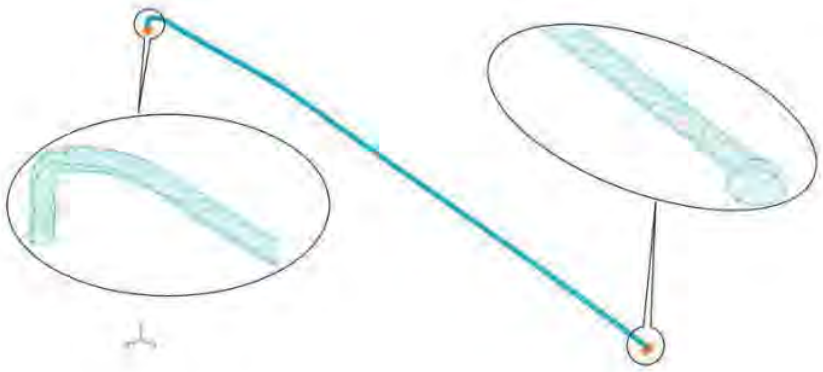

Figure 3.29 Meshed wire for ABAQUS analysis of actual size PBGA.

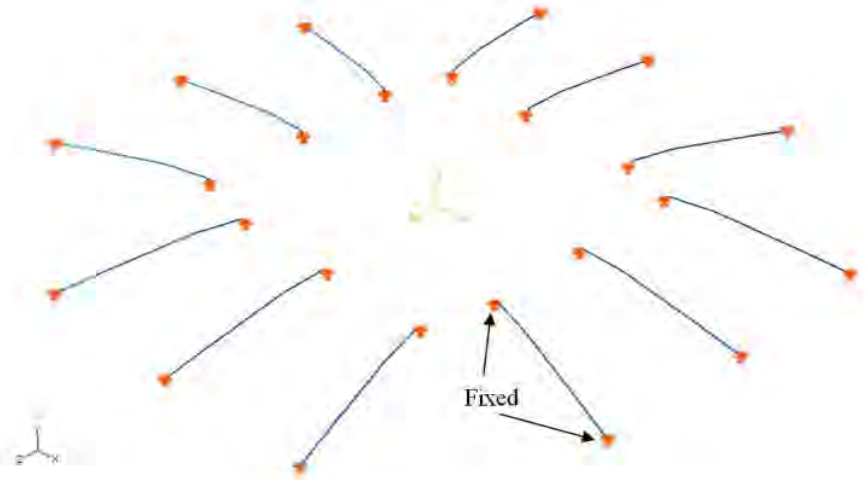

Figure3.30 Boundary condition of wire in ABAQUS of actual size PBGA.

3.6 Optimization Using RSM of PBGA Encapsulation Process

3.6.1 Design Optimization

The design, mathematical modelling and optimization of this study were performed using Design Expert 6.0.6 software. Central composite design (CCD) was used to model the response surface methodology (RSM) in the design. The former is the most widely used numerical design for fitting a second order response surface (Kapoor et al., 2004). The independent variables (factor) used in this numerical study were inlet pressure, wire diameter, and vent height and coded as *A*, *B* and *C* respectively (Table 3.3). The independent variables were varied over three levels, between−1, 0 and +1, and the range was determined based on literature review. In the literature review the ranges of inlet pressure from 5 MPa (Teng and Hwang, 2008) to 10 MPa (Wang et al., 2010). Another factor that was concern in this study is the wire diameter. The maximum value for the wire diameter was set at 0.05 mm in order to reduce the wire deformation in encapsulation process. The wire diameter was varied from 0.03 mm to 0.05 mm. The wire diameter was designed based on the research work conducted by Kung et al.

(2006a). Effect of mould vent size was introduced by Chai and Zohar (1999). The mould vent size may influence the filling time of the encapsulation process.

Generally, the CCD consists of a 2^k full factorial design with $2k$ axial or star runs, a total of 20 simulations were performed to assess the three factors, according to the equation CCD = $2^k + 2k + 6$, where k is the number of factors. Fourteen simulations were improved with six replications at the design centre to evaluate the pure error, (Montgomery, 2009). Eq. (3.23) shows the quadratic model used to estimate the optimal point (Adlan et al., 2011, Khor and Abdullah, 2012b):

$$Y = \beta_o + \sum_{i=1}^{k} \beta_i X_i + \sum_{i=1}^{k} \beta_{ii} X_i^2 + \sum_{i<j}^{k} \sum_{j}^{k} \beta_{ij} X_i X_j + \cdots + e \qquad (3.23)$$

where Y is the response; X_i and X_j are the variables; β_0 is a constant coefficient; β_i, β_{ii}, and β_{ij} are the interaction coefficients of linear, quadratic and second-order terms, respectively; k is the number of studied factors; and e is the random error.

The coefficient of determination (R^2) was used to identify the quality of the fit of polynomial model and the P-value associated with the 95% confidence level was used to evaluate the variables and the interactions between them. The significance and adequacy of the model was assessed according to the calculated F-value (Fisher variation ratio), probability value (Prob > F), and Adequate Precision.

Table 3.3 Actual and coded value for the independent variable of the CCD design.

Factor (Symbol)	Coded value		
	-1	0	1
	Actual value		
A. Inlet Pressure (MPa)	5	7.5	10
B. Wire Diameter (mm)	0.03	0.04	0.05
C. Vent height (mm)	0.04	0.22	0.40

The regression analysis was performed using Design Expert 6.0.6 software to fit the simulation data into the second-order polynomial equation, and evaluate the variable and interaction between them. The statistical significance of the equation developed was also estimated through the software.

3.6.2 Modelling

The FSI simulation modelling consists of the fluid flow and structural analysis. Finite volume-based (FLUENT) and finite element-based (ABAQUS) software were used to perform the analysis of the PBGA encapsulation process. The basic idea of the current FSI is the real-time coupling (Khor et al., 2012a) between both analysis codes through the Mesh-based parallel Code Coupling Interface (MpCCI) method. During the simulation, the forces induced from the fluid flow (FLUENT) are transferred to the ABAQUS for simultaneous structural analysis. The deformation, stress concentration on the structures (wires), and EMC fluid flow were analyzed in the FSI analysis. The FSI phenomenon in the cavity focused on the fluid feeding until the final stage, before the plunger isretracted from the fluid cylinder. Figure 3.27depicts the boundary conditions of the PBGA in fluid analysis. The meshed model of the PBGA was a mould cavity as illustrated in Figure 3.28, which provides a fluid domain for FLUENT analysis, and was created and meshed using GAMBIT software. The 3D model with different variables was meshed with 350000–500000 tetrahedral elements. A 75 ^{o}C pre-heated temperature was set at inlet gate for EMC, and 175 ^{o}C was set as the mould temperature. The Optimisation material properties of EMC are summarized in Table 3.1 (Case B in Table 3.2). The EMC material was selected based on Case B of previous study (in Section 3.5.1). The EMC more stable in flow front profile and can reduce the wire sweep in PBGA encapsulation process.

In the FEM modelling, the wires were meshed using hexahedral elements with sweep method, as illustrated in Figure 3.29. Similarly, several assumptions have been made for the present structural analysis included the fixed boundary of the model is shown in Figure 3.30. Homogeneous and isotropic in the elastic behaviour of structures were considered in the finite element (FE) analysis. The mechanical properties of wire are summarized in Table 3.4.

Table 3.4 Mechanical properties of wires (Chen, 1990)

Parameter	Wire
Elastic modulus, E (GPa)	34
Poisson ratio, v	0.42
Solid density, ρ_s (kg/m^3)	19330

3.7 Summary

A 3-D computational analysis was used to predict the wire sweep in the imitation of scaled-up and the actual size PBGA encapsulation process. The FVM- and FEM-based software coupled with MpCCI were used to perform the study of FSI in virtual modelling of the encapsulation process. Moreover, the VOF technique was applied to track the flow front of EMC.

This research also discussed the optimisation of physical and process parameters of the actual size PBGA package by using RSM model in the analysis of wire sweep, filling time and void occurrence during the encapsulation process.

CHAPTER4: SIMULATIONS AND EXPERIMENTS ON PBGA ENCAPSULATION PROCESS

This chapter presents the simulations and experiments on PBGA encapsulation process and a detailed discussion with the observation. The results obtained from experimental results of a scaled-up eight-wire PBGA prototype encapsulation process with different stacked dies and inlet gates orientation and the simulation of melt front behaviour, pressure distribution within cavity, wire sweep profile and wire stress, also comparison between simulation, experiment, and previous experimental results of melt-front profile and wire sweep. The wire sweep considering rheological effect and optimization of an encapsulation process on actual size of PBGA through the simulations is discussed in this chapter.

4.1 Grid Independence Test

Grid independence test was performed to obtain the optimum mesh size. Five different mesh sizes were tested, and the corresponding filling percentage was estimated for a PBGA package that consisted of a single die and scaled-up four wires PBGA with stacked die and scaled-up eight-wire and also included an actual size PBGA. The simulations were performed by using a PC with an Intel Core 2 Duo processor E7500, 2.93 GHz with 2 GB of RAM; it took around seventy-four hours for each case to complete 15000 iterations for a case with 2 vents of scaled-up four wires PBGA. Then, for Case 3 (single and stacked die of scale-up eight-wire PBGA),it took around four hours for each case to complete 4000 iterations, and took around twelve hours for each case to complete 12000 iteration for Case B of actual size PBGA in optimum time steps of 0.001s (Khor et al., 2011b).

The encapsulation process took about 13 s, 4 s and 12 s to fill completely for a scaled-up four-wire PBGA, a scale-up eight-wire PBGA and an actual size PBGA, respectively. Concerning the finest mesh size of 459697, 586617,634341(Test4) and experimental results for scaled-up four-wire PBGA, single and stacked die of scaled-up eight-wire PBGA and actual size PBGA respectively, the discrepancies in the filling volume of tests 1, 2, 3 and 4 at 13 s, 4 s and 12 s are calculated. As summarized in Table 4.1- 4.4 and Figure 4.1, the deviations of Test 2 and 3 from 4are found to be the same and nominal (0.29% (scale-up four-wire PBGA), 0.30% (single die of scale-up

eight-wire PBGA), 0.25% (stacked die of scale-up eight-wire PBGA) and 0.13% (actual size PBGA)). Hence, for the present study, Test2 with 395498, 446143, 564465 and 478822elements are chosen as the optimum and closely with the experiment results of fluid volume, in terms of accuracy and computational cost.

Table 4.1 Summary of grid independency test of single die of a scale-up four-wire PBGA for 2 vents Case

Test	1	2	3	4	Exp.
Element	357,844	395,498	398,900	459,697	-
% filling volume at 13 s	83.46	84.13	84.13	84.42	84.00
Deviation from size 5	0.96	0.29	0.29	-	-

Table 4.2 Summary of grid independency test of single die of a scale-up eight-wire PBGA for Case 3

Test	1	2	3	4	Exp.
Element	406,852	446,143	493,407	586,617	-
% filling volume at 4 s	97.83	98.02	98.02	98.32	99.00
Deviation from size 5	0.49	0.30	0.30	-	-

Table 4.3 Summary of grid independency test of stacked die of a scale-up eight-wire PBGA for Case 3

Test	1	2	3	4	Exp.
Element	498,072	564,465	598,483	634,341	-
% filling volume at 4 s	93.16	97.00	97.00	97.25	98.5
Deviation from size 5	4.24	0.25	0.25	-	-

Table 4.4 Summary of grid independency test of an actual size PBGA for Case B

Test	1	2	3	4	Exp.
Element	467,092	478,822	499,614	537,192	-
% filling volume at 12 s	78.95	83.66	83.50	82.52	87.13
Deviation from size 5	8.18	3.47	3.63	4.61	-

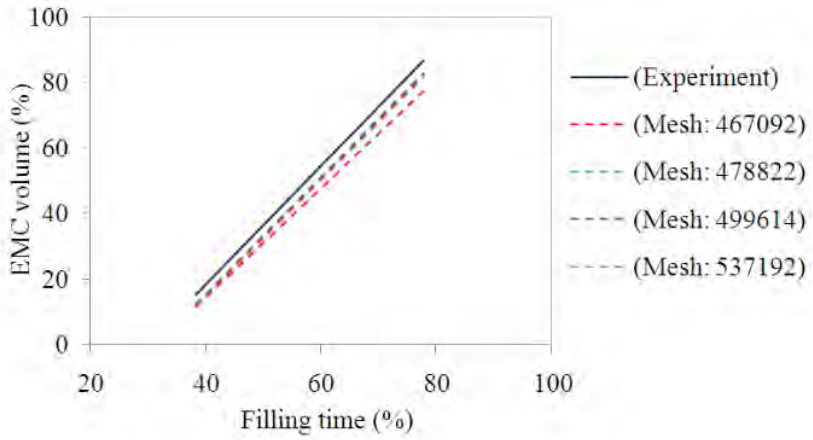

Figure 4.1 Grid independent test of an actual size PBGA for Case B.

4.2 Experiment and Model Validation

4.2.1 Scaled-up Four-wire PBGA Encapsulation Process

4.2.1.1 Fluid Flow

The present simulation results of fluid flow (package with 2 vents) were validated with the experimental results of Yang et al. (2000) who investigated the flow behaviour of epoxy resin (D.E.R.331, Dow Chemical). Figure4.2 shows the comparison of predicted and experimental flow profiles of the scaled-up four-wire PBGA encapsulation process from 33% to 84% of filling. The simulation results showed separate profiles for wire sweep and EMC filling, at various stages of filling. The predicted EMC flow profiles showed a good agreement with the experimental results, at all percentage volume steps. Wire displacement phenomenon was observed when the EMC flow around the wire region. The percentage of EMC volume versus filling time for the simulation and the experiment was also plotted and compared as depicted in Figure4.3; 6.7 % of maximum discrepancy was found for both results.

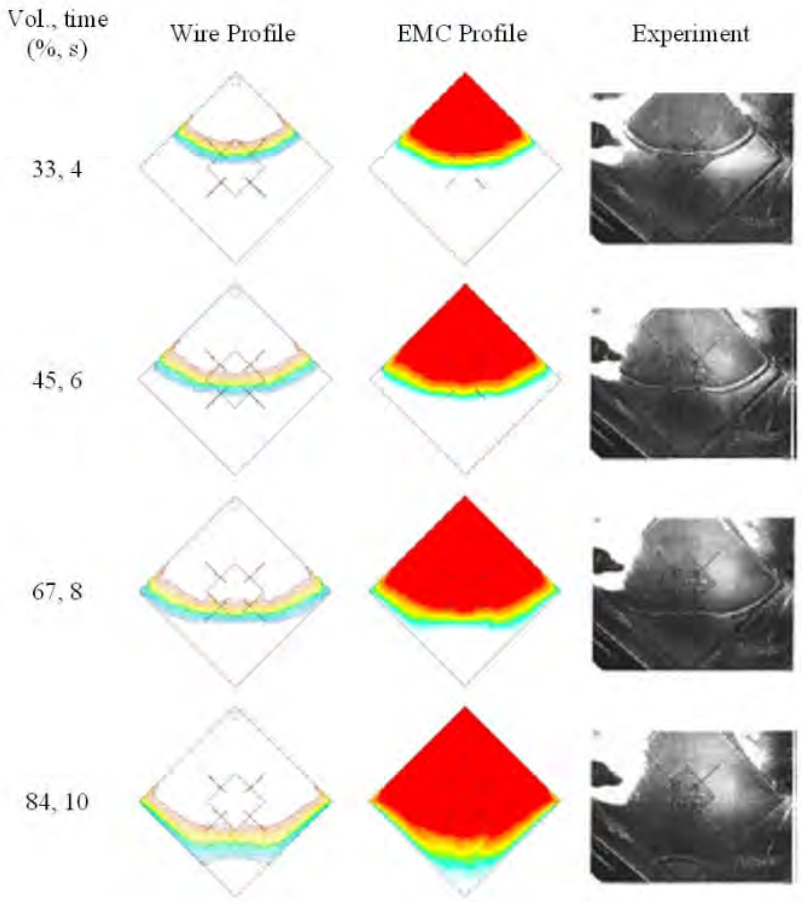

Figure 4.2 Comparison of simulation and experiment of scale-up four-wire PBGA(Yang et al.,2000) for wire deformation and EMC flow profiles (2 vents case).

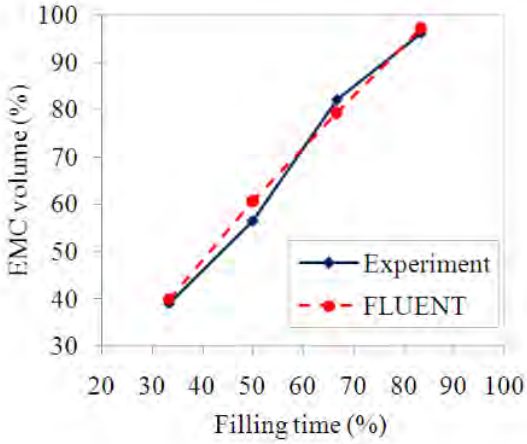

Figure 4.3 Comparison of EMC filled volume for experiment (Yang et al., 2000) and simulation (2 vents case) of scale-up four-wire PBGA.

4.2.1.2 Wire Deformation

Furthermore, the wire deformation was validated by using analytical method that proposed by Kung et al. (2006a). The comparison between simulation and their analytical results of wire sweep deformation for wire 4, which presented in x-direction, is shown in Figure 4.4. The analytical calculation was referred to Eq. 3.18 with f_B = 0.165, f_T = 0.00165 and H/L = 0.175. The average deviation at maximum displacement (after 60% filling time) is found to be 6.5 %. The result had demonstrated a good quantitative agreement.

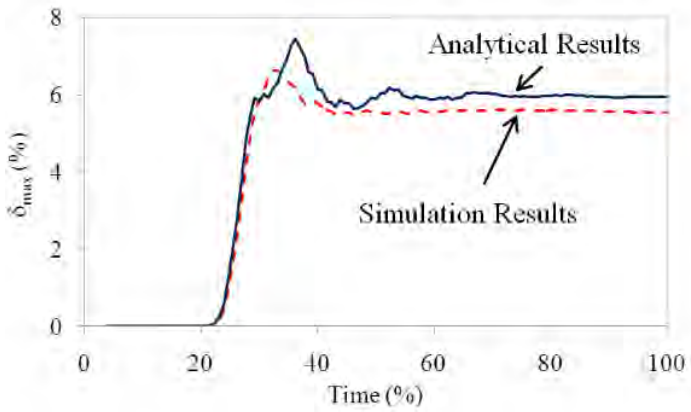

Figure 4.4 Comparison simulation and analytical results (Kung et al., 2006a) of wire sweep deformation for wire 4 in x-direction (2 vents case) of scale-up four-wire PBGA.

4.2.2 Scaled-up Eight-wire PBGA Encapsulation Process –Centre Inlet

4.2.2.1 Fluid Flow of Single Die and Stacked Die

The experiment was conducted for a scaled-up eight-wire PBGA prototype with a centre inlet. This experiment focuses on the FSI phenomenon and flow mechanism. Therefore temperature effect was not considered in experiment. The temperature of inlet boundary was similar to room temperature. The filling process of the viscous fluid into the cavity was recorded on top of the transparent mould. FSI simulation was also performed on the imitated package with a single die and a stacked die, as presented in Figure 3.11of Chapter 3. The flow front advancement of the simulation results were compared with the experimental results. The results showed that flow front predictions from the simulation code have nearly identical profile with the experimental results at different filling volumes of the test fluid. Figure4.5and Figure 4.6show the comparison of FSI predicted and experimental flow profiles of the scaled-up eight-wire PBGA with centre inlet encapsulation process from 27% to 75%and 25% to 78% of the filling stages, which included the wire sweep for a single die and a stacked die of scale-up eight-wire PBGA with centre inlet, respectively. The simulation result is substantiated by the experimental results by using similar scaled-up eight-wire PBGA with centre inlet size, operating condition and material properties as used in the present numerical

study. The predictions of flow front profiles and percentage of mould filling were well matched with the experimental results at all filling stages. The percentage of filled volume at various stages versus percentage filling time for Case 3 is compared in Figure4.7,the maximum discrepancy is found at 2.86% and 3.09% for single die and stacked die of scale-up eight-wire PBGA with centre inlet, respectively. The predicted fluid flow profiles showed a good agreement with the experimental results at all percentage of filling stages.

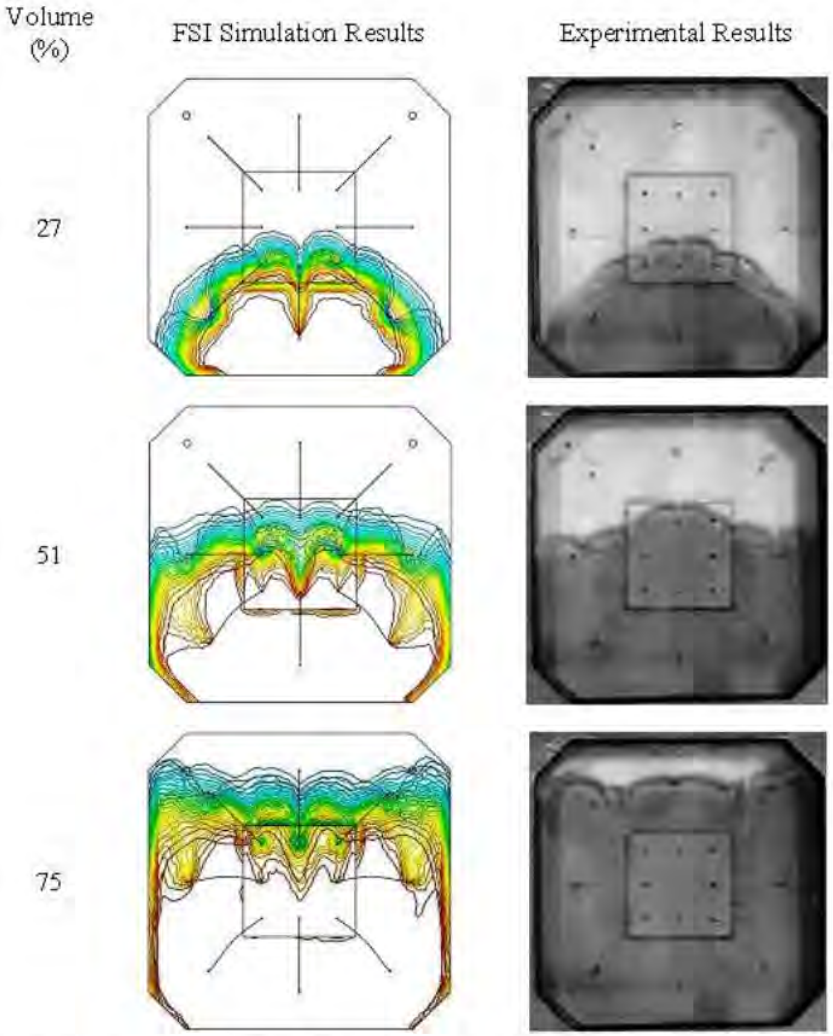

Figure 4.5 Comparison of FSI and experimental result of fluid flow front of single die of a scale-up eight-wire PBGA with centre inlet for Case 3.

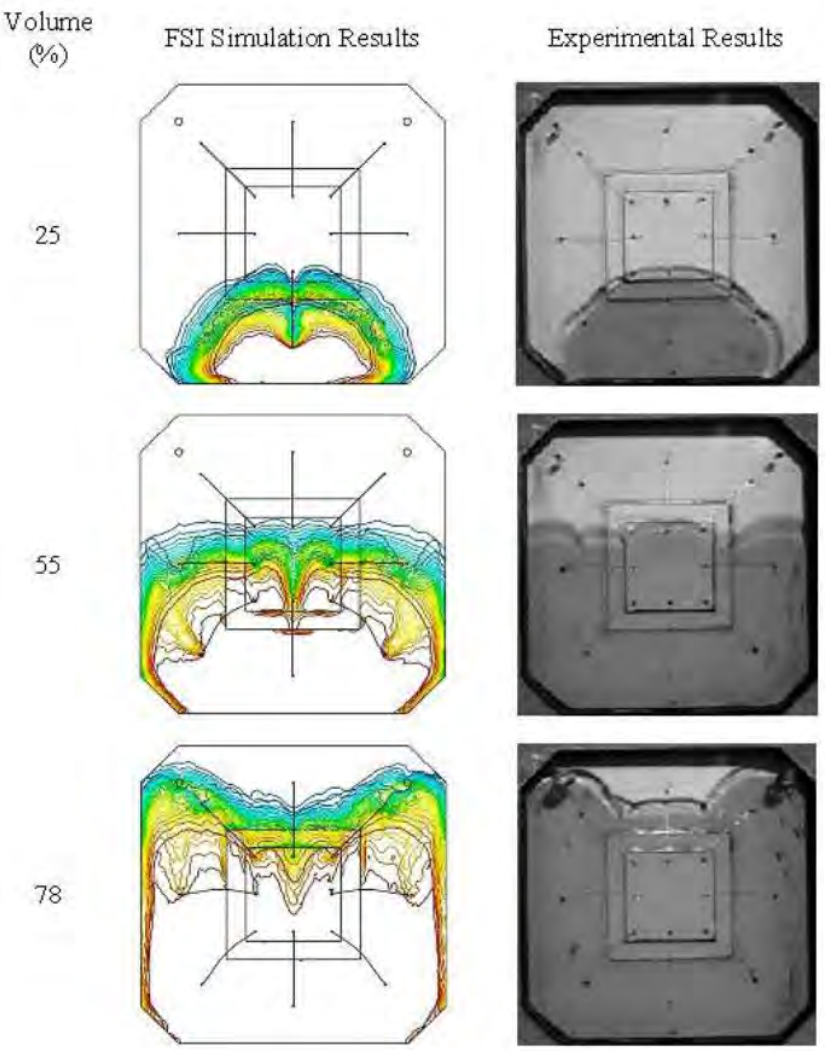

Figure 4.6 Comparison of FSI and experimental result of fluid flow front of stacked die of a scale-up eight-wire PBGA with centre inlet for Case 3.

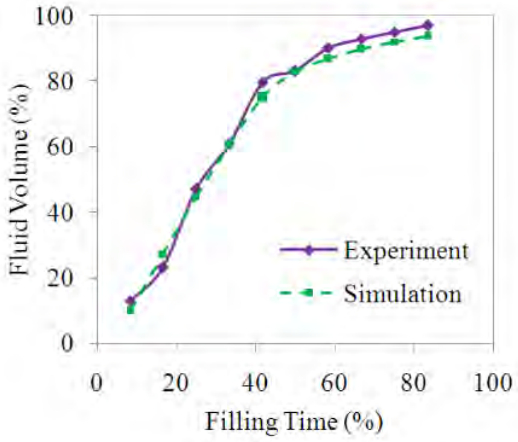

(a) Single die.

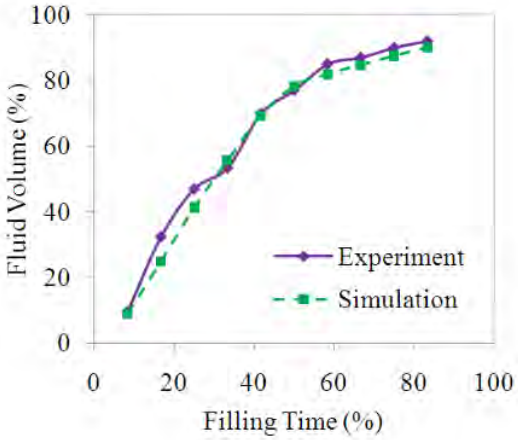

(b) Stacked die.

Figure 4.7 Percentage of filled volume versus percentage filling time of a scale-up eight-wire PBGA with centre inlet for Case 3: (a) Single die and (b) Stacked die.

4.2.2.2 Wire Sweep of Single Die and Stacked Die

Wire displacement phenomenon was observed when the test fluid flows around the wire region. Figure 4.8 shows the FSI simulation and the experimental results of the wire deformation, which has approximately the similar trends. In the FSI simulation the PBGA encapsulation was carried out in ideal condition. However, there may be an

unexpected uncertainty in the scaled-up experiment. Thus, this situation causes FSI result slight over-predict the wire sweep. The average discrepancy of maximum wire deformation was only 7.74 % for single die and 6.92 % for stacked die of a scale-up eight-wire PBGA with centre inlet. Therefore, the present modelling techniques yielded reliable predictions in handling the moulded packaging problem.

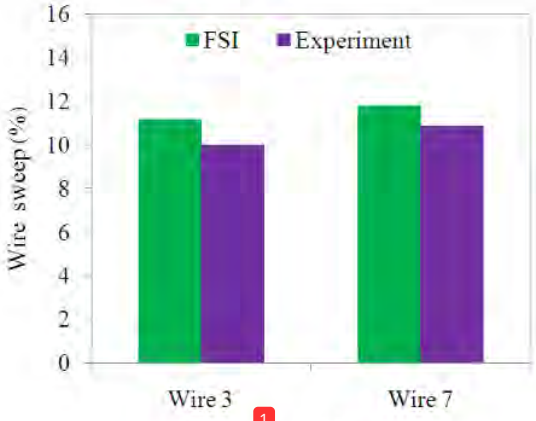

(a) Single die.

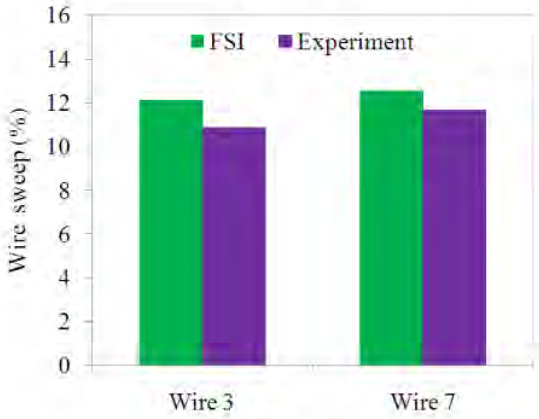

(b) Stacked die.

Figure 4.8 Percentage of wire sweep of wires 3 and 7of a scale-up eight-wire PBGA with centre inlet for Case 3: (a) Single die and (b) Stacked die.

In the last stage of filling process, as depicted in Figures 4.5 and 4.6, the dominant direction of deformation was found corresponds to the fluid flow, as clearly observed for wires 3 and wire 7 (Tay and Lee, 2002). Therefore, only these wires were focused in term of maximum displacement and stress distribution. Comparison of the

wire deformation for a single and a stacked die of wires 3 and 7 in Case 3 are shown in Figure 4.9.

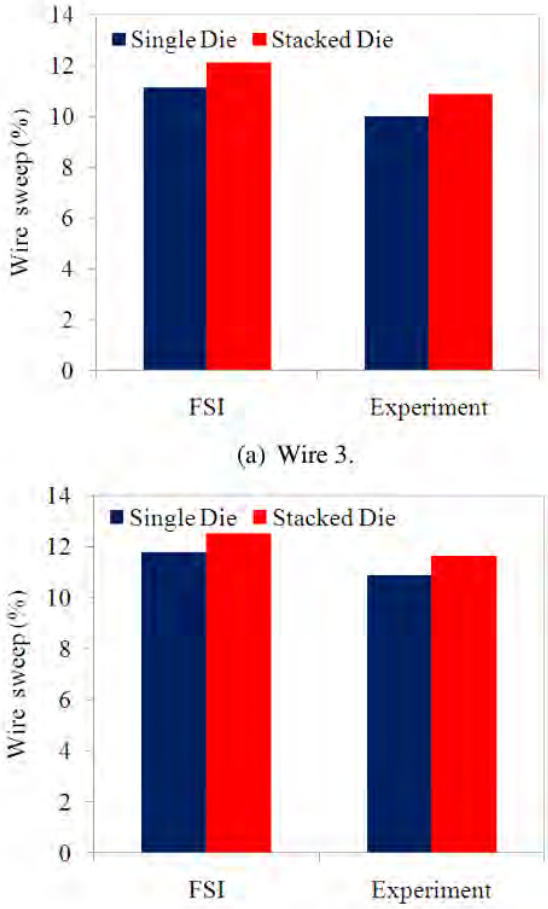

(a) Wire 3.

(b) Wire 7.

Figure 4.9 Comparison of wire sweep of single and stacked die of a scale-up eight-wire PBGA with centre inlet for Case 3: (a) Wire 3 and (b) Wire 7.

4.2.3 Scaled-up Eight-wire PBGA Encapsulation Process –Corner Inlet

4.2.3.1 Fluid Flow of Single Die and Stacked Die

Similarly, the experiments of encapsulation process were also conducted for a

scaled-up eight-wire PBGA prototype with corner inlet. The filling process of the viscous fluid into the cavity was recorded on top of the transparent mould. FSI simulation was also performed on the imitated package with single die and stacked die, as presented in Figure 3.12 of Chapter 3. The flow front advancement of the simulation results was compared with the experimental results. The results showed that flow front predictions from the simulation code had nearly the same profile with the experimental results at different filling volumes. Figure4.10and Figure 4.11shows the comparison of predicted FSI and experimental flow profiles for the scale-up eight-wire PBGA with corner-inlet encapsulation process from 21% to 78%and 19% to 80% of filling, which includes wire sweep for single die and stacked die respectively. The simulation result was substantiated by the experimental results by using the similar scaled-up eight-wire PBGA with corner inlet size, operating condition and material properties in the present numerical study. The predictions of flow front profiles and percentage of mould filling were well matching with the experimental results at all stage of filling. The percentage of filled volume at various stages versus percentage filling time for Case 3 was compared in Figure4.12; the maximum discrepancy was found about 6.0% and 4.97% for single die and stacked die respectively of a scale-up eight-wire PBGA with corner inlet. The predicted test fluid flow profiles showed a good agreement with the experimental results, at all percentage of filling stages.

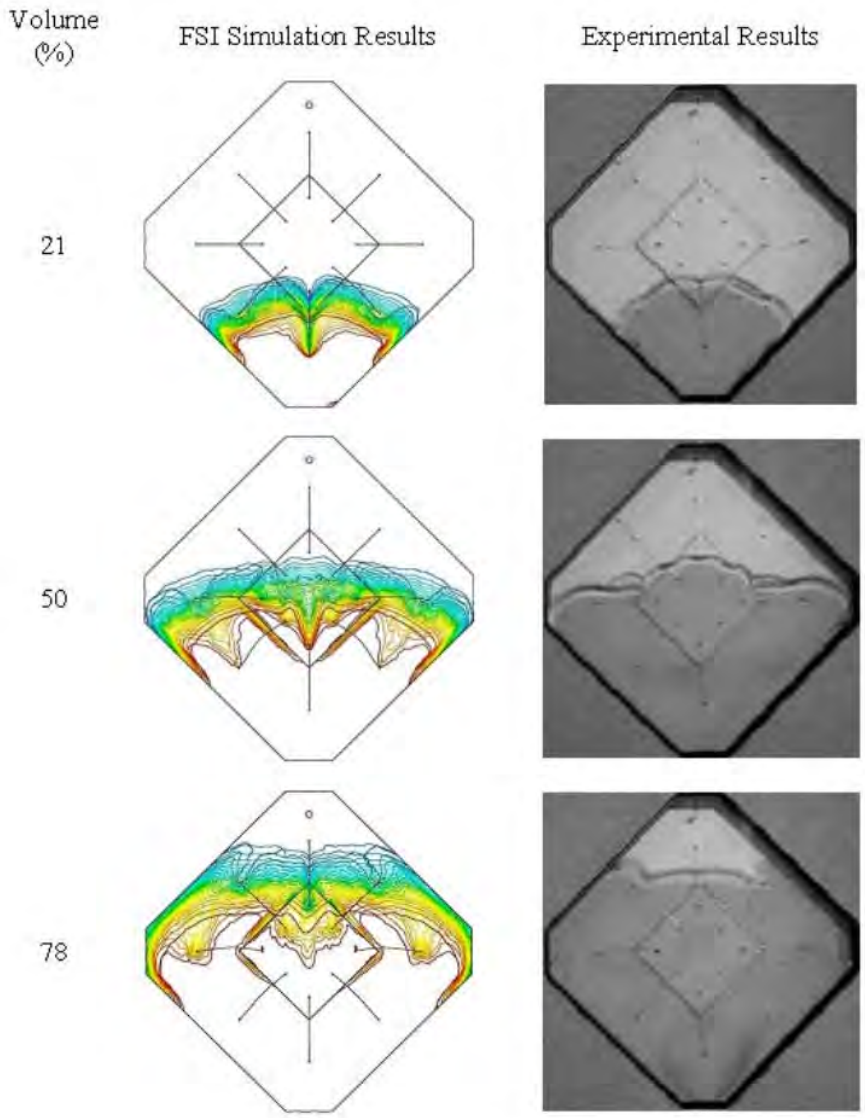

Figure 4.10 Comparison of FSI and experimental result of fluid flow front of single die of a scale-up eight-wire PBGA with corner inlet for Case 3.

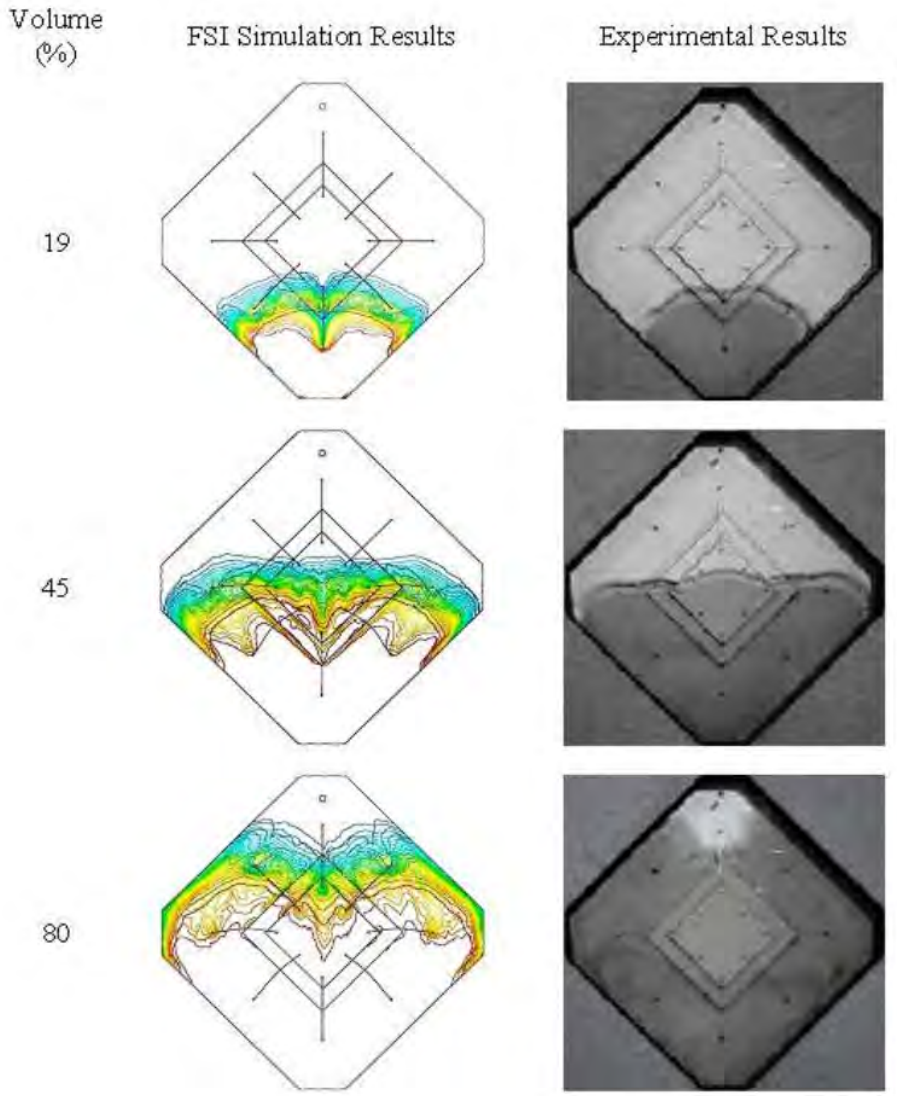

Figure 4.11 Comparison of FSI and experimental result of fluid flow front of stacked die of a scale-up eight-wire PBGA with corner inlet for Case 3.

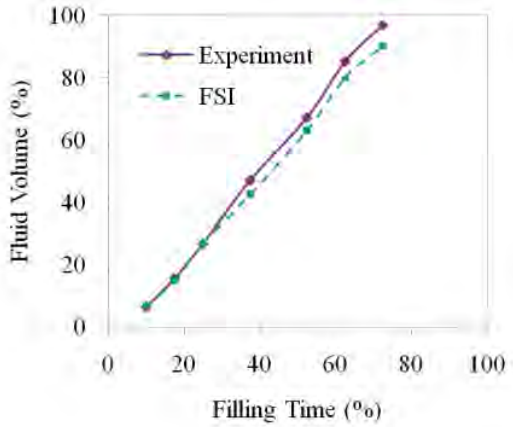

(a) Single die.

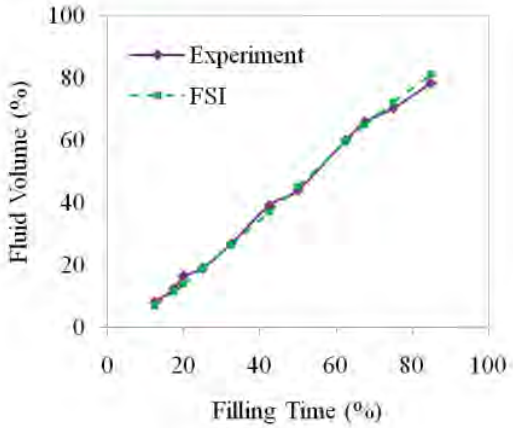

(b) Stacked die.

Figure 4.12 Percentage of filled volume versus filling time of a scale-up eight-wire PBGA with corner inlet for Case 3: (a) Single Die and (b) Stacked Die.

4.2.3.2 Wire Sweep of Single Die and Stacked Die

Wire displacement phenomenon was also observed when the test fluid flow around the wire region. Figure 4.13 shows FSI simulation and experimental results of wire deformation of a scale-up eight-wire PBGA with corner inlet, which was found approximately in identical trend. The average discrepancy of maximum wire deformation was only 4.95 % for single die and 8.45% for stacked die of a scaled-up

eight-wire PBGA with corner inlet. Therefore, the present modelling techniques yielded reliable predictions in handling moulded packaging problem.

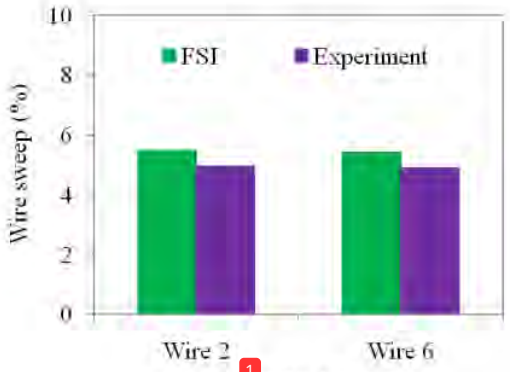

(a) Single die.

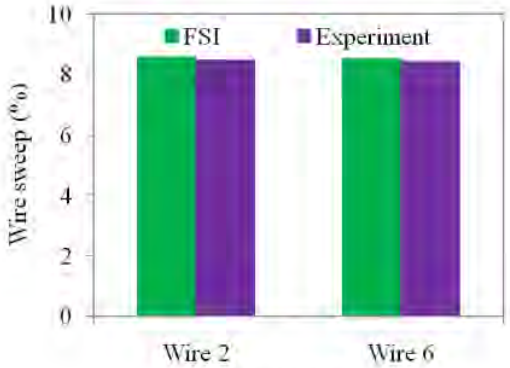

(b) Stacked die.

Figure 4.13 Percentage of wire sweep of wires 2 and 6 of a scale-up eight-wire PBGA with corner inlet for Case 3: (a) Single Die and (b) Stacked Die.

In the last stage of filling process as depicted Figure 4.10 and 4.11, the dominant direction of deformation was found corresponded to the fluid flow as clearly observed for wire 2 and wire 6 (Tay and Lee, 2002). Therefore, only these wires for a scale-up eight-wire PBGA with corner inlet were focused in term of maximum displacement and stress distribution. Comparison of wire deformation for single and stacked die of wire 2 and 6 in Case 3 is shown in Figure 4.14of a scale-up eight-wire PBGA with corner inlet respectively.

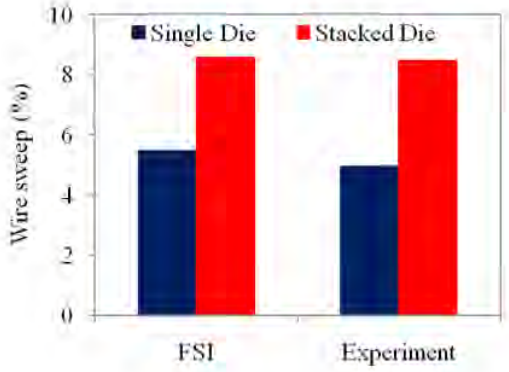

(a) Wire 2.

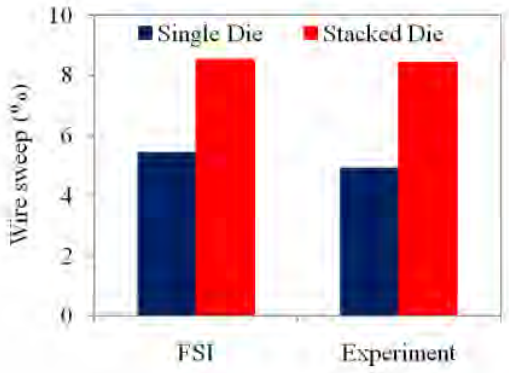

(b) Wire 6.

Figure 4.14 Comparison of wire sweep of single and stacked die of a scale-up eight-wire PBGA with corner inlet for Case 3: (a) Wire 2 and (b) Wire 6.

Based on the previous FSI simulations and experiment, it seemed that both the centre and corner inlet the die height could affect the sweep of the wires (Han et al., 2011b). Thus, the ratio of die height was introduced as an index to estimate the ratio effect on wire sweep behaviour. Figure 4.9 and Figure 4.14 demonstrated the wire sweep results in detail.

4.2.3.3 Measurement and Validation of Inlet Pressure

The pressure in the mould cavity and inlet gate was measured by using pressure sensor and pressure gauge, respectively. The pressure gauge was installed between asteel cylinder (barrel) and the inlet gate. The pressure in cavity was measured by using pressure sensor that was placed on the top centre and corner of the cavity. The position of both sensors is displayed in Figures 4.15 and 4.16, respectively.

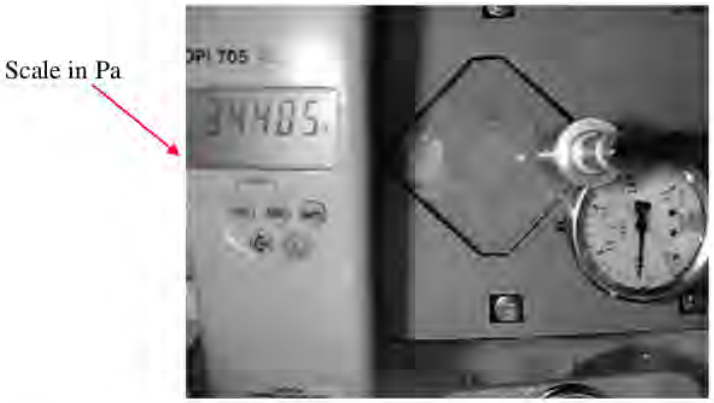

Figure 4.15 Pressure Validation on top corner position of pressure sensor at full filled.

Figure 4.15 shows the result when the mould cavity was fully filled. The pressure gauge displayed inlet pressure of 0.5 kg. f/cm^2. Then, the pressure value was used in the simulation. The simulation result of the maximum pressure inside cavity on the top corner was 34.7 kPa. However, the pressure sensor displayed 34.405 kPa as maximum pressure in the same position and the deviation for both results is only 0.85%.

At different positions of pressure sensor, the increase of inlet pressure is shown in Figure 4.16. In this experiment, the inlet pressure was measured by using a pressure gauge and it showed pressure of 1.3 kg.f/cm^2. Similarly, this value was used as an inlet pressure parameter in the simulation. The maximum pressure value on top centre of the cavity of simulation result is 114.3 kPa, and the pressure sensor displayed of the maximum pressure in the same position was obtained at 113.8 kPa, and the deviation for

both results is only 0.45%. Detailed of fluid flow pressure gauge calibration graphically is shown in Appendix F.

Figure 4.16 Pressure Validation on top centre position of pressure sensor at full filled.

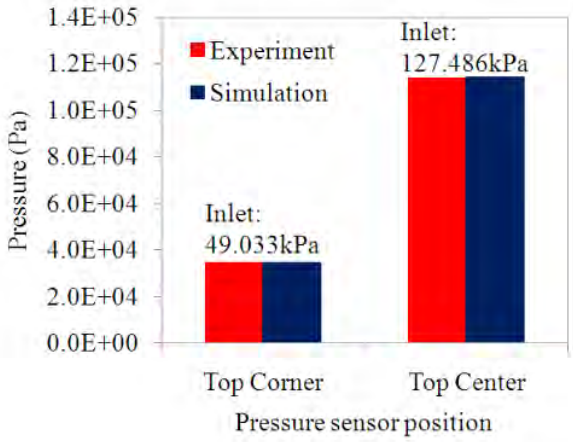

Figure 4.17 Comparison of pressure on top cavity for different pressure sensor position and inlet pressure.

The comparison of simulation and experimental results for the pressure at top of cavity for different positions and inlet pressure is described in Figure 4.17. The

comparison shows a good agreement; therefore, this has demonstrated that the measurement of inlet pressure was reasonable in the experimental and simulation studies of the current research.

4.2.4 Actual Size of PBGA Encapsulation Process

4.2.4.1 Fluid Flow Profiles

This simulation result was substantiated by the experimental results of Chen (1990) by using similar size of PBGA, operating condition, and material properties in the present study. The comparison of Case B simulation and experimental results for the melt-front profiles is shown in Figure4.18. The predictions of flow-front profiles and percentage of mould filling matched well with the experimental results in all stages of mould filling. The percentage of the filled volume at various stages versus percentage of time of Case B is compared in Figure 4.19.

UDFs allow the user to customize FLUENT, and it can significantly enhance its capabilities. Based on the observation (Figure4.18), the experiment and simulation of the melt-front closely match each other except on a number of voids observed in the experiment. The shape of the melt-front begins to diverge as it contacts the leading edge of the die. One melt-front is located directly above the dies, and the other on either side of the dies. The effect of dies is clearly shown in the melt fronts. The flow is retarded in this region due to flow resistance, causing the flows in other regions to advance. These results indicate that the simulation results are in good agreement with those of the experiments.

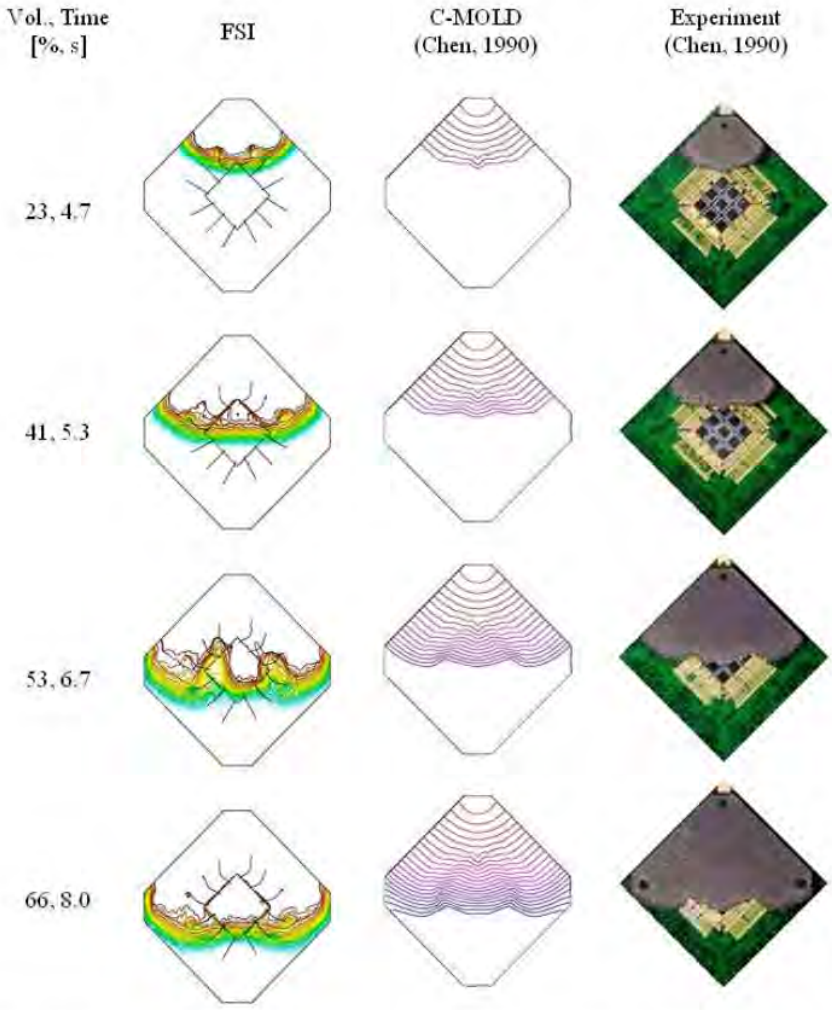

Figure4.18 Comparison between experimental (Chen, 1990), C-MOLD simulation (Chen, 1990) and simulation results of EMC Flow of Case B of actual size PBGA.

The experimental results of short shot at the different percentage of filled volume are compared with the simulation results. Figure4.18 demonstrates the melt-front advancement of actual size PBGA for both experimental and simulation results from 23, 41, 53 and 66 percentage of EMC filled volume. The experimental results were obtained by from previous work (Chen, 1990). At the initial stage, 23% of EMC filled the volume; a top view of the current simulation result shows an almost similar flow-front profile as in the experiment. This is obviously shown in 41% of the EMC filled volumes, the simulation results is well matched with the experimental result. For 53 and

66% of EMC filled volume, the flow-front on top of the die was concave, while the flow-front around was convex. The simulation results show that the flow-front on top of the die dropped behind the experimental results except in the middle of the die. The difference with the experimental result might be attributed to the geometric model. The results show the faster flow-front at the free region which has no silicon die presence. However, at 66% of filling stage, good agreement of the flow profile is found for both results. Overall, the FLUENT prediction gives the better agreement to experimental results.

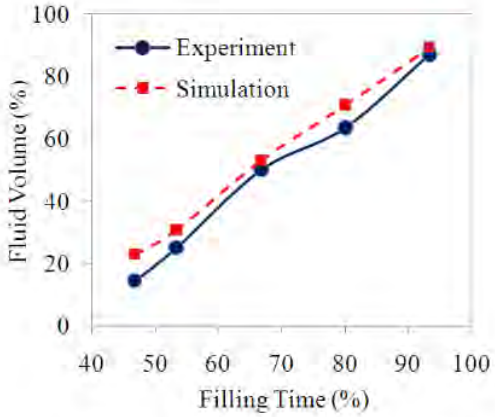

Figure4.19 Comparison between experimental (Chen, 1990) and simulation results of percentage EMC Volume of Case B of actual size PBGA.

Figure4.19 shows the percentage volume of the melt-fronts during the filling process. The approximate volume of the melt fronts is calculated from the experimental work (Chen, 1990) by taking the area of the melt-front. The results also show the comparison between experimental measurement and numerical simulation, which shows the good conformity.

4.2.4.2Wires Sweep

Figure 4.20 shows the comparison between experimental (Chen, 1990) and FSI simulation of the maximum and minimum wire sweep of Case B. From the comparison, the average discrepancy of the maximum and minimum of wire sweeps between the

present FSI predictions and experimental results (Chen, 1990) is approximately 8%. This demonstrates the realistic predictions of present FSI in solving the wire sweep during the encapsulation process.

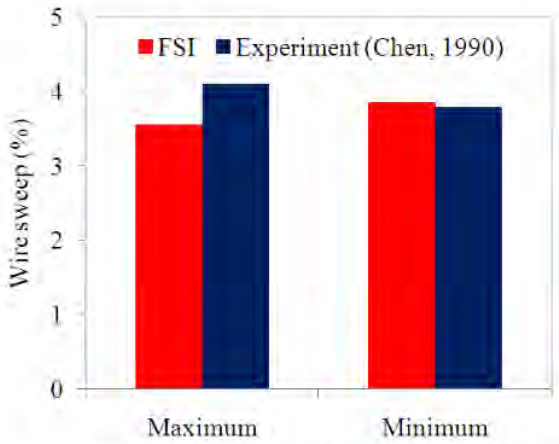

Figure4.20 Comparison between experimental (Chen, 1990) and FSI simulation of wire sweep of Case B of actual size PBGA.

4.3 Influence of Number of Mould Cavity Vents and Inlet Gate on Wire Sweep in Scale-up Four-wire PBGA Encapsulation

4.3.1 Melt Front Profile

First of all, the effect of number of vents on the melt front profile is visualized for various stages of filling, as presented in Figure 4.21. It is observed that the melt flow pattern exhibits almost similar trend in all the cases; this indicates that the melt front advancement is not significantly influenced by the number of vents.

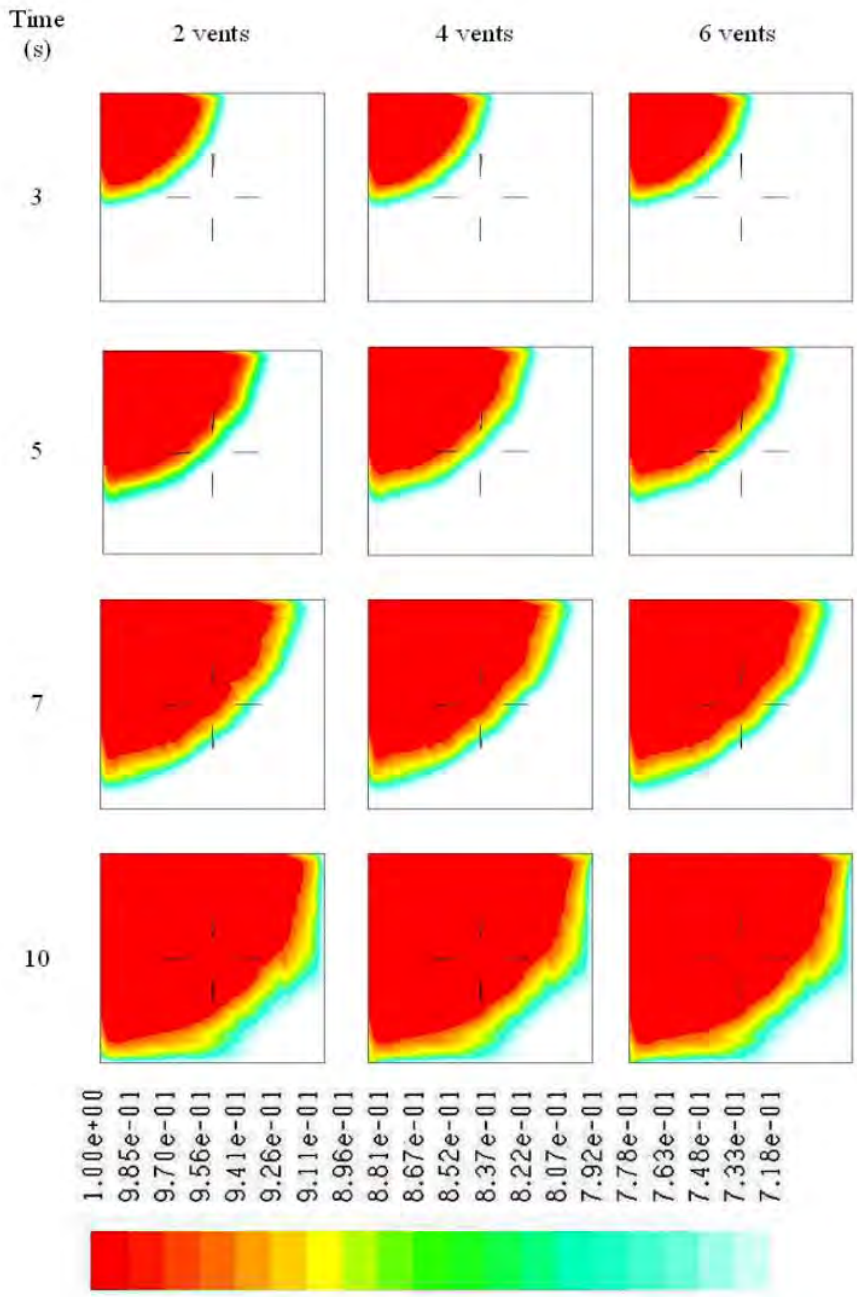

Figure 4.21 Melt front profiles of scale-up four-wire PBGA of three cases at various filling stages.

4.3.2 Wire Sweep

Figure 4.22 illustrates the phenomenon of wire deformation, predicted by ABAQUS. The deformation has been calculated at Point A (Figure 4.23). The wire sweep of wire 1 and wire 4 for all cases are shown in Table 4.5. Figure4.24 shows the wire deformation in x, y and z directions for all wires of two-outlet vent arrangement. It can be clearly understood that the wires deformed to the horizontal (x) and vertical (y) axes (Yao, et al., 2005). For the wire 1, the deformation is the tendency in the z-direction and wire 2 in the x-direction respectively. The comparison of deformation magnitudes of wires 1 to 4 are shown in Figure 4.25. It is found that wire 4 has the highest deformation in the x-direction (Figure 4.23(a)). However, wire 1 has larger deformation in y and z directions as shown Figures 4.23(b-c). These deformations are due to the positioning of wire and the directions of wire bond span. In Figure 4.25, wires 1 and 4 show, higher deformation compared to wires 2 and 3. This is due to their orientation and the direction of EMC flow during the encapsulation process. The magnitude of wire deformation for each wire is also estimated and plotted as shown in Figure4.26. It is clear that the wires 1 and 4 are significantly deformed compared to wires 2 and 3, in all cases. At the same time, it is worth noting that, as the number of vents increases, the sweep tendency decreases, presumably due the reduced pressure force inside the cavity.

Table 4.5 Wire deformation predicted by ABAQUS of different outlet vent

Number of vents/No. of wire	Wire sweep (mm)	
	Wire 1	Wire 4
2 vents	0.65	0.60
4 vents	0.49	0.57
6 vents	0.37	0.55
Uncertainty deformation on real wire sweep in industry (Jong et al., 2005)	0.80	

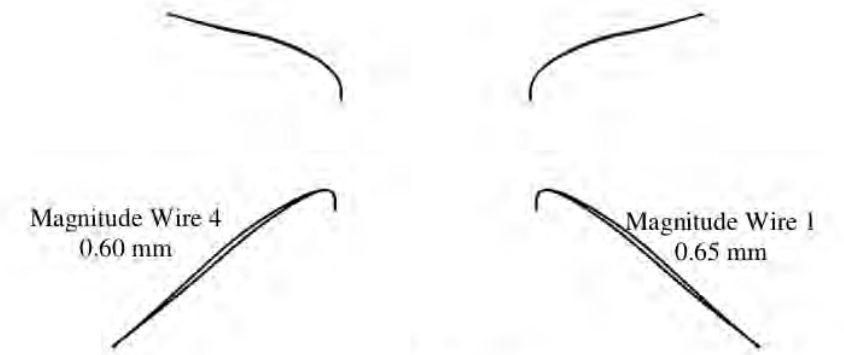

a) 2 vents

Figure 4.22 Illustration of wire sweep predicted by ABAQUS of scale-up four-wire PBGA: (a) 2 vents

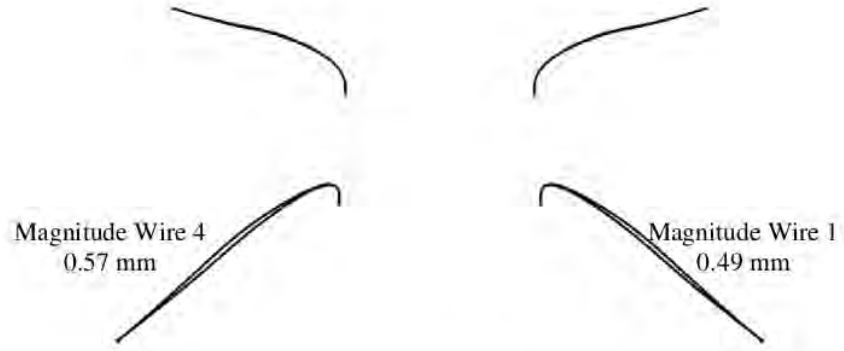

b) 4 vents

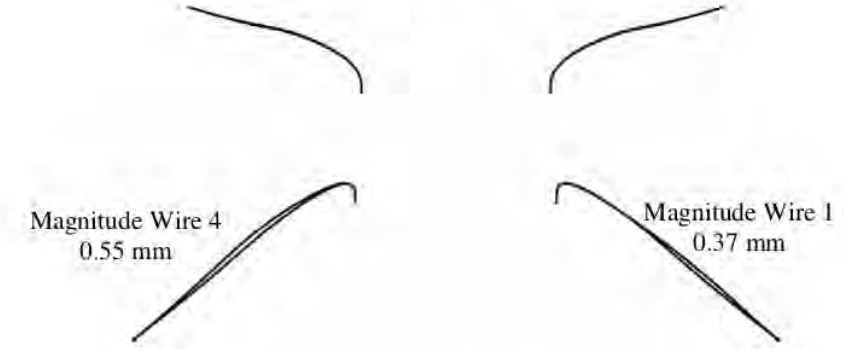

c) 6 vents

Figure 4.22 Illustration of wire sweep predicted by ABAQUS of scale-up four-wire PBGA: (b) 4 vents and (c) 6 vents.

Figure 4.23 Measurement of wire deformation at Point A.

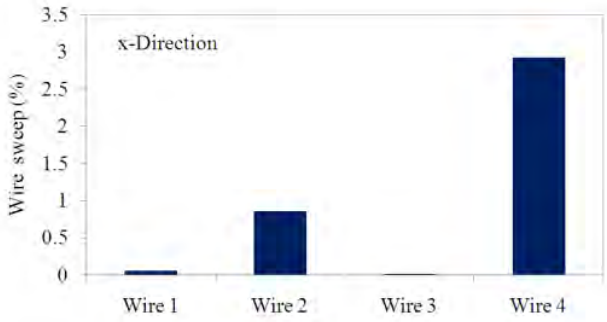

(a) x-direction.

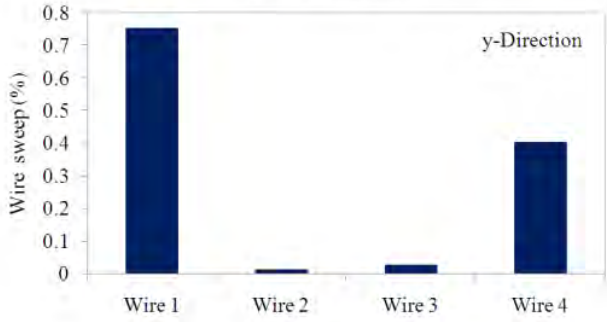

(b) y-direction.

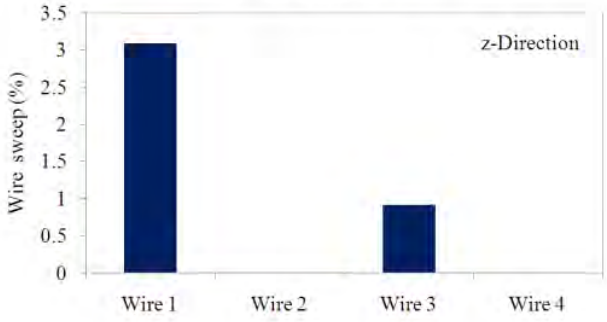

(c) z-direction.

Figure 4.24Comparison of four wire deformation of two outlet vents arrangement at Point A: (a) x-direction, (b) y-direction and (c) z-direction.

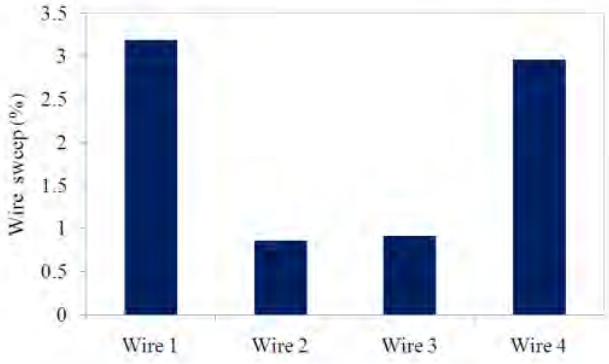

Figure 4.25 Comparison of wire sweep for all wires of two outlet vents arrangement at Point A.

Figure4.26shows the effect of the number of outlet vents on the wire deformation. The results show that the deformation of all wires is lower for six outlet vents compared to two outlet vents arrangements. The results illustrated the drag force induced by the EMC flow is lower for the case of six outlet vents arrangement. The lower the drag force will provide less stress concentration on the wire and will reduce the tension on the wire. Thus, number of outlet vents does influence on the wire deformation during the encapsulation process.

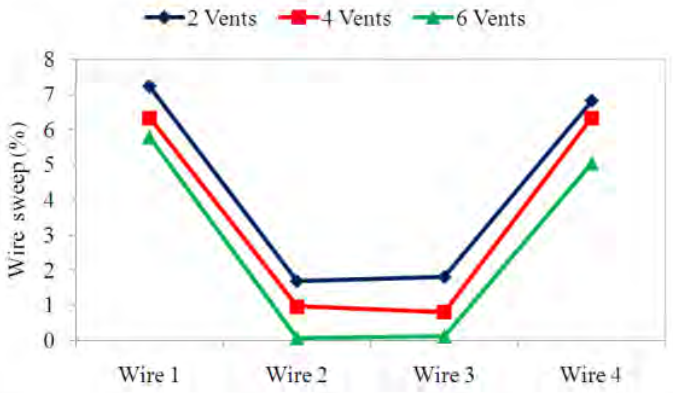

Figure 4.26 Comparison of deformation of wires 1-4 for all the cases of scale-up four-wire PBGA.

The results also shown that the wires 2 and 3 have lower deformation compared to wires 1 and 2 since the locations of wires 2 and 3 are behind the silicon die. The wires 1 and 4 are located near to the inlet gate have experienced higher induced drag force, thus, both wire has higher stress concentration. The phenomena will help the engineers to decide the appropriate location for the wire in order to avoid the wire overlap that might cause a short circuit or failure during the encapsulation process.

4.3.3 Pressure Distribution

Figure 4.27 shows the locations of pressure measurement of each wire during the encapsulation process, and Figure 4.28 shows the corresponding plots as a function of position point. The increase of pressure is due to the presence of EMC. As can be seen, pressure at Point 1 is the maximum due to the impact of incoming flow, gradually reduces with flow advancement as evident from the medium pressures at the identical locations Point 2 and Point 4, and the location Point 3 (near the exit) which shows the minimum pressure. The pressure directly influences the wire displacement and drag force acting on the wire structure, during the filling process. Thus, wires situated at high pressure location are expected to deform more compared to those at the low pressure region, as is clear from the increased sweep of wires 1 and 4 located near to Point 1. It is also worth noting from Figure4.28 that, as the number of vents increases, the pressure decreases, leading to possible reduction in wire sweep.

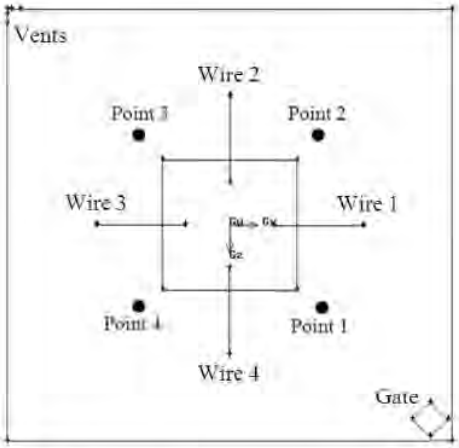

Figure 4.27 Locations of pressure measurement of scale-up four-wire PBGA.

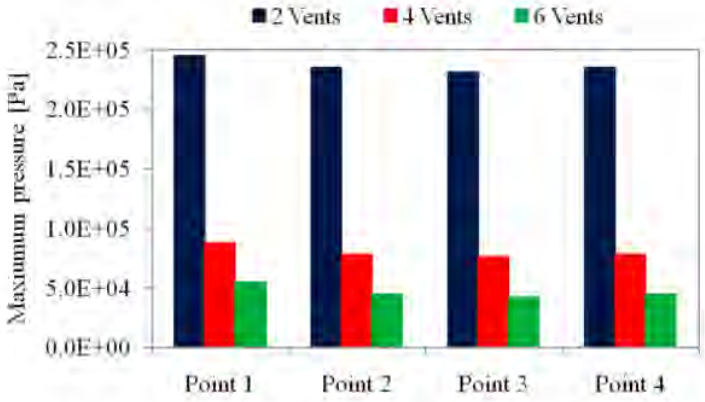

Figure 4.28 Comparison of maximum pressure at locations 1-4 for the three cases of scale-up four-wire PBGA.

4.3.4 Von-Mises Stress Distribution

The consolidated data of maximum Von-Mises stress developed in each wire for the three cases is given in Table 4.5. It is clear that wires 1 and 4 are subjected to maximum stress, owing to the influence of higher pressure force on them. However, the stress decreases significantly with the increase in the number of vents. Detailed view of stress distribution for wires 1 and 4, in maximum displacement is shown in Figure4.29a, 4.29b, 4.30a and 4.30b respectively, which demonstrates that the highest stress is around un-deformed fixed boundary, especially near to the wire bonds. This means the sweep displacement of wire is dominated by the twisting moment instead of the bending moment (Kung et al., 2006). For clarity, only the two bond regions where stress is significant, are shown, that too only for the highly deformed wires (1 and 4). From Table 4.5, it is also worth noting that the maximum stresses in the case of 2 vents are alarmingly above the ultimate stress of the wire material (gold), which is 2.2×10^8 Pa (Liuet al., (2004b), and this failure threat is significantly eliminated by increasing the number of vents. Increase in number of vent reduces the pressure within the package (Figure 4.28), which also decrease the fluid induced forces on the wire. Thus the von-Mises stress subjected to the wire also decreases.

Table 4.6 Maximum Von-Mises stress in each wire for different cases during encapsulation process of scale-up four-wire PBGA.

Wire	Maximum Von-Mises stress (Pa)		
	2 vents	4 vents	6 vents
1	3.748×10^8	1.522×10^8	1.289×10^8
2	3.091×10^8	3.988×10^7	2.696×10^7
3	2.696×10^8	4.495×10^7	2.463×10^7
4	3.499×10^8	1.678×10^8	1.518×10^8

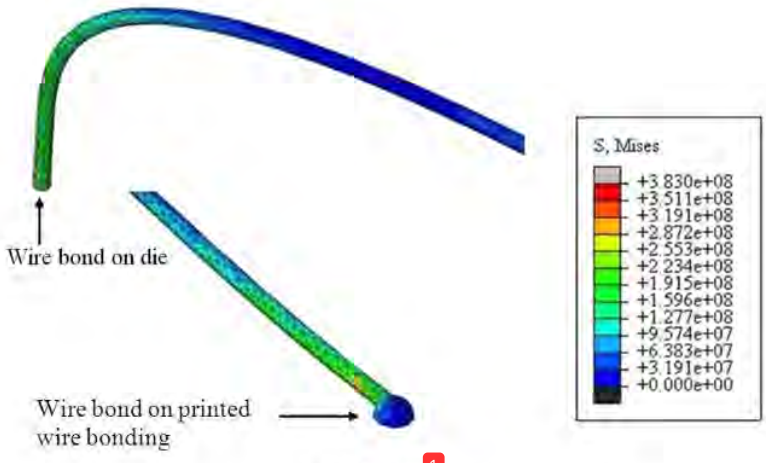

(a) Wire 1-2 vents.

Figure 4.29a Detailed view of von-Mises stress distribution for wire 1for various numbers of vents of scale-up four-wire PBGA: (a) Wire 1-2 vents

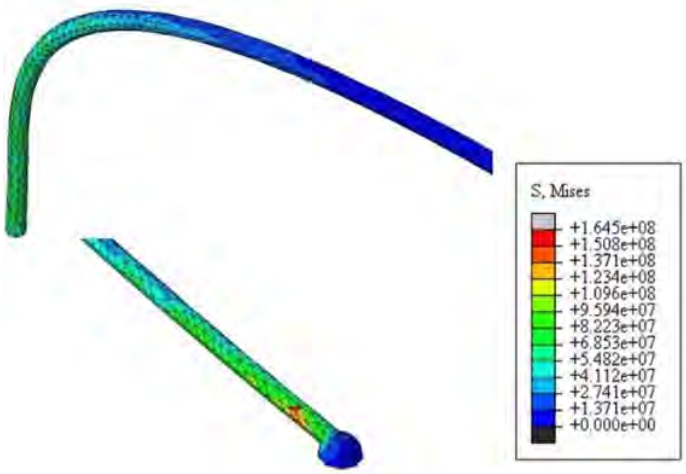

(b) Wire 1-4 vents.

Figure 4.29a Detailed view of von-Mises stress distribution for wire 1for various numbers of vents of scale-up four-wire PBGA: (b) Wire 1-4 vents.

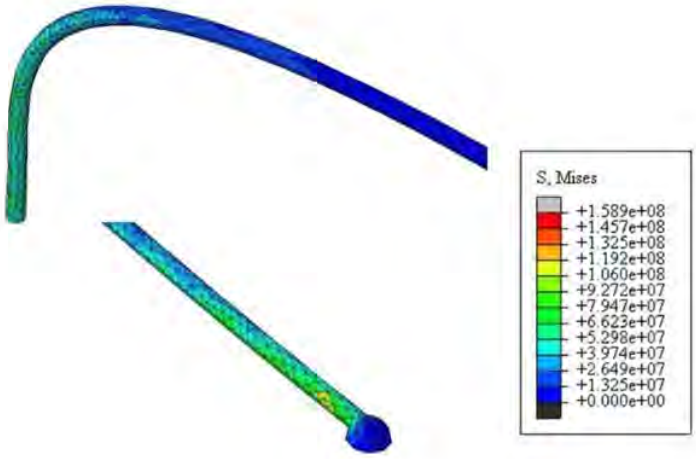

(c)Wire 1-6 vents.

Figure 4.29bDetailed view of von-Mises stress distribution for wire 1for various numbers of vents of scale-up four-wire PBGA: (c) Wire 1-6 vents (continued).

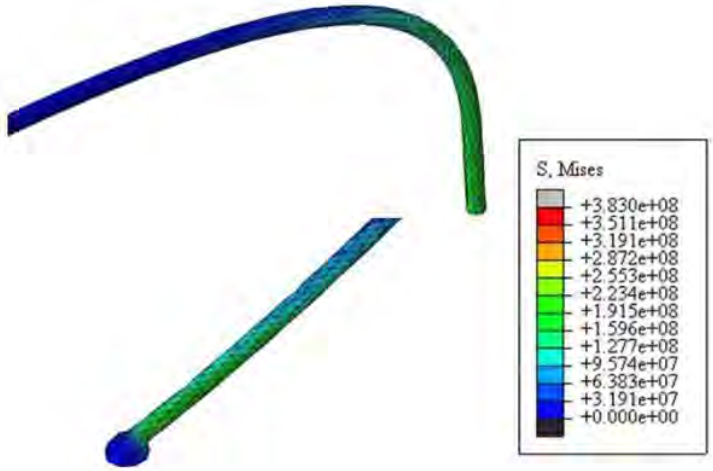

(a) Wire 4-2 vents.

Figure 4.30a Detailed view of von-Mises stress distribution for wire 4 for various numbers of vents of scale-up four-wire PBGA: (a) Wire 4-2 vents

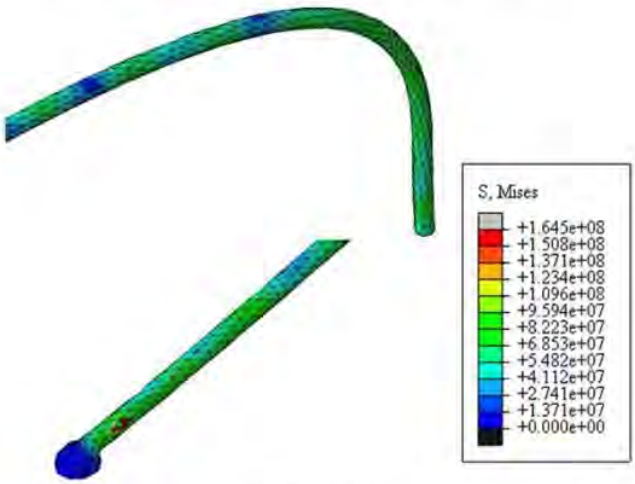

(b) Wire 4-4 vents.

Figure 4.30b Detailed view of von-Mises stress distribution for wire 4 for various numbers of vents of scale-up four-wire PBGA: (b) Wire 4-4 vents

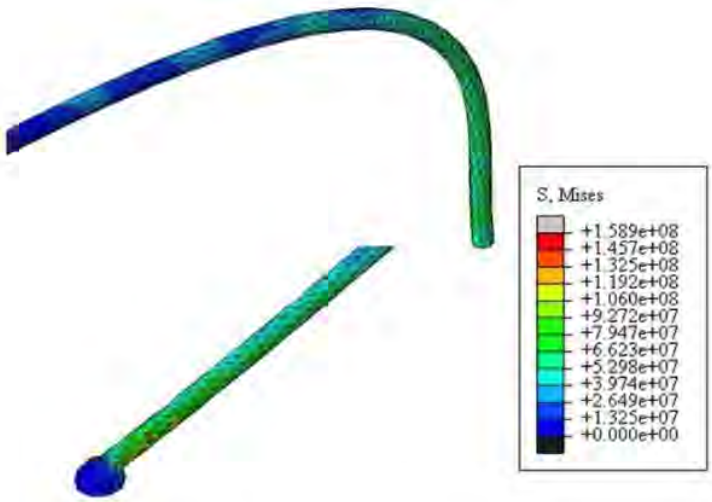

(c)Wire 4-6 vents.

Figure 4.30bDetailed view of von-Mises stress distribution for wire 4 for various numbers of vents of scale-up four-wire PBGA: (c) Wire 4-6 vents (continued).

4.3.5 Void Occurrence

It has been shown in the previous sections that the increasing in number of vents could reduce the wire sweep. However, it would be interesting to study the limiting factors of increasing the vents for a given mould cavity and number of gate. Thus in the present study, an attempt is also made to observe how the number of vents influence the development of voids during the encapsulation process. Figure4.31 shows the melt front profiles showing the void locations for various cases, and Figure4.32 shows the graphical comparison of the respective percentages of voids. It is observed that, as the number of vents increases, the void formation increases significantly; this apparently imposes restriction on the number of vents. However, as is clear from Figure4.31, since the voids are situated near the walls, and the wire zone is not affected, the increased number of vents does not presumably pose significant threat on the quality of mould filling.

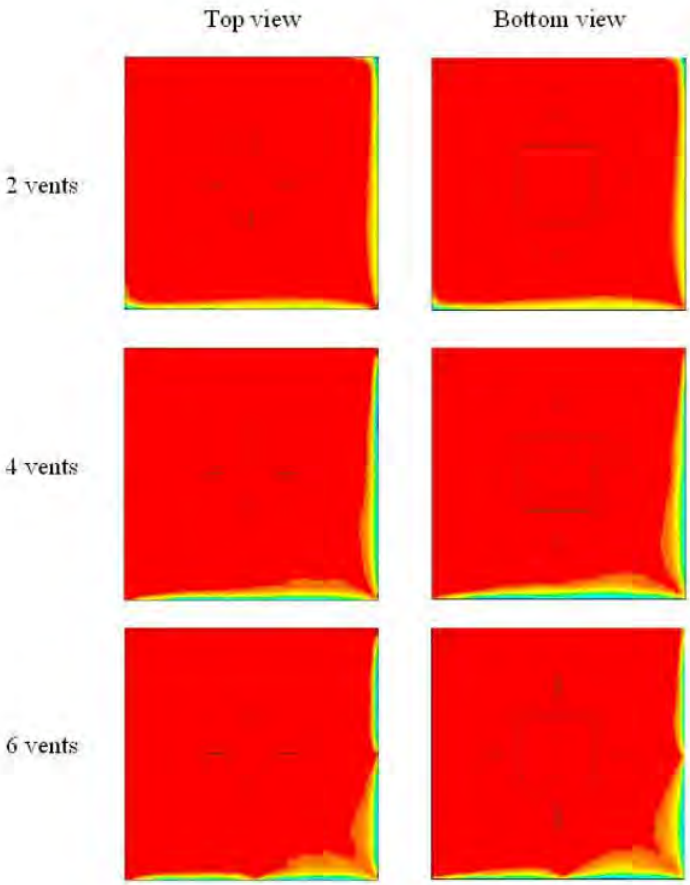

Figure 4.31Mould filling contours for various cases after 15s, showing voids of scale-up four-wire PBGA.

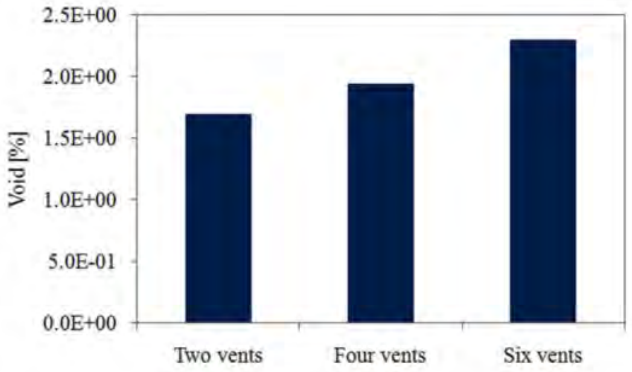

Figure 4.32 Voids percentage in various cases after 15sof scale-up four-wire PBGA.

4.3.6 Conversion of the compound

Degree of conversion reflects the cure development of the moulding compound with time and it can be quite straight forward to follow if the cure process occurred in static mode.

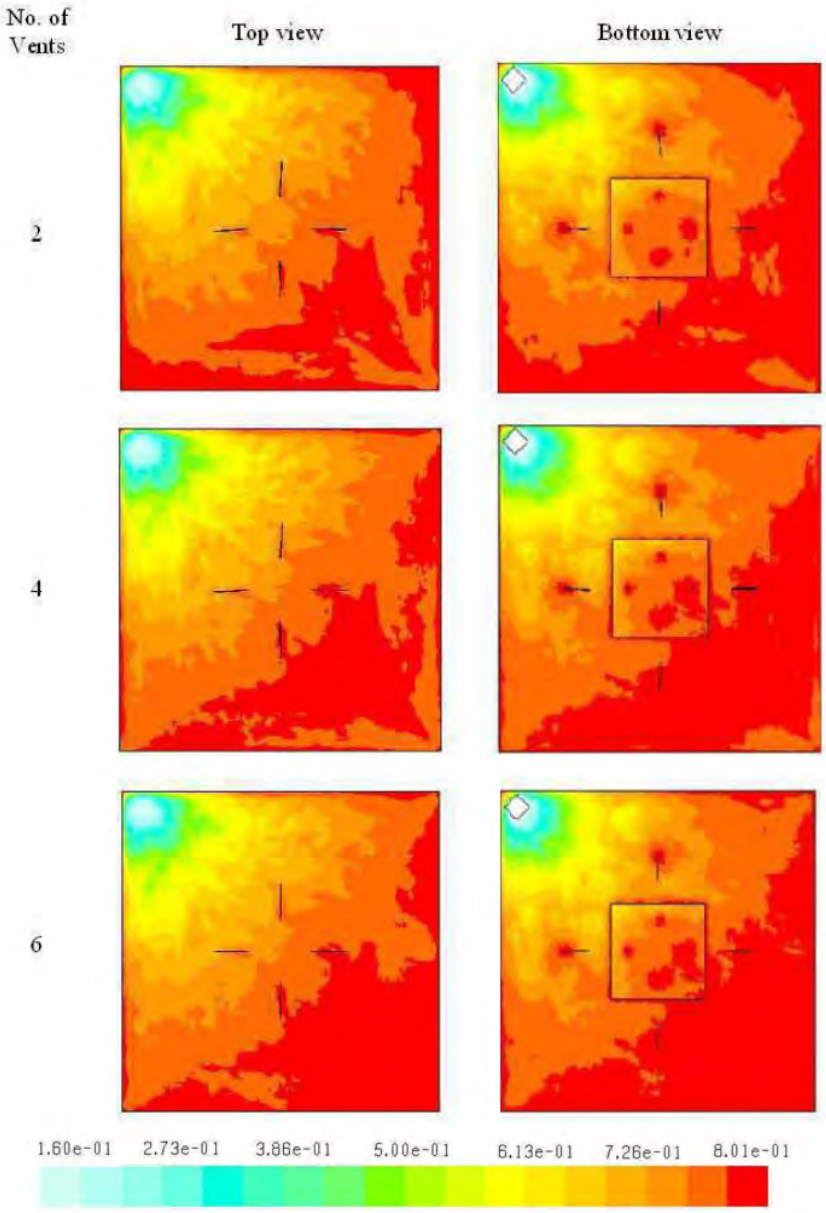

Figure 4.33 Predicted conversion of the mould compound at top and bottom view

However, during dynamic mould filling process, other factors such filling pressure, temperature change due to non-Newtonian flow behaviour of the moulding packages for different number of vents of scale-up four-wire PBGA.

Figure 4.33 Predicted conversion of the mould compound at top and bottom view of the compound and shear rate variation within the mould cavity make the prediction of conversion level to be quite difficult. The top and bottom view of conversion distribution of the packages is presented in Figure 4.33 for different number of outlet vents. It is observed that the conversion level is quite low at the cavity inlet gate and outlet vents, but higher around the package region. The predicted conversion of the mould compound at 15 s is 8.01e-01 for 2, 4, and 6 vents. This phenomenon is reasonable with the vents number variation. This is predictable since the combination of the Castro-Macosko viscosity model and the Kamal cure kinetics model have taken into account of two important factors, i.e. the dependence viscosity toward shear rate and dependence of conversion level (which also affects the viscosity of the moulding compound) toward temperature.

Mould filling of thermoset polymers consists of two competing events which usually occur simultaneously during the process. These events are: a) reduction of viscosity with shear rate due to non-Newtonian behaviour of the polymer fluid and b) increase in viscosity as the results of chemical reaction that occur during thermoset curing (Ardebiri and Pecht, 2009). The success of the mould filling process for thermoset polymer relies greatly on the compromise of both events and their dependence on process temperature. The filling must be as fast as possible to take full advantage of the first event; but when it comes to intricate and restricted moulding process such as IC packages encapsulations, the filling process would not be as smooth as anticipated, due to the second event. This is quite true in the vicinity of the package region where it is estimated that the melt front velocity is slower enough to cause initiation of the second event. In addition, the slower the fluid flows in these regions; more contact time is available for the compound to absorb heat from the mould surfaces which enhances the degree of conversion as observed in the simulation results.

4.3.7 Melt Front Profile and Wire Sweep Behaviour of Different inlet Gate of Scale-up four-wire PBGA

Increasing of the number of inlet gates resulted in the reducing of the wire sweep and minimizing the filling time. Figure 4.34a and 4.34b shows the melt front profile of different inlet gates to the wire sweep in the cavity. Wire sweep of each cases are presented in Figure 4.35a and 4.35b.As reported by Khor et al. (2011), increased of inlet gate had raised the pressure distribution within the cavity during encapsulation process. However, they only focused on the fluid flow analysis. As the extension from their work, the multi-inlet gate was considered in the current study by focusing on the wire sweep phenomenon.

As a result, from the simulation analysis, it was found that the increased in number of inlet gates raised the wire sweep during the encapsulation process. The wire that normal to the flow direction was found has higher deformation. This is because the wire experienced higher drag force when interaction occurs. Besides, the knit lines were form because of the interaction between two separating flows, which may increase the tendency of void formation in the package. More inlet gates yielded shorter filling time, but caused higher wire deformation. Therefore, the design of the IC package is significant to eliminate void and wire sweep during the encapsulation process.

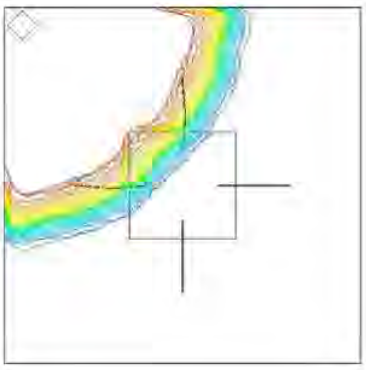

(a) 1 inlet gate.

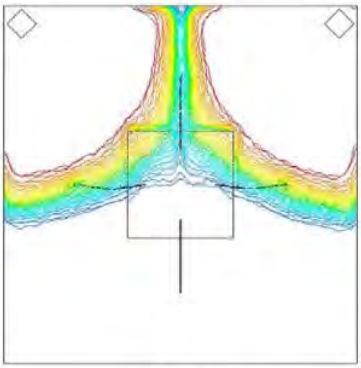

(c) 2 inlet gates.

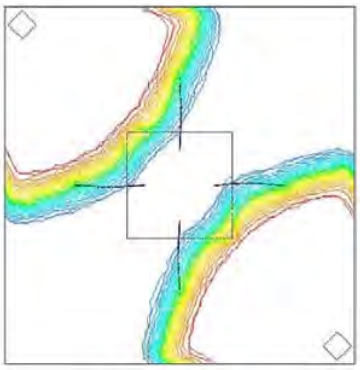

(d) 2 inlet gates diagonal.

Figure 4.34a Melt front and wire sweep profile of scale-up four-wire PBGA: (a) 1 inlet gate, (b) 2 inlet gates and (c) 2 inlet gates diagonal.

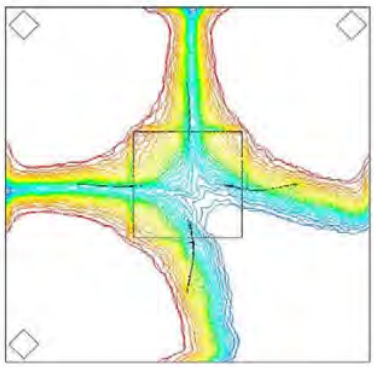

(d)3 inlet gates.

Figure 4.34bMelt front and wire sweepprofile of scale-up four-wire PBGA: (d) 3 inlet gates (continued).

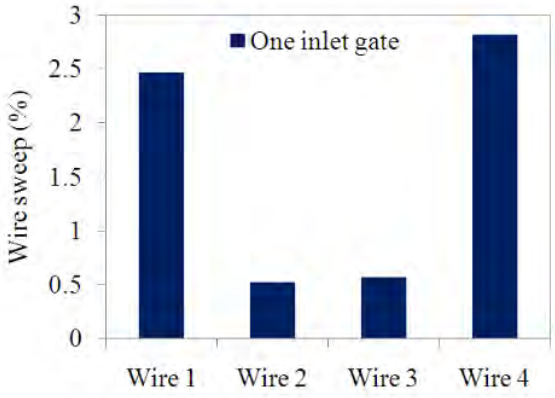

(a) 1 inlet gate.

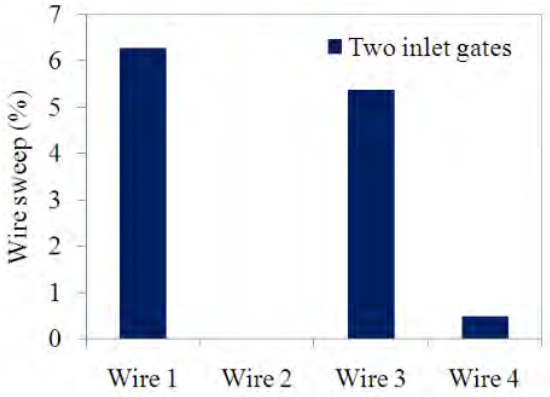

(b) 2 inlet gates.

Figure 4.35a Magnitude of deformation each wire of scale-up four-wire PBGA:

(a) 1 inlet gate and (b) 2 inlet gates.

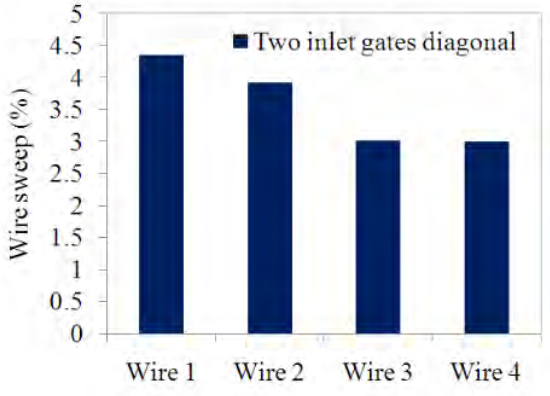

(b) 2 inlet gates diagonal.

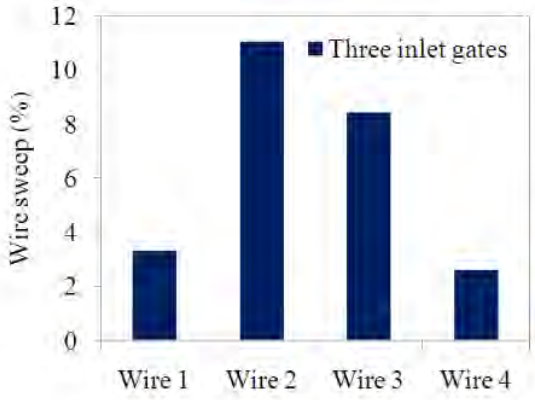

(d)3 inlet gates

Figure 4.35b Magnitude of deformation each wire of scale-up four-wire PBGA: (c) 2 inlet gates diagonal and (d) 3 inlet gates (continued).

4.4 Wire Sweep Considering Stacked Die Effect of Scale-up eight-wire PBGA Encapsulation Process-Centre Inlet

4.4.1 Analysis of Inlet Pressure Effect in Packaging of Single and Stacked Die

During the wire deformation, largest wire sweep occurred at the middle of the silicon die (Wu et al. 1998). This was because of wire bonds (at the middle region) that positioned normal to the flow direction of the moulding compound. During the encapsulation process, wire at this region experienced higher lateral flow load, which resulted in large deformation of about 14.5% of wire sweep during 27s of filling time (Wu et al. 1998). In a typical scaled-up eight-wire PBGA with inlet centre, tension on the excess wire resulted from sweep, because it offered small resistance to the traverse forces imposed by the moulding compound. However, with the lateral looping approach, the excess wire present in the lateral direction provided the required tension (Brunner et al. 2004). Lower deformation was found on lateral loop of wire shape (3.3 %) when compared to the standard loop (6%) using moulding compound EME-G760. Kunget al. (2006) had demonstrated that deformation of wire was dominated by the twisting moment instead of the bending moment. The wire loop shape has significant effect on the deformation in IC encapsulation. Yao et al. (2003) found that the normal

shape of the wire loop possessed weak bend resistance at the middle region of wires, which resulted in more deformations when compared to M shape.

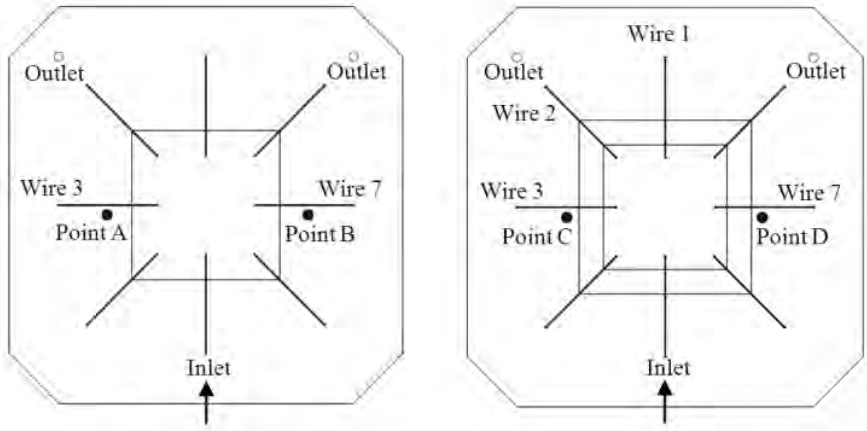

(a) Single die. (b) Stacked die.

Figure 4.36 Points position of pressure measurement on maximum wire deformation of scale-up eight-wire PBGA with centre inlet: (a) Single die and (b) Stacked die.

As mentioned inSection4.2.2.2, the wires 3 and 7, which positioned at middle region of package, experienced the dominant deformations in the encapsulation process. Therefore, only the pressure around wire 3 and wire 7 are evaluated for the comparison.Figure4.36 shows the locations of pressure measurement at Point A and Point B for single die package and Point C and Point D for stacked die package during the encapsulation process.Figure4.37a and 4.37b shows the corresponding bar chart of pressure acting of each point for all cases for single and stacked die packages. The different inlet pressures of single and stacked die packages for all cases of wires 3 and 7 were shown in Figure 4.38a and 4.38b and percentage of filled volume versus filling time at different cases were plotted in Figure 4.39.The increase of inlet pressure is due to the presence of test fluid. As can be seen, pressure at Point A and Pont B (single die package) and Point C and Point D (stacked die package) is high due to the impact of continuous incoming flow.

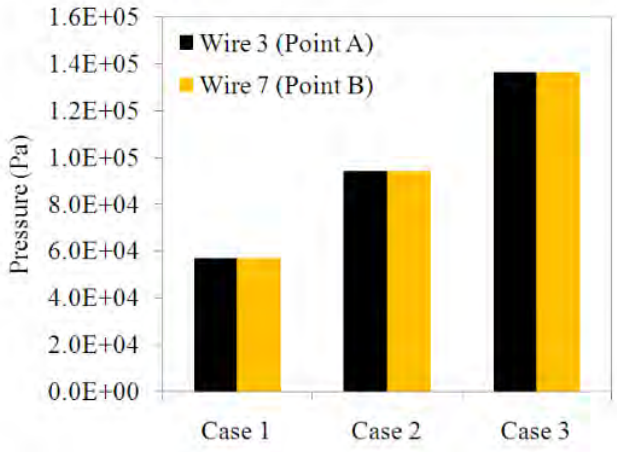

(a) Single die.

Figure 4.37a Pressure acting on wires 3 and 7 for all cases in single and stacked die packages of scale-up eight-wire PBGA with centre inlet: (a) Single die.

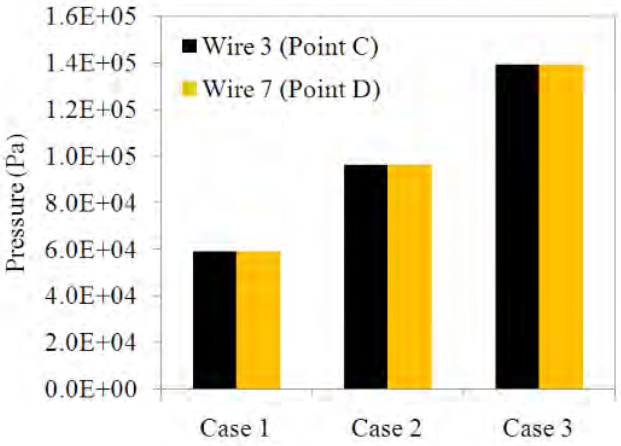

(c) Stacked die.

Figure 4.37bPressure acting on wires 3 and 7 for all cases in single and stacked die packages of scale-up eight-wire PBGA with centre inlet: (b) Stacked die (continued).

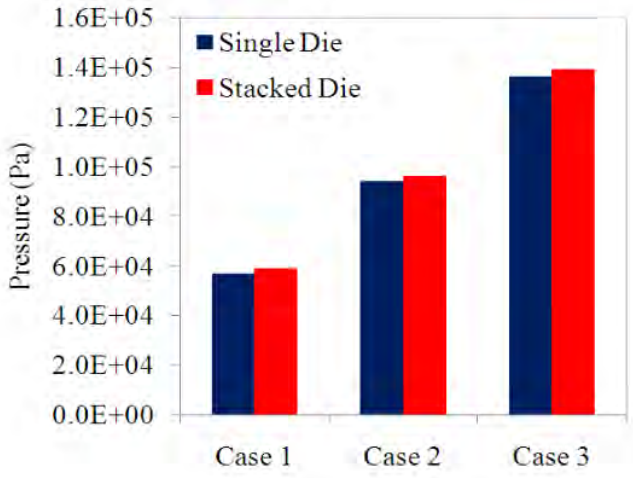

(a) Wire 3.

Figure 4.38a Different pressures at single and stacked die packages for all cases of wires 3 and 7 of scale-up eight-wire PBGA with centre inlet: (a) Wire 3.

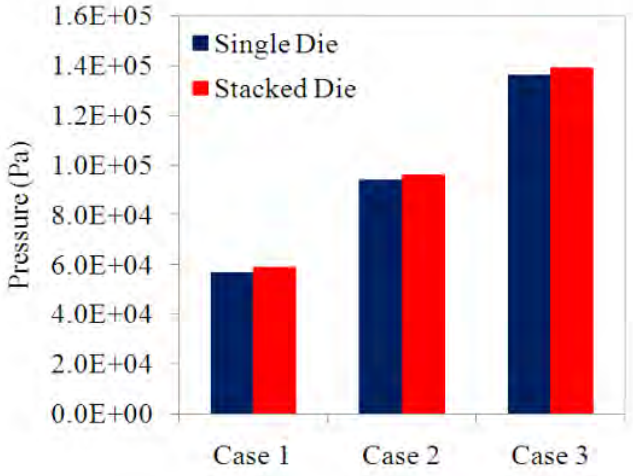

(b) Wire 7.

Figure 4.38b Different pressures at single and stacked die packages for all cases of wires 3 and 7 of scale-up eight-wire PBGA with centre inlet: (b) Wire 7 (continued).

The pressure directly influences the wire displacement and the drag force that acting on the wire structure, during the filling process (Figure 4.40). Thus, the wires which experienced higher pressure are expected to cause higher deformation compared to those at the low pressure. At the same time, it is worth noting that, as the inlet pressure increased, the wire sweep tendency increased, presumably due the increase of pressure force inside the cavity.

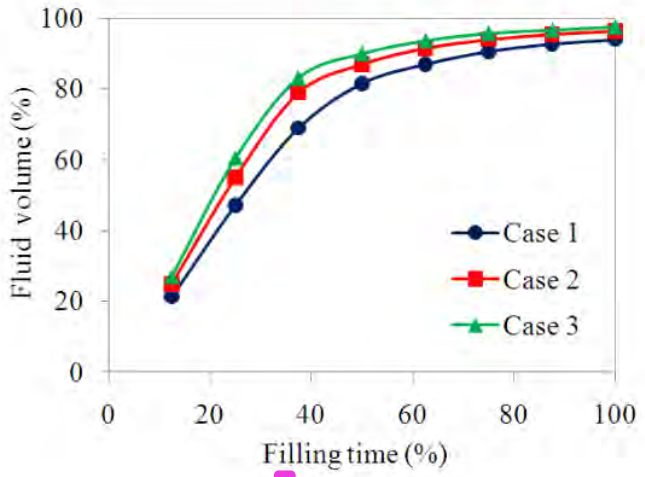

(a) Single die.

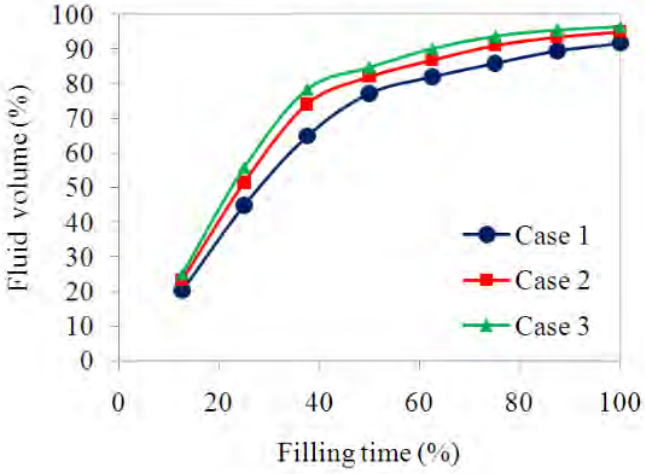

(b) Stacked die.

Figure 4.39 Percentage of filled volume versus filling time for different cases of scale-up eight-wire PBGA with centre inlet: (a) Single die and (b) Stacked die.

(a) Wire 3.

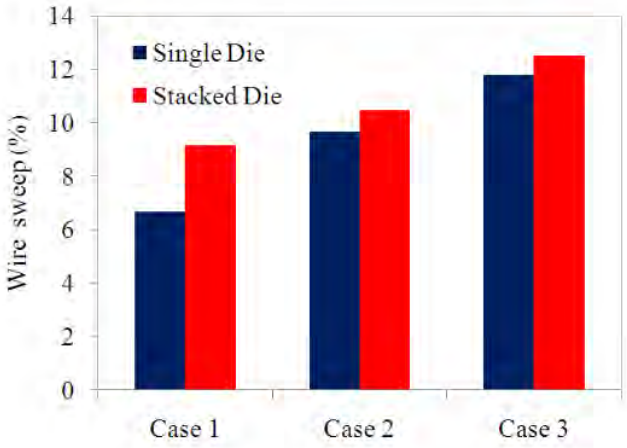

(b) Wire 7.

Figure 4.40 Deformations of wires 3 and 7 of scale-up eight-wire PBGA with centre inlet for all cases: (a) Wire 5 and (b) Wire 7.

4.4.2 Stress Analysis (Shear Stress)

The FSI modelling technique is capable to handle the prediction and simulation of complicated geometry in the structural analysis. In the actual experiment and in the

industry, the stress of the structures during FSI is difficult to determine and costly, especially for miniaturised IC packaging. Therefore, this technique is essential for the continuous improvement and the investigation of microelectronic reliability.

Figure 4.41a-4.46 illustrate the phenomenon of wire deformation, which predicted by ABAQUS. Detailed view of maximum stress distribution of all cases of wire 7, at maximum displacement is shown in Figure 4.41a, 4.41b, 4.42a and 4.42b that demonstrates the highest stress around un-deformed fixed boundary, especially near to the wire bonds for single and stacked die respectively. According to the simulation, stress distribution varied according to the fluid force. At 2.0s, maximum stress was concentrated at the joint between the die and the bumps (bending region). This means the sweep displacement of wire is dominated by the bending moment instead of the twisting moment (Kung et al., 2006). For clarity, only the two bond regions are shown where the stress was concentrated for the higher deformation of wires (3 and 7).The consolidated data of maximum Von-Mises stress in wire 3 and wire 7for the three cases is given in Figure 4.43a and 4.43b. It is clearly shown that wires 3 and 7were subjected to maximum stress, owing to the influence of higher pressure force. It is noting that the stress increased significantly with the increased in the inlet pressure.

Figure 4.44a, 4.44b, 4.45a and 4.45b shows the shear stress of the structures during the filling process for single and stacked die respectively. The fluid flow into the cavity subjected force upon the structure and induced stress in x and z direction as shown in Figure 3.22 of Chapter 3.The maximum shear stress distribution was concentrated at the twisting region. The consolidated data of maximum shear stress in wire 3 and wire 7 for the three cases is given in Figure 4.46.Comparison of von Mises and Shear stress of Wire 3 and Wire 7 of scale-up eight-wire PBGA with centre inlet is shown in Appendix G.

In the actual IC packaging, improper process control may lead the unintended occurrences on the wire such as overstress and serious deformation. These may cause failures or short circuit in the packaging. High shear stress can cause the reduction of reliability; the wire may degrade or fail, due to the overstress. Therefore, the FSI phenomenon during encapsulation for the actual-size of PBGA, and 3D packaging and integration should be considered in the process.

(a) Case 1.

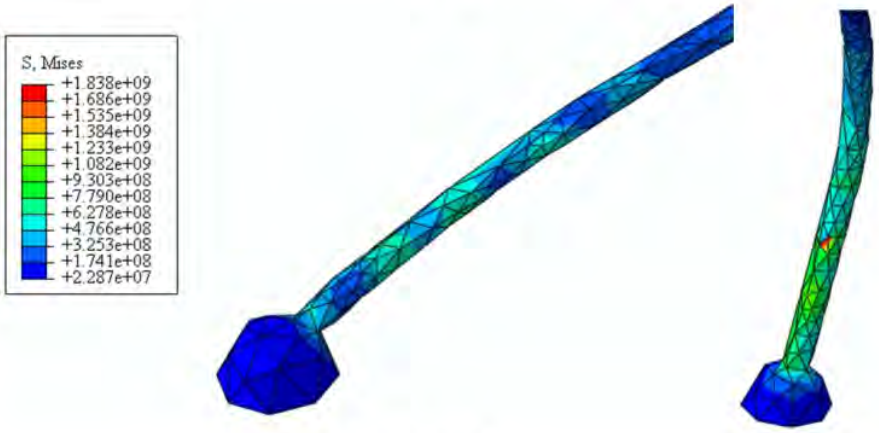

(b) Case 2.

Figure 4.41a Detailed view of maximum von Mises stress distribution for all cases of single die of scale-up eight-wire PBGA with centre inlet for wire 7: (a) Case 1 and (b) Case 2.

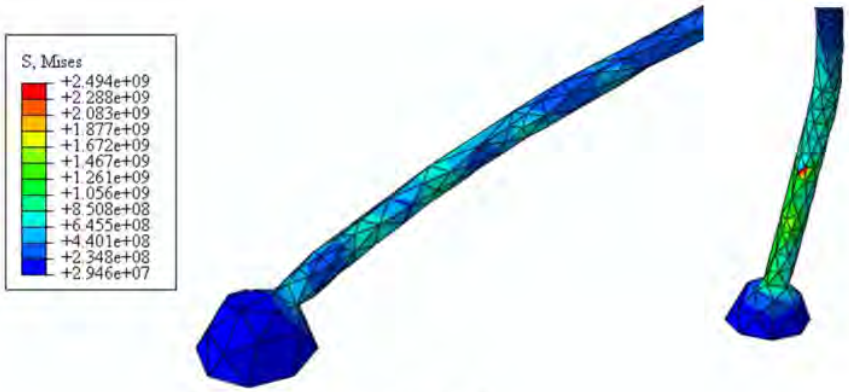

(b) Case 3.

Figure 4.41b Detailed view of maximum von Mises stress distribution for all cases of single die of scale-up eight-wire PBGA with centre inlet for wire 7: (c) Case 3 (continued).

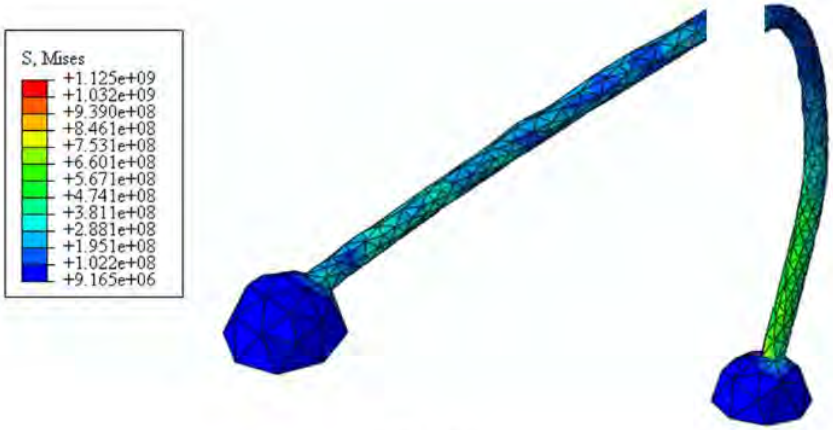

(a)Case 1.

Figure 4.42a Detailed view of maximum von Mises stress distribution for all cases of stacked die of scale-up eight-wire PBGA with centre inlet for wire 7: (a) Case 1.

(c) Case 2.

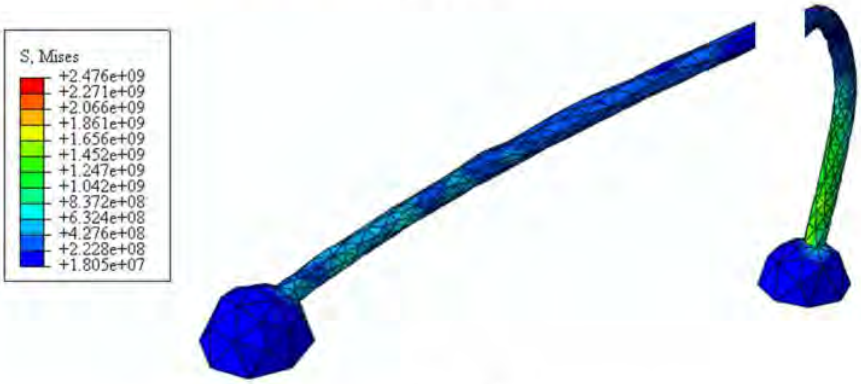

(d) Case 3.

Figure 4.42b Detailed view of maximum von Mises stress distribution for all cases of stacked die of scale-up eight-wire PBGA with centre inlet for wire 7: (b) Case 2 and (c) Case 3 (continued).

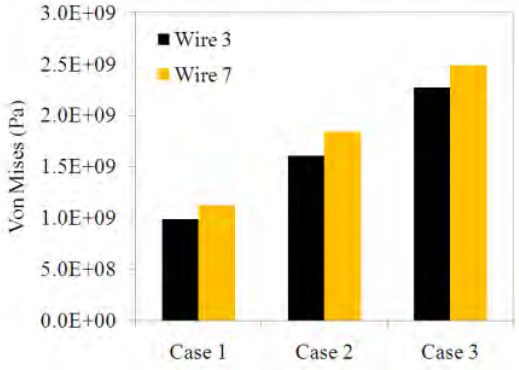

(a) Single die.

Figure 4.43a Maximum von Mises for all cases of scale-up eight-wire PBGA with centre inlet: (a) Single die.

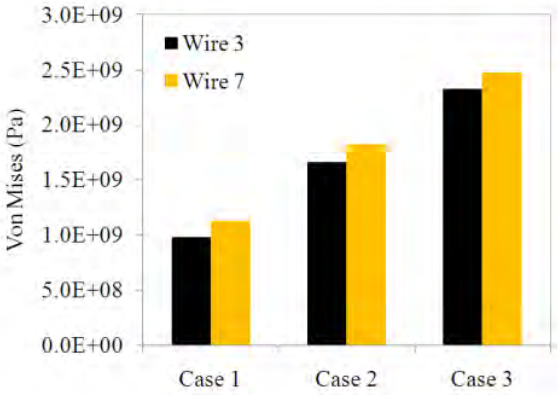

(b) Stacked Die.

Figure 4.43b Maximum von Mises for all cases of scale-up eight-wire PBGA with centre inlet: (b) Stacked die (continued).

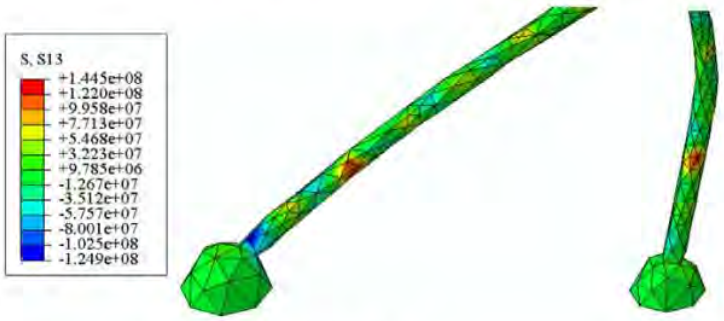

(a) Case 1.

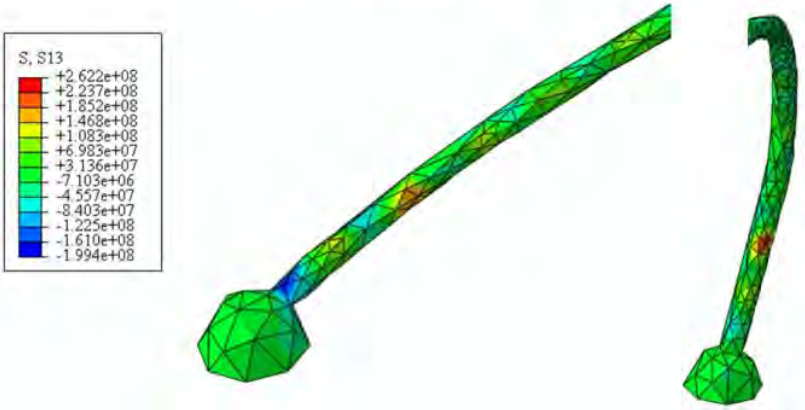

(b) Case 2.

Figure 4.44a Detailed view of maximum shear stress distributions for all cases of single die of scale-up eight-wire PBGA with centre inlet for wire 7: (a) Case 1 and (b) Case 2.

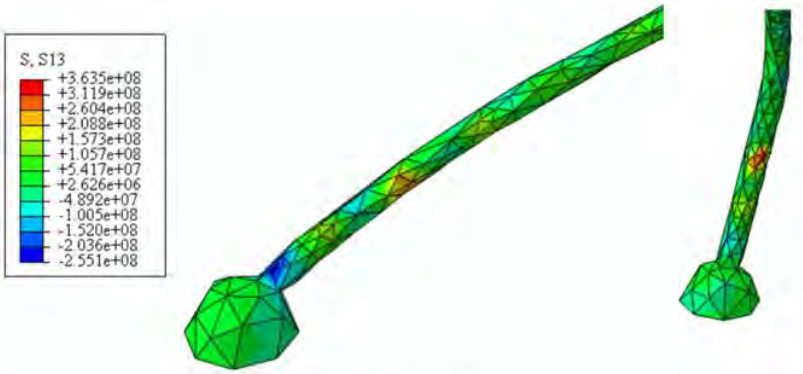

(c) Case 3.

Figure 4.44b Detailed view of maximum shear stress distributions for all cases of single die of scale-up eight-wire PBGA with centre inlet for wire 7: (c) Case 3 (continued).

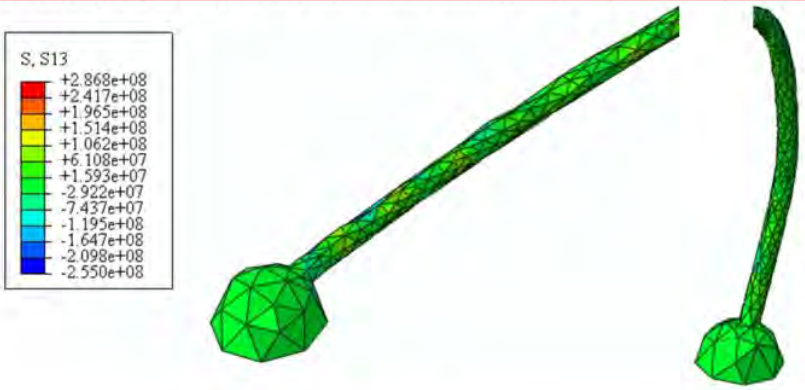

(a) Case 1.

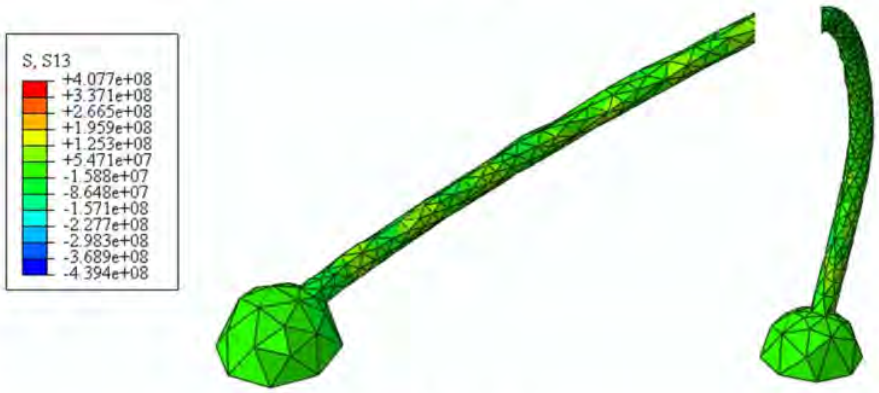

(b) Case 2.

Figure 4.45a Detailed view of maximum shear stress distributions for all cases of stacked die of scale-up eight-wire PBGA with centre inlet for wire 7: (a) Case 1 and (b) Case 2.

(c) Case 3.

Figure 4.45bDetailed view of maximum shear stress distributions for all cases of stacked die of scale-up eight-wire PBGA with centre inlet for wire 7: (c) Case 3 (continued).

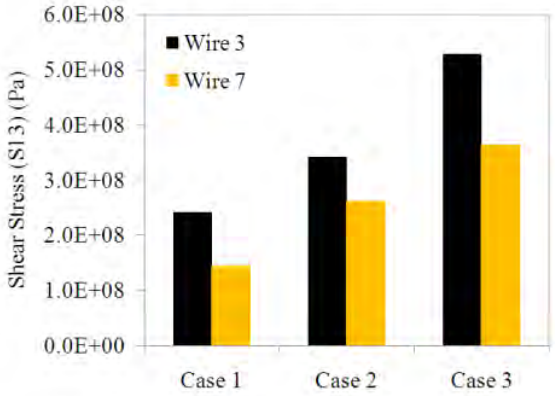

(a) Single die.

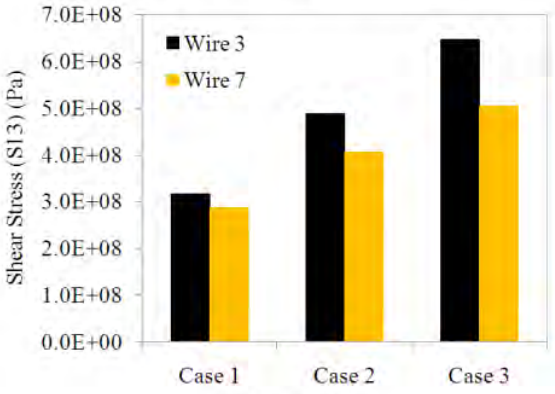

(b) Stacked Die.

Figure 4.46 Maximum shear stress for all cases of scale-up eight-wire PBGA with centre inlet: (a) Single die and (b) Stacked die.

4.5 Wire Sweep Considering Stacked Die Effect of Scale-up eight-wire PBGA Encapsulation Process –Corner Inlet

4.5.1 Analysis of Pressure Effect in Packaging of Single and Stacked Die

During the wire deformation, largest wire sweep occurred at the middle of the silicon die (Wu et al., 1998). This was due to the fact that wire bonds (at the middle region) were positioned normal to the flow direction of the moulding compound. During the encapsulation process, wire at this region experienced higher lateral flow load, which resulted in large deformation of about 14.5% of wire sweep during 27s of filling time (Wu et al., 1998). In a typical PBGA, tension on the excess wire resulted from sweep, because it offered small resistance to the traverse forces imposed by the moulding compound. However, with the lateral looping approach, the excess wire present in the lateral direction provided the required tension (Brunner et al., 2004). Lower deformation was found on lateral loop of wire shape (3.3 %) when compared to the standard loop (6%) using moulding compound EME-G760. Kung et al.,(2006a) had demonstrated the deformation of wire was dominated by the twisting moment instead of the bending moment. The wire loop shape has significant effect on the deformation in IC encapsulation. Yao et al.,(2003) found that the normal shape of the wire loop possessed weak bend resistance at the middle region of wires, which resulted in more deformations when compared to M shape.

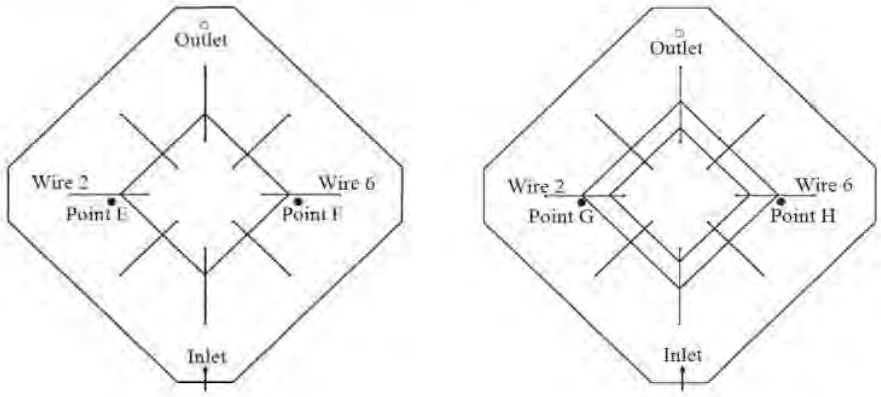

(a) Single die. (b) Stacked die.

Figure 4.47 Points position of pressure measurement on maximum wire deformation of PBGA with corner inlet: (a) Single die and (b) Stacked die.

As mentioned in Section 4.2.4.2 in above, the wires 2 and 6, which positioned at middle region of package experienced the dominant deformations in the encapsulation process. Therefore, only the pressure around wire 2 and wire 6 are evaluated for the comparison. Figure 4.47 shows the locations of pressure measurement at Point E and Point F for single die package and Point G and Point H for stacked die package during the encapsulation process.Figure4.48 shows the corresponding bar chart of pressure acting of each point for all cases for single and stacked die packages. The different inlet pressures of single and stacked die packages for all cases of wires 2 and 6 were shown in Figure 4.49 and percentage of filled volume versus filling time at different cases were plotted in Figure 4.50.The increase of inlet pressure is due to the presence of test fluid. As can be seen, pressure at Point E and Pont F (single die package) and Point G and Point H (stacked die package) is high due to the impact of continuous incoming flow. The pressure directly influences the wire displacement and the drag force that acting on the wire structure, during the filling process (Figure 4.51). Thus, the wires which experienced higher pressure are expected to cause higher deformation compared to those at the low pressure. At the same time, it is worth noting that, as the inlet pressure increased, the wire sweep tendency increased, presumably due the increase of pressure force inside the cavity.

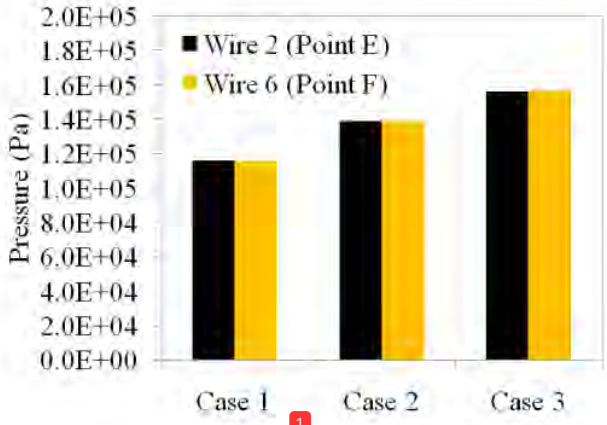

(a) Single die.

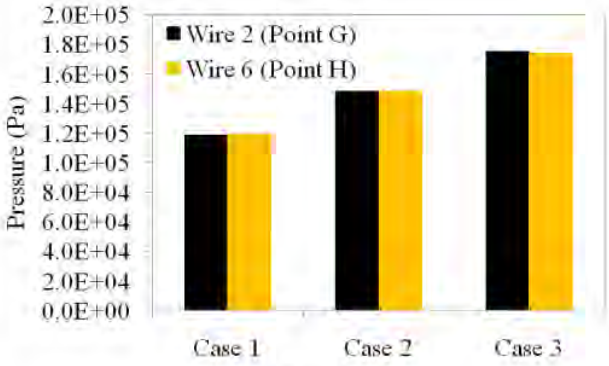

(b) Stacked die.

Figure 4.48 Pressure acting on wires 2 and 6 for all cases in single and stacked die packages of scale-up eight-wire PBGA with corner inlet: (a) Single die and (b) Stacked die.

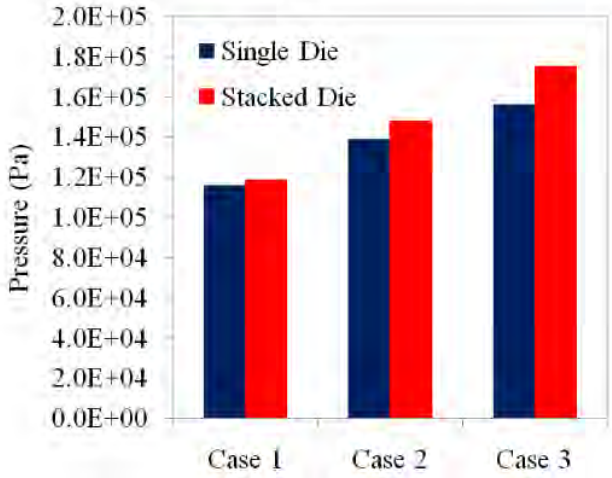

(a) Wire 2.

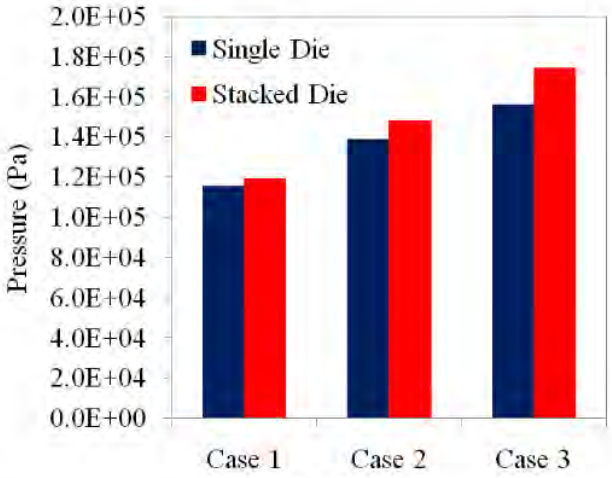

(b) Wire 6.

Figure 4.49 Different pressures at single and stacked die packages for all cases of wires 2 and 6 of scale-up eight-wire PBGA with corner inlet: (a) Wire 2 and (b) Wire 6.

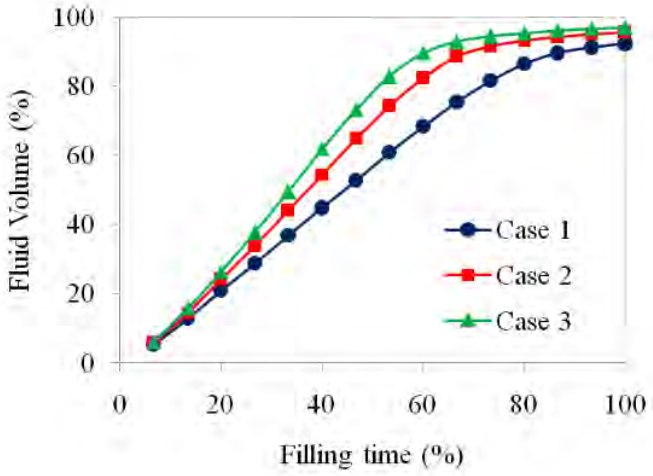

(a) Single die.

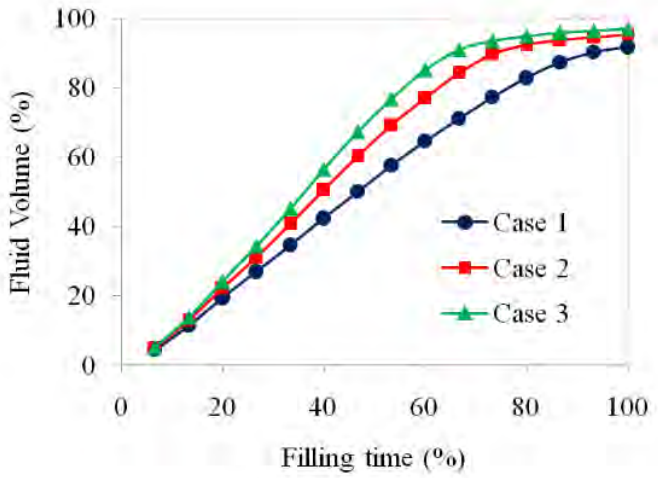

(b) Stacked die.

Figure 4.50 Percentage of filled volume versus filling time for different cases of scale-up eight-wire PBGA with corner inlet: (a) Single die and (b) Stacked die.

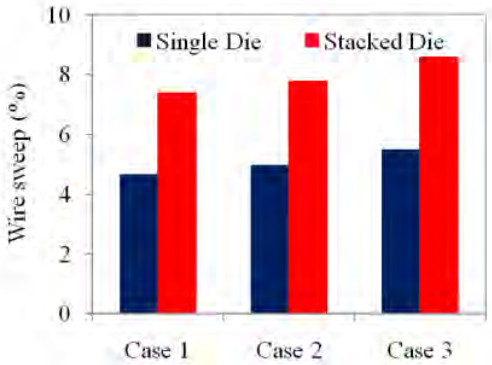

(a) Wire 2.

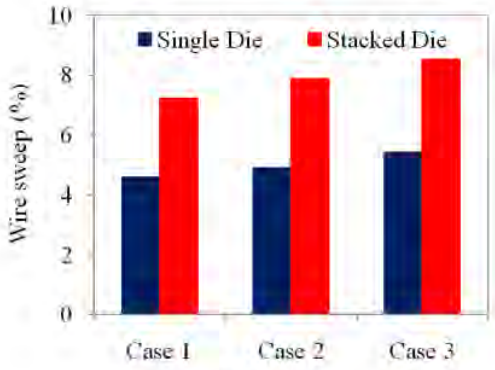

(b) Wire 6.

Figure 4.51 Deformations of wires 2 and 6of scale-up eight-wire PBGA with corner inlet for all case: (a) Wire 2 and (b) Wire 6.

4.5.2 Stress Analysis (Shear Stress)

The FSI modelling technique is capable to handle the prediction and simulation of complicated geometry in the structural analysis. In the actual experiment and in the industry, the stress of the structures during FSI is difficult to determine and costly, especially for miniaturised IC packaging. Therefore, this technique is essential for the continuous improvement and the investigation of microelectronic reliability.

Figure4.52a- 4.57 illustrate the phenomenon of wire deformation, which predicted by ABAQUS. Detailed view of stress distribution of wires 2 and 6, at maximum displacement is shown in Figure4.52a, 4.52b, 4.53a and 4.53bthat demonstrates the highest stress around un-deformed fixed boundary, especially near to the wire bonds for single and stacked die respectively. According to the simulation, stress distribution varied according to the fluid force. At 2.0s, maximum stress was concentrated at the joint between the die and the bumps (bending region). This means the sweep displacement of wire is dominated by the bending moment instead of the twisting moment (Kung, 2006a). For clarity, only the two bond regions are shown where the stress was concentrated for the higher deformation of wires (2 and 6).The consolidated data of maximum Von-Mises stress in wire 2 and wire 6 for the three cases is given in Figure 4.54. It is clearly shown that wires 2 and 6were subjected to

maximum stress, owing to the influence of higher pressure force. It is noting that the stress increased significantly with the increased in the inlet pressure.

Figure 4.55and Figure 4.56shows the shear stress of the structures during the filling process for single and stacked die. The fluid flow into the cavity subjected force upon the structure and induced stress in x and z direction such as shown in Figure 3.22 of Chapter 3.The maximum of shear stress distribution was concentrated at the twisting region. The consolidated data of maximum shear stress in wire 2 and wire 6 for the three cases is given in Figure 4.57.Comparison of von Mises and Shear stress of Wire 2 and Wire 6 of scale-up eight-wire PBGA with corner inlet is shown in Appendix H.

In the actual IC packaging, improper process control could lead the unintended occurrences on the wire such as overstress, serious deformation, and its may causing failure or short circuit in the packaging. High shear stress can cause the reduction of reliability; the wire may degrade or fail, due to the overstress. Therefore, the FSI phenomenon during encapsulation for actual-size of PBGA, and 3D packaging and integration should be considered in the process.

(a) Case 1.

(b) Case 2.

Figure 4.52a Detailed view of maximum von Mises stress distribution for single die of scale-up eight-wire PBGA with corner inlet for all cases for wire 6: (a) Case 1 and (b) Case 2.

(c) Case 3.

Figure 4.52b Detailed view of maximum von Mises stress distribution for single die of scale-up eight-wire PBGA with corner inlet for all cases for wire 6: (c) Case 3 (continued).

(a) Case 1.

(b) Case 2.

Figure 4.53a Detailed view of maximum von Mises stress distribution for stacked die of scale-up eight-wire PBGA with corner inlet for all cases for wire 6: (a) Case 1 and (b) Case 2.

(c) Case 3.

Figure 4.53b Detailed view of maximum von Mises stress distribution for stacked dieof scale-up eight-wire PBGA with corner inlet for all cases for wire 6: (c) Case 3 (continued).

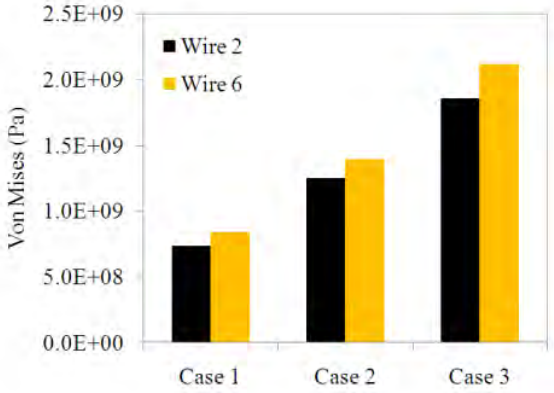

(a) Single die.

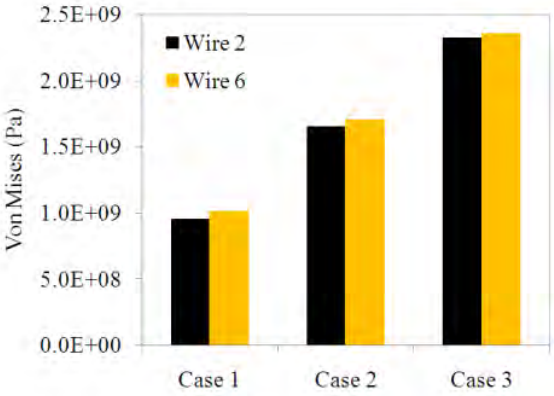

(b) Stacked Die.

Figure 4.54 Maximum von Mises for all cases of scale-up eight-wire PBGA with corner inlet: (a) Single die and (b) Stacked die.

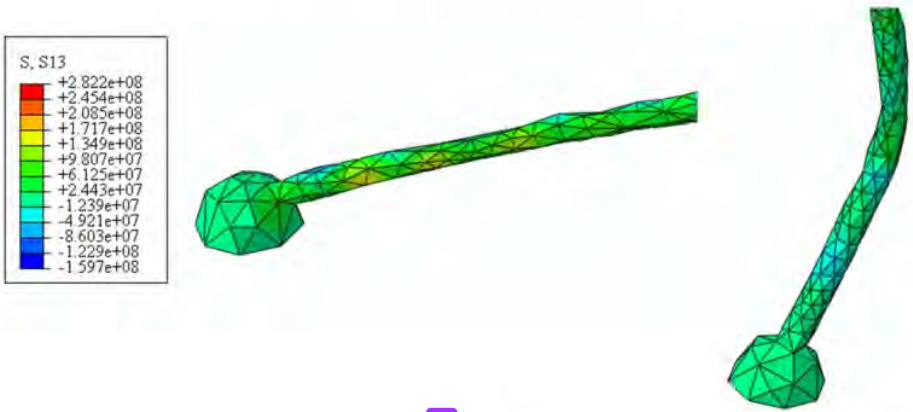

(a) Case 1.

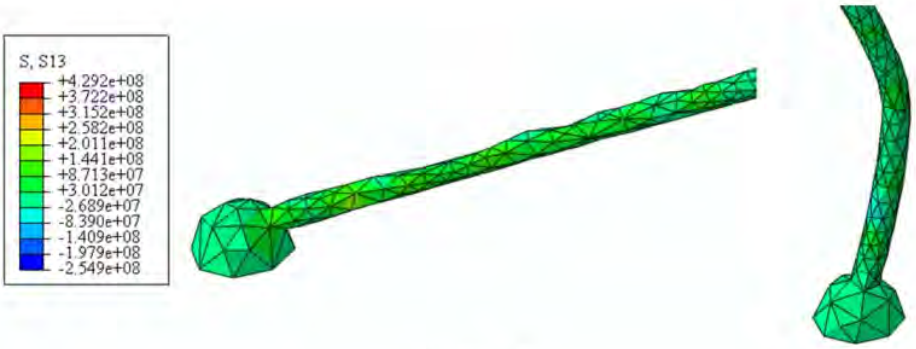

(b) Case 2.

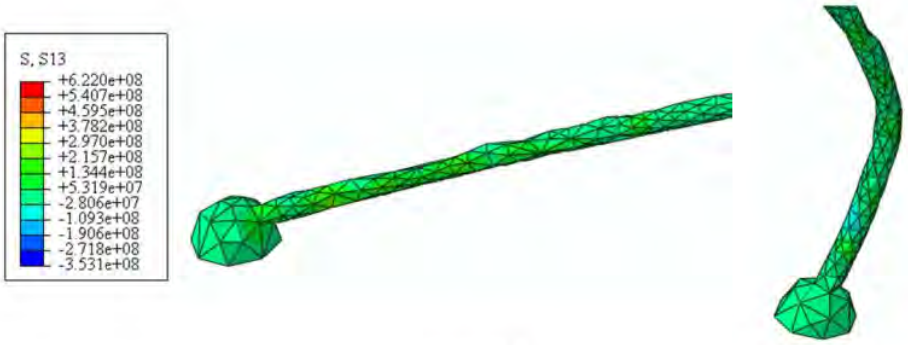

(c) Case 3.

Figure 4.55 Detailed views of maximum shear stress distributions for single die of scale-up eight-wire PBGA with corner inlet for all cases for wire 6: (a) Case 1, (b) Case 2 and (c) Case 3.

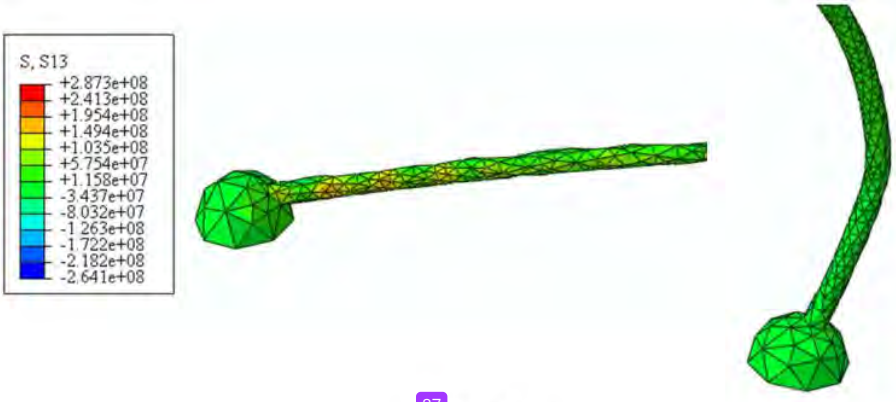

(a) Case 1.

(b) Case 2.

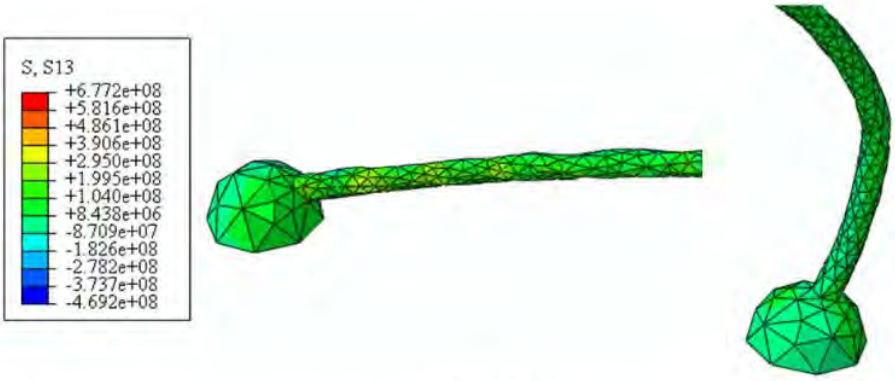

(c) Case 3.

Figure 4.56Detailed views of maximum shear stress distributions for stacked die of scale-up eight-wire PBGA with corner inlet for all cases for wire 6: (a) Case 1, (b) Case 2 and (c) Case 3.

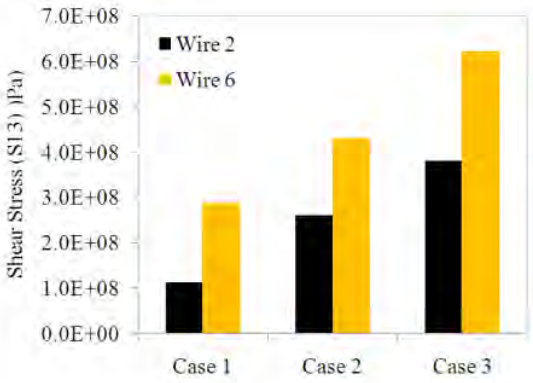

(a) Single die.

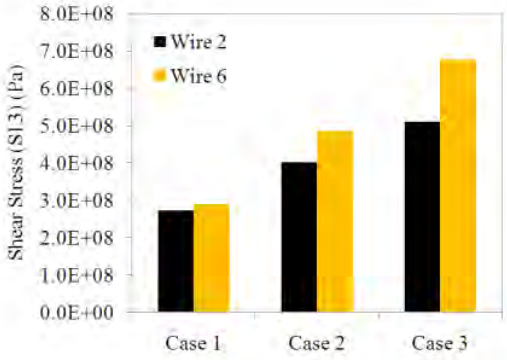

(b) Stacked Die.

Figure 4.57 Maximum shear stress for all cases of scale-up eight-wire PBGA with corner inlet: (a) Single die and (b) Stacked die.

4.6 Effects of Die Heights and Inlet Arrangement on Wire Sweep Behaviour

4.6.1 Effects of Die Heights on Wire Sweep behaviour

To investigate the die height effect on wire sweep behaviour, two die heights, i.e. 1.1 mm and 2.2mm were used to analyze the wire sweep values, which were compared with that from the FSI simulation and the experiment. Besides, to make the wire sweep of different die height comparable, the wire loop heights were considered as a constant (1.5 mm) for these designs. Figure 3.15 indicates the two die height designs.

Wire sweep results from a scale-up eight-wire PBGA with centre and corner inlet gate for Case 3 are illustrated in Figure 4.58. As shown in Figure 4.58, the trends of wire sweep distribution with different die heights are similar. However, higher die height brings about bigger wire sweep (Han et al., 2011b).

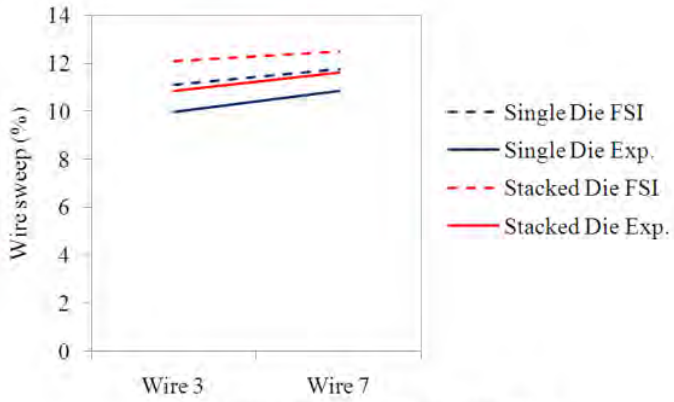

(a) Centreinlet of Wire 3and Wire 7.

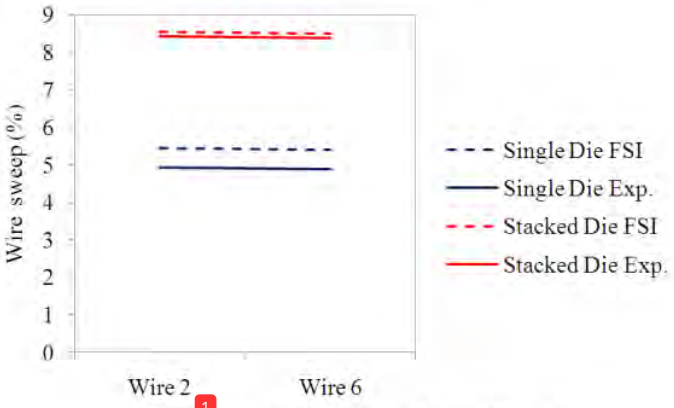

(c) Corner inlet of Wire 2 and Wire 6.

Figure 4.58 Comparison of wire sweep of single and stacked die of a scale-up eight-wire PBGA for Case 3: (a) Centre inlet of Wire 3and Wire 7 and (b) Corner inlet of Wire 2 and Wire 6.

4.6.2 Effects of Inlet Arrangements on Wire Sweep Behaviour

4.6.2.1 PBGA Package with Centre Inlet

The wirebond profiles at several stages of filled fluid percentage volume are shown in Figure 4.5 and Figure 4.6. It can be seen that the wirebonds were deflected in the direction of the mould front. The greatest wire sweep occurs in the middle portion of the die because these wirebonds being orthogonal to the melt-front generally are subjected to higher flow-induced forces.

4.6.2.2 PBGA Package with Corner Inlet

The wirebond profiles at several stages of filled fluid percentage volume are shown in Figure 4.10 and Figure 4.11. It can be observed that inlet gate position has a significant effect on wire sweep. The shifting of the inlet gate from the centre to the corner changes the flow pattern in the cavity and the pattern of wirebond deformation. In this case, the melt front meets at the corner opposite the gate. Even though the wirebonds in the region where the melt fronts meet may be deflected in directions opposite to each other, the risk of wirebond shorting may be lower than that with a centre inlet gate because the space between wirebonds at the corner inlet of the package is normally larger.

4.7 Wire Sweep Considering Rheology Effect of Actual Size PBGA Encapsulation Process

Different EMC material properties show the different flow behaviours during the encapsulation process. The characteristic of EMC material properties in electronic packaging gives significant effect to the package during encapsulation such as void formation and warpage on silicon die. EMC material properties with highest viscosity may require the proper setting in processing parameter to reduce the void formation and filling time. Thus, the EMC characteristic may cause the unpredicted flow front profile in the encapsulation process. Three types of moulding compound with different material properties have been utilized in the actual size PBGA encapsulation process, which is

available in the literatures. The EMC fluid behaves according to non-uniform flow profiles and viscosity variation during filling process. The behaviour of moulding compound is also influenced by the filler content. The filler content in the EMC gives the important effect to the warpage trend, and it is dominant in the compound properties (Yong, 2006). Besides, the type and percentage of filler content also affect the thermal conductivity, thermal expansion coefficient and dielectric constants (Kim et al., 1999). The Al-N (Aluminium Nitride) filler improved the thermal conductivity until 7-8 times compared with crystalline silica at 70% of EMC volume.

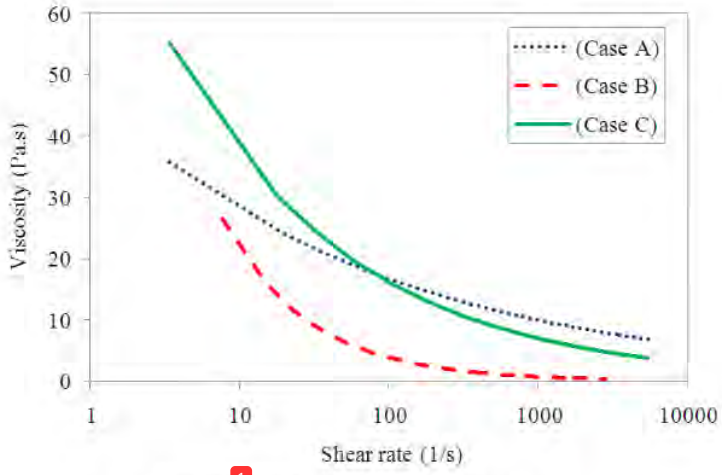

Figure 4.59 Viscosity versus shear rate.

Figure 4.59 illustrates the viscosity variation versus shear rate for three different EMC material properties that were used in the present study. The curves show an exponential relation of viscosity variation where the viscosity reduces with the shear rate. EMC material properties used in Case B shows the higher viscosity variation, followed by Case A and Case C. The variations of viscosity-shear rate in Figure4.59 were obtained from the FLUENT simulation results. The FLUENT software calculated the variation of the viscosity shear-rate for EMC material properties during the encapsulation process depending on the material properties. The capability of the FLUENT in handling this problem was reported by Khor et al. (2010c) in their experimental and simulation of polymer rheology during injection moulding process. Hence, the realistic predictions could be achieved by using FLUENT software. In the polymer fluid processing, viscosity is normally independent of pressure, but liquids

under extreme pressure often experience an increase in viscosity (Liang, 2001). Since liquids are normally incompressible, an increase in pressure does not really bring the molecules significantly closer together.

4.7.1 Analysis of Pressure Effect in Packaging

Pressure distribution during the mould filling process is also important in electronic packaging, especially for the wire bonding and lead frame. Dissimilarity of the pressures may give the undesirable effect to the wire such as serious deformation, failure or fracture; hence, reduce the package reliability. Point position of measured pressure is shown in Figure4.60. Thus, the pressure distributions during the PBGA encapsulation process are observed in the present study. Pressure distribution of all cases at Point 1, 2, 3 and 4 are shown in Figure4.61a and 4.61b and pressure behaviour of each point of Case C is shown in Figure 4.62. From Figure 4.61, the similarity of the pressure trends of Case B and Case C may be due to the viscosity behaviour that mainly influenced by the complex rheological of the EMCs. This is evidently from the Figure 4.59, where they show the almost similar trend of the viscosity-shear rate although with different values compared to the EMC of Case A. As illustrated in Figure4.62, the maximum pressure at Point 1 is due to the impact of continuous flow from the inlet gate. The pressure gradually reduces with flow front advancement as evident from the pressures at the symmetric locations of Point 2 and Point 4, and the lower pressure at the location Point 3, which near to the outlet vent.

Pressure distributions contour for Case A, Case B and Case C are shown in Figure4.63. The contour colours represent the pressure drop around package during the filling process; higher pressures are observed near the inlet gates and lower pressures around the outlet vent.

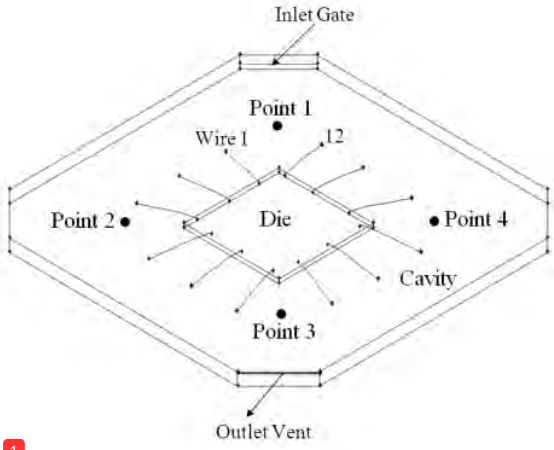

Figure4.60 Point position of measured pressure of actual size PBGA.

The pressure at all locations shows the similar pressure distribution contour for all cases of filling process. From the results, the relationship between pressure and types of EMC are obvious, Case A with maximum viscosity (as illustrates in Figure 4.59) the higher pressure distributions. Besides, the pressure around outlet vents is found lower compare to pressure nearer to inlet gates. From the simulation analysis, filling process of Case A shows the highest pressure with comparing to Case B, and Case C. This phenomenon is caused by the flow interaction from the different parameter of EMC properties.

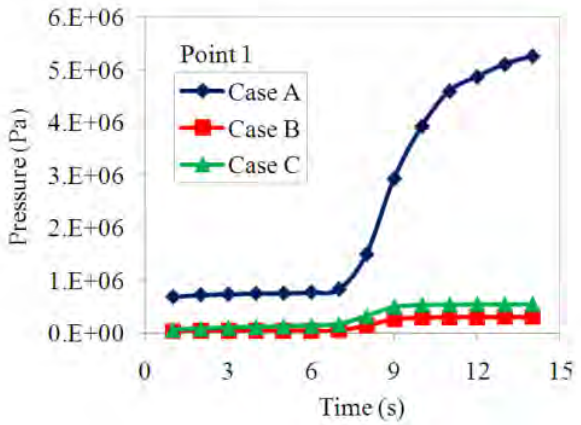

(a) Point 1.

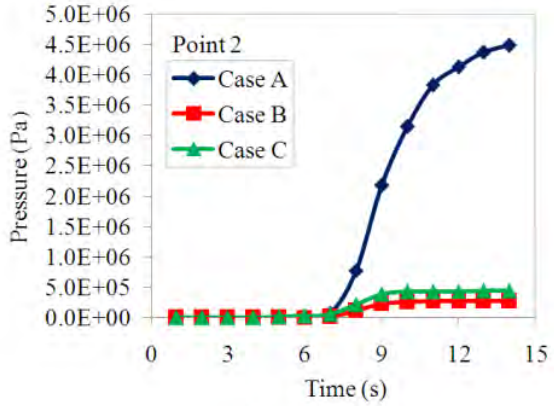

(b) Point 2.

Figure 4.61a Pressure distributions of all Cases of actual size PBGA: (a) Point 1 and (b) Point 2.

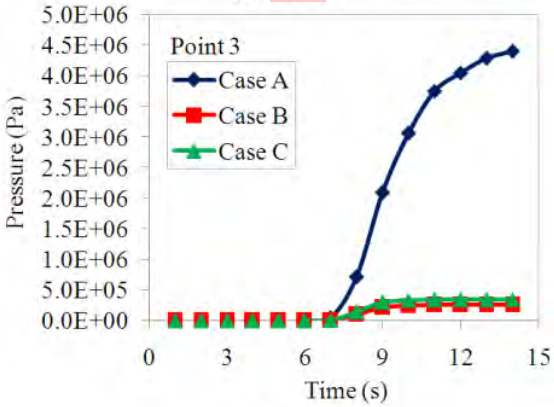

(c) Point 3.

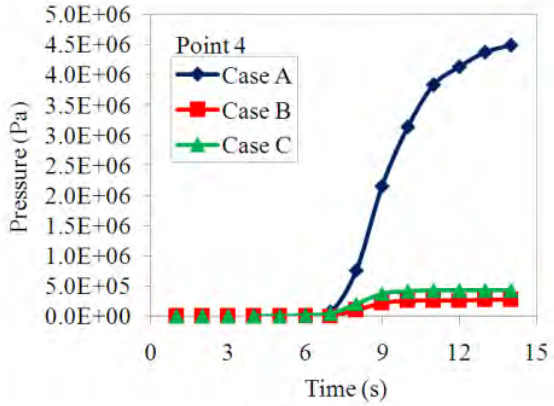

(d) Point 4.

Figure4.61b Pressure distributions of all Cases of actual size PBGA: (c) Point 3 and (d) Point 4 (continued).

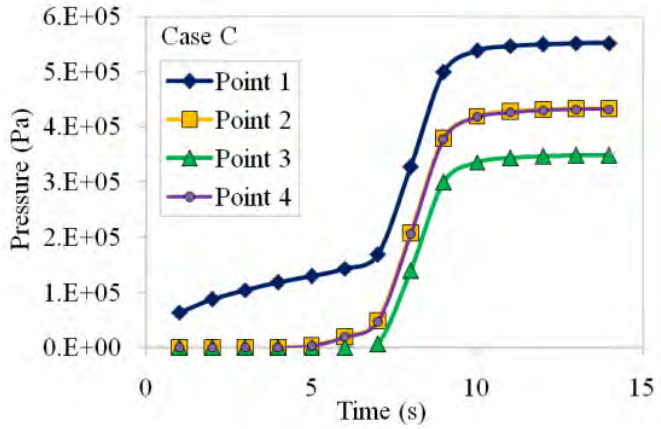

Figure 4.62 Pressure behaviour of each point of Case C of actual size PBGA.

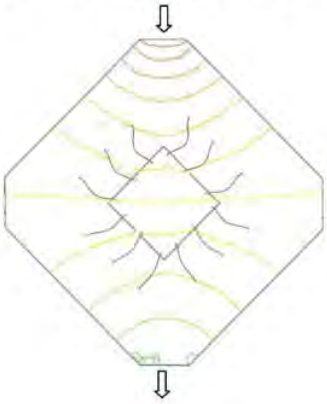

117

(a) Case A.

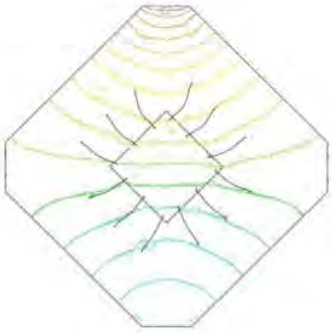

(b) Case B.

(c) Case C.

Figure 4.63 Pressure profiles for different parameter of material properties of actual size PBGA: (a) Case A, (b) Case B and (c) Case C.

4.7.2 Void Occurrence

The possibility of air trap or incomplete filling in the package is observed in the present case. Three cases of different properties of EMC are used in the analysis. Figure4.64a and 4.64b shows the possibility of the air trap or incomplete filling at 14 s of the package for all cases. The circles show in Figure4.64a and 4.64bis the location of the high possibility of void formation that causes by air trap or incomplete filling during the process. Case B (Figure 4.64b) is found to have the lowest air trap volume during filling process. This is clearly presented in Figure 4.65, which shown fewer and smaller air trap regions for Case B. Decreasing of viscosity may be the need for Case A, Case Band Case C to reduce the possibility of the air trap in the package. Comparison of EMC filling volume for the three cases with different parameters is presented in Figure 4.66. The results are obtained from simulation analysis show the Case B and Case C have higher and faster filling of the EMC volume compared to Case A. These filling phenomena are obviously shown in Figure 4.59 where the EMC with lowest viscosity (Case C) and the changes of the viscosity in Case B have significantly affected the EMC filling during the encapsulation process.

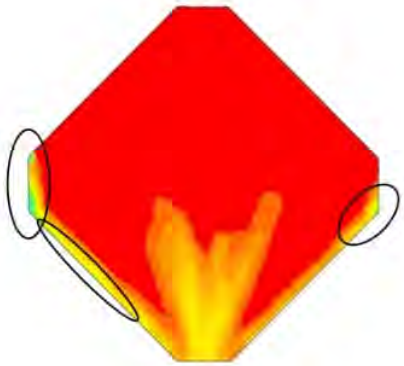

(a) Case A.

Figure 4.64a Comparison position posibility of void at 14 s of actual size PBGA:

(a) Case A.

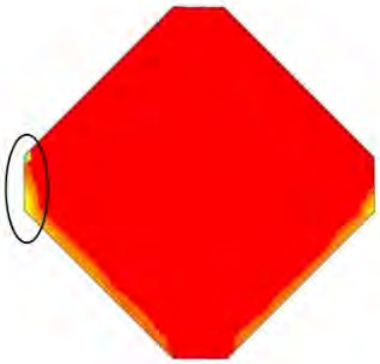

(b) Case B.

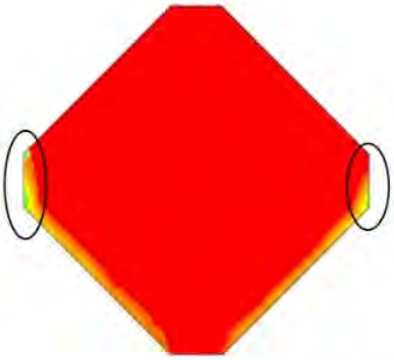

(c) Case C.

Figure4.64b Comparison position posibility of void at 14 s of actual size PBGA: (b) Case B and (c) Case C (continued).

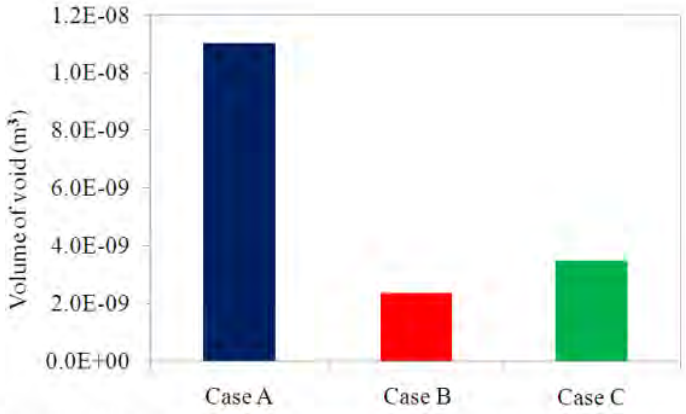

Figure 4.65 Volume of air trap (void) for all cases of actual size PBGA.

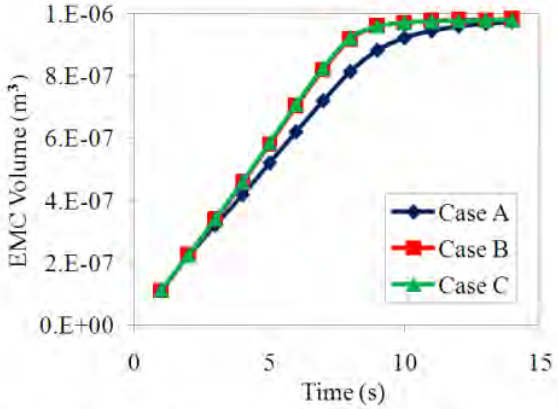

Figure 4.66 EMC volume of each Case of actual size PBGA.

4.7.3 Melt Front Profile

The comparison of simulation results between all Cases at 3, 7 and 11s is shown in Figure4.67. The predicted flow front shows different profiles for three cases. At the initial stage (1 s), the simulation flow-front profile is similar in all cases. The EMC flowed into the cavity without any obstacles before it reached the die or gold wires. So the EMC expanded ahead synchronously, and the melt front during this time tended to have a smooth curve shape. This may be attributed to the lower flow resistance around the inlet gate as the encapsulant is allowed to enter freely through the inlet gate. However, at 3s of filling time, the simulation displays different between Case A, Case B and Case C. In this state, the EMC encapsulant has already covered more than half of

the silicon die and the flow front of Case A shows a non-uniform profile around the silicon die region compared to the uniform profiles for Case B and Case C. The effect of the gold wires and the die is obviously shown in the flow front profiles. The EMC in this region was retarded. At 7s of filling time, the flow front on the top of the die was concave, while the flow front around was convex. At 11 s, the EMC completely flowed over the area of the die and the gold wires, and filled the whole cavity. Case B and Case C show a faster flow compared to Case A, which is observed at 11s of filling time during the simulation.

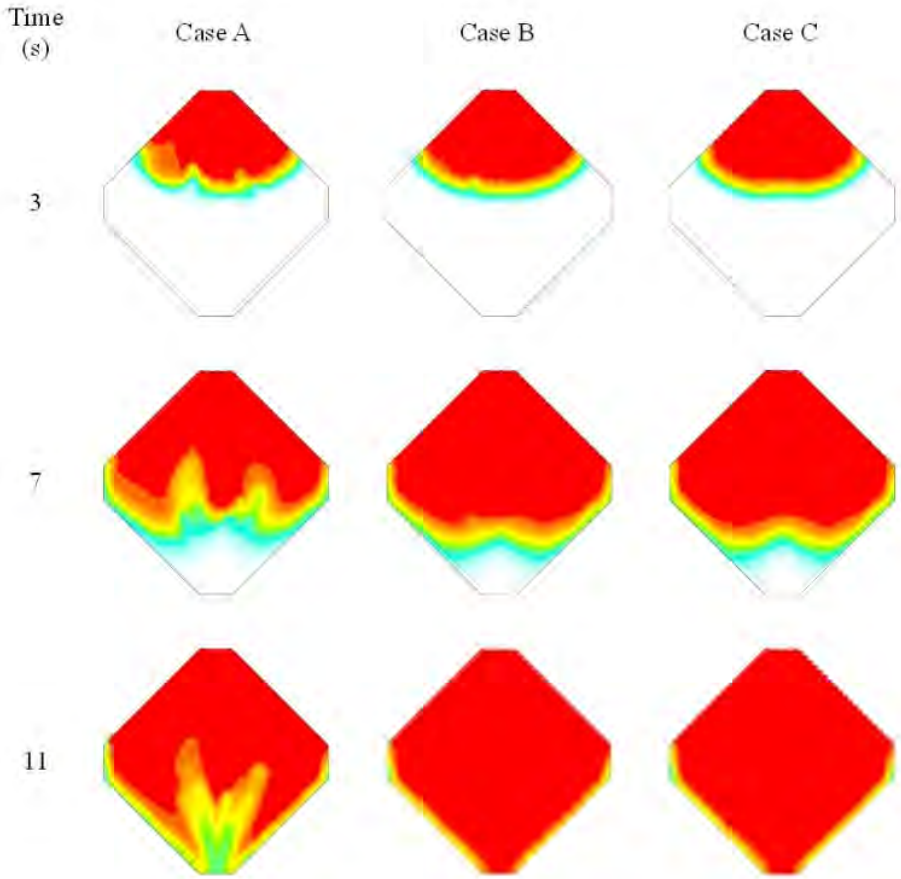

Figure 4.67 Simulation comparisons between different EMC parameters of actual size PBGA.

4.7.4 Conversion of the Compound

Degree of conversion within the mould cavity had been explained by Khoret al.,(2010a). The top view of conversion distribution of the packages is presented in Figure 4.68a and 4.68b for different cases of material properties. It is observed that the conversion level is quite low at the cavity inlet gate but higher around the package region. The predicted conversion of the mould compound at 14 s is 8.06e-01, 8.02e-01 and 7.75e-01 for Case A, Case B and Case C, respectively. This phenomenon is reasonable with the viscosity variation that is shown in Figure 4.59. This is predictable because the combination of the Castro–Macosko viscosity model and the Kamal curing kinetics model has taken into account two important factors, i.e. the dependence viscosity on the shear rate and the dependence of conversion level (which also affects the viscosity of the moulding compound) on the temperature.

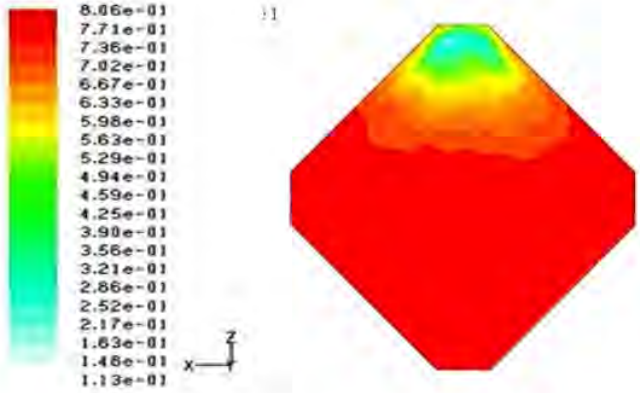

(a) Case A.

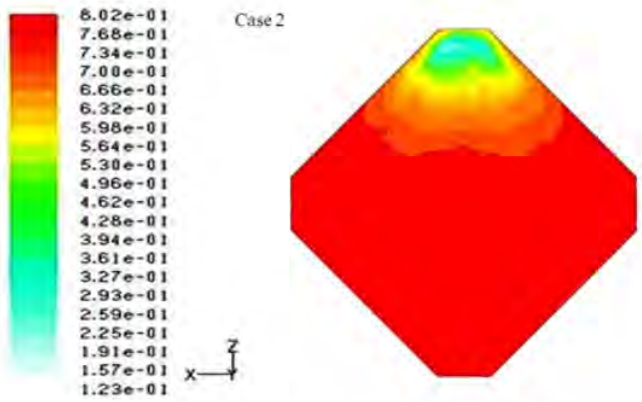

(b) Case B.

Figure 4.68a Predicted conversion of the mould compound at top of the package for different parameter of material properties at 14 s of actual size PBGA: (a) Case A and (b) Case B.

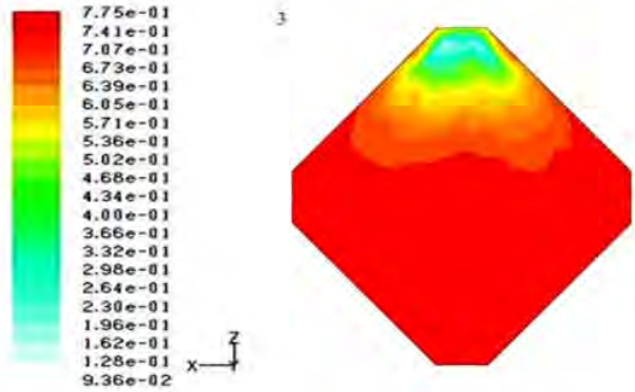

(c) Case C.

Figure 4.68b Predicted conversion of the mould compound at top of the package for different parameter of material properties at 14 s of actual size PBGA: (c) Case C (continued).

4.7.5 Wire Sweep Analysis

Figure4.69 illustrates the melt-front advancement for the PBGA package obtained from FLUENT, and the phenomenon of wire deformation predicted by ABAQUS. At the initial filling stage as shown in Figure4.69 (2s), two wire deformations are observed. However, the wire deformation occurs when EMC fills and covers the die and the wires in the package, or the wire sweep occurs when EMC interacts with the solid surface of the wire, as observed in Figure 4.69 (4 to 14s). Figure 4.70 shows the percentage of maximum wire sweep of each wire, and Figure 4.71 describes the percentage of wire sweep in Case C at 6, 10 and 12 s. In the present study, the effect of viscosity on pressure is found to directly influence the wire displacement and drag force that act on the wire structure, during the filling process. Thus, wires that experience a high viscosity flow or high pressure distribution are expected to deform more compared to those at a low viscosity or pressure, as is clear from the increase of wire sweep at wires 1 and 12, which are closer to Point 1.

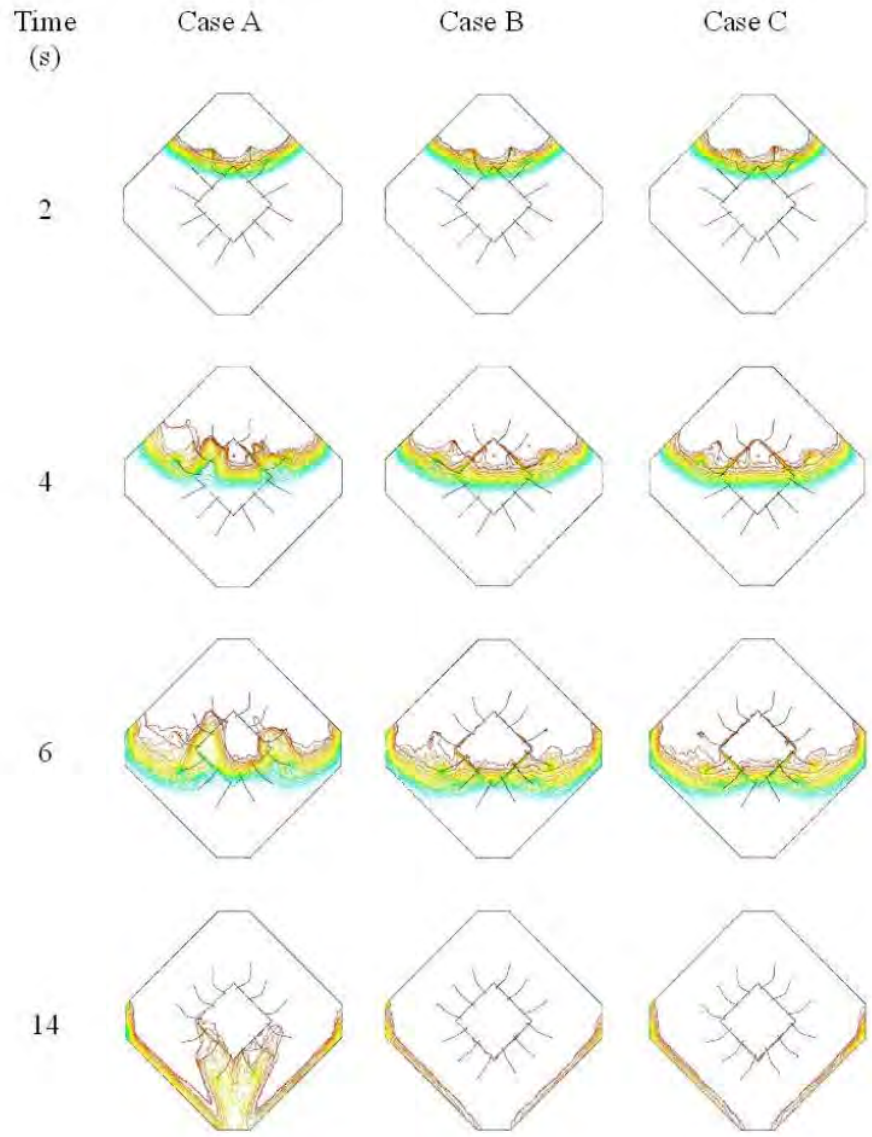

Figure 4.69 Behaviour of wire sweep of actual size PBGA of Case A, Case B and Case C at 2s, 4s, 6s and 14s.

Figure4.70 Percentage maximum wire sweep of each wire of actual size PBGA.

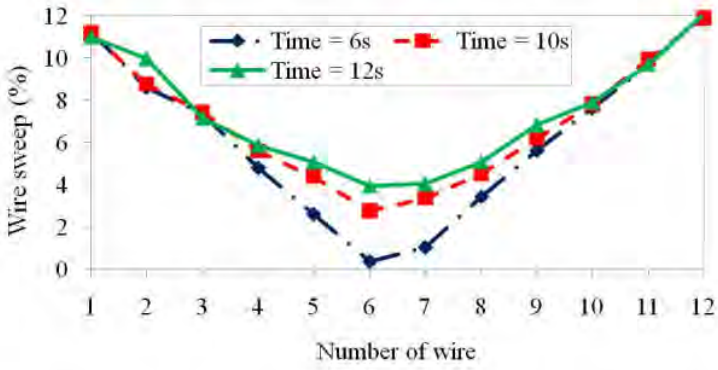

Figure 4.71 Percentage wire sweep of Case C at 6 s, 10 s and 12 s of actual size PBGA.

4.8 Optimisation Using RSM on Actual Size PBGA Encapsulation Process

4.8.1 Result of the Central Composite Design

In this numerical analysis, a total of 20 CCD batch runs were conducted (Table 4.6). The targets of the study are to minimize the wire sweep (Y_1), filled time (Y_2), and void in package (Y_3) during the actual size PBGA encapsulation process. The wire deformation on the structures will cause unintended defects to the package reliability, especially for high-density of wire applications. Void formation in the package might

induce delamination (Tay and Lin, 1999) on the interface of the actual size PBGA. Proper control of filling time can reduce production cycle time and cost.

Table 4.7Results of the central composite design

Run	Factor (codec)			Response (Y)					
				Simulation			Model Prediction		
	A	*B*	*C*	*1*	*2*	*3*	*1*	*2*	*3*
1	0	0	1	0.71874	4	0.09955	0.7065	4.1125	0.28031
2	-1	0	0	0.64396	10.5	0.80213	0.57339	10.7625	1.48013
3	0	0	0	0.87091	7.5	0.22754	0.86492	7.7125	0.26589
4	1	0	0	1.11645	5	0.08949	1.15645	4.6625	-0.9483
5	0	0	-1	0.94459	11.5	8.73617	1.02334	11.3125	7.41965
6	1	1	-1	0.42154	6.5	7.83664	0.48823	6.6375	7.5028
7	0	0	0	0.87091	7.5	0.22754	0.86492	7.7125	0.26589
8	0	0	0	0.87091	7.5	0.22754	0.86492	7.7125	0.26589
9	0	0	0	0.87091	7.5	0.22754	0.86492	7.7125	0.26589
10	0	-1	0	1.78421	7.25	0.23322	1.66608	7.7125	-0.4299
11	-1	-1	1	0.96508	6	0.78257	0.93666	5.5375	1.40034
12	0	1	0	0.3527	7.5	0.16884	0.31776	7.7125	0.96169
13	-1	1	-1	0.23983	16.5	10.1431	0.16786	15.9875	10.7712
14	-1	1	1	0.21518	5.75	0.34034	0.33226	5.5375	-0.7968
15	0	0	0	0.87091	7.5	0.22754	0.86492	7.7125	0.26589
16	1	-1	1	1.67217	3	0.15591	1.7824	2.6875	-0.1882
17	1	-1	-1	2.65929	7	1.10144	2.58048	6.6375	2.52249
18	1	1	1	0.35954	2.75	0.02316	0.28268	2.6875	0.7059
19	0	0	0	0.87091	7.5	0.22754	0.86492	7.7125	0.26589
20	-1	-1	-1	1.24965	16	9.28092	1.36478	15.9875	8.88213

A, *B*, and *C* = inlet pressure, diameter of wire, vent height.

1, 2 and 3 = wire sweep, filling time and void.

In the actual size PBGA encapsulation process, the stress and deformation of wire imposed on the structure are resulted from the fluid–structure interaction. Thus, wire sweep (Y_1) was evaluated during the encapsulation process. However, package

filling time (Y_2) and void in the package (Y_3) were estimated at the final of the process. From the CCD batch runs, the maximum wire deformation is 2.65 mm, when high inlet pressure (5 MPa) is applied to 0.03 mm of diameter of wire, and 0.40 vent height. Therefore, this situation should be avoided in the PBGA encapsulation. Moreover, the lowest void formation is found on run 18, whereas the middle inlet pressure, wire diameter and vent height applied. This condition may be attributed to the large pressure, which gives lower resistance to the EMC to freely flow through. The fastest filling time (3 s) for run 16 is achieved at the highest inlet pressure (A) with 0.04 mm for factors B, and 0.22 mm for factor C.

4.8.2 Regression Model Equation and Analysis of Variance (ANOVA)

The regression models for responses, maximum wire sweep (Y_1) filled time (Y_2) and void in package (Y_3), and were selected based on the highest-order polynomials, the significant additional terms and the absence of aliased models through the software. The best fitting was the quadratic model (Eqs. (4.1)– (4.3)) for all significant model terms (values of ''Prob> F'' less than 0.05) as suggested by the software.

Based on the sequential model sum of squares, the models for wire sweep and filling time percentages reduce were selected based on the highest order polynomials where the additional terms were significant and the models were not aliased. The models were coded as Y_1, $Y_2$and $Y_3$for wire sweep, filling time and void respectively.

The quadratic model for wire sweep, filling time and void terms, Y_1, $Y_2$and Y_3 were selected as suggested by the software and are shown in Eqs. (4.1), (4.2) and (4.3). The independent variables in the models were inlet pressure, wire diameter and vent height and were coded as A, B, and C, respectively. The final empirical models used to generate coded factors for each variable are as follows:

$$Y_1 = 0.8649215 + 0.2915288A - 0.6741609B - 0.1584183C + 0.1269982B^2 - 0.2238325AB - 0.09248875AC + 0.14813BC \quad (4.1)$$

$$Y_2 = 7.7125 - 3.05A - 3.6C + 1.625AC \quad (4.2)$$

$$Y_3 = 0.265893 - 1.21424A + 0.6958B - 3.56967C + 3.584086C^2 + 0.772815AB + 1.192763AC - 1.02154BC \quad (4.3)$$

The quality of the model was evaluated based on the coefficient of determination in addition to the ANOVA statistical analysis. The ANOVA results for the quadratic model for wire sweep, filling time and void percentage reduce are shown in Table 4.6 – 4.8.

Tables 4.7 – 4.9 show the ANOVA results for the models (Y_1–Y_3). In the ANOVA analysis, the quality of the model was evaluated according to the coefficient of determination (R^2). The information from the ANOVA analysis showed the R^2 for every empirical equation (Eqs. (4.1)–(4.3)) were 0.98, 0.99, and 0.96 for responses Y_1 to Y_3; meanwhile, the standard deviations of each model were 0.08, 0.31, and 0.88. The R^2 values of all models were considerably high. Thus, the percentages of total variability of each empirical model were 98% (Y_1), 99% (Y_2), and 96% (Y_3), respectively.

Table 4.8 ANOVA of quadratic model for maximum wire sweep (Y_1) with operating parameters (Inlet pressure (A), Wire diameter (B), and Vent height (C))

Source	Sum of Squares	DF	Mean Square	F Value	Prob> F
Model (Y_1)	6.371207	7	0.91017	121.371	< 0.0001
A	0.84989	1	0.84989	113.333	< 0.0001
B	4.544929	1	4.54493	606.065	< 0.0001
C	0.250964	1	0.25096	33.4659	< 0.0001
B2	0.080643	1	0.08064	10.7537	0.0066
AB	0.400808	1	0.40081	53.4477	< 0.0001
AC	0.068433	1	0.06843	9.12557	0.0106
BC	0.17554	1	0.17554	23.4082	0.0004
Residual	0.089989	12	0.0075		
Lack of Fit	0.089989	7	0.01286		
Pure Error	0	5	0		
Std. Dev.	0.086597		R-Squared	0.98607	
Mean	0.928421		Adj R-Squared	0.97795	
C.V.	9.327366		Pred R-Squared	0.80463	
PRESS	1.262305		Adeq Precision	44.0509	

Sample ANOVA calculations for maximum wire sweep (Y_1) are presented in Appendix I.

Table 4.9 ANOVA of quadratic model for filling time (Y_2) with operating parameters (Inlet pressure (A), Wire diameter (B), and Vent height (C))

Source	Sum of Squares	DF	Mean Square	F Value	Prob> F
Model (Y_2)	243.75	3	81.25	847.251	< 0.0001
A	93.025	1	93.025	970.037	< 0.0001
C	129.6	1	129.6	1351.43	< 0.0001
AC	21.125	1	21.125	220.285	< 0.0001
Residual	1.534375	16	0.0959		
Lack of Fit	1.534375	11	0.13949		
Pure Error	0	5	0		
Std. Dev.	0.309675		R-Squared	0.99374	
Mean	7.7125		Adj R-Squared	0.99257	
C.V.	4.015231		Pred R-Squared	0.98823	
PRESS	2.887262		Adeq Precision	96.0353	

Table 4.10 ANOVA of quadratic model for void in package (Y_3) with operating parameters (Inlet pressure (A), Wire diameter (B), and Vent height (C))

Source	Sum of Squares	DF	Mean Square	F Value	Prob> F
Model (Y_3)	235.7469	7	33.6781	43.346	< 0.0001
A	14.74382	1	14.7438	18.9763	0.0009
B	4.841383	1	4.84138	6.23119	0.0281
C	127.4256	1	127.426	164.005	< 0.0001
$C2$	64.22837	1	64.2284	82.6663	< 0.0001
AB	4.77794	1	4.77794	6.14953	0.0290
AC	11.38147	1	11.3815	14.6487	0.0024
BC	8.348394	1	8.34839	10.745	0.0066
Residual	9.323517	12	0.77696		
Lack of Fit	9.323517	7	1.33193		
Pure Error	0	5	0		
Std. Dev.	0.881453		R-Squared	0.96196	
Mean	2.057936		Adj R-Squared	0.93976	
C.V.	42.83191		Pred R-Squared	0.57362	
PRESS	104.4925		Adeq Precision	21.0223	

4.8.3 Effect of Factors on Wire Sweep, Filling Time and Void

The sensitivity of each factor was identified through the perturbation plots as presented in Figure 4.72a and 7.72b for (a) wire sweep, (b) filling time and (c) void. Wire sweep was mostly influenced by inlet pressure and wire diameter as compared to the outlet vent height (Figure 4.72a). Inlet pressure and vent height appeared to be the most influential factor for filling time and void (Figure 4.72b).However, the vent height had shown a dominant effect to percentage of void in the encapsulation process (Figure 4.72 (c)).

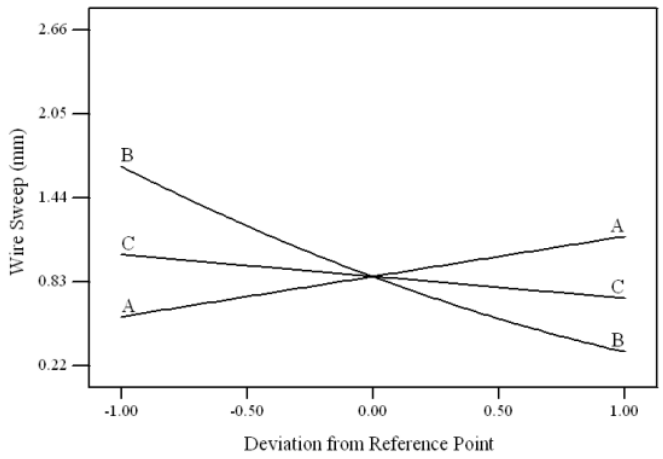

(a) Wire sweep

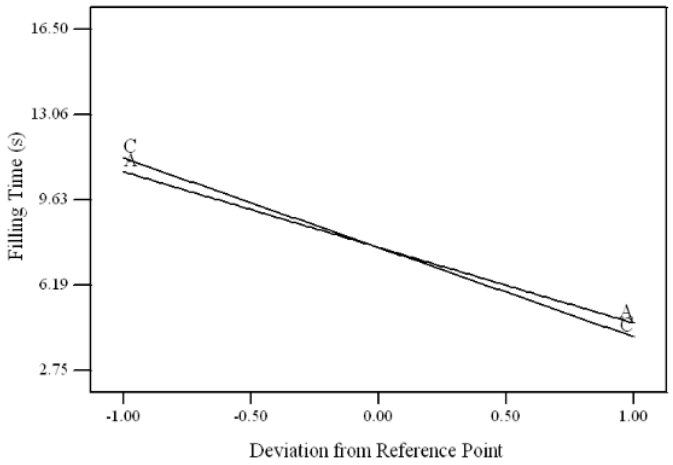

(b) Filling time

Figure 4.72a Perturbation plot for: (a) Wire sweep and (b) Filling time. Coded values for each factor are referring to the actual values listed in Table 3.2. (Note: *A* = inlet pressure, *B* = wire diameter, and *C* = vent height)

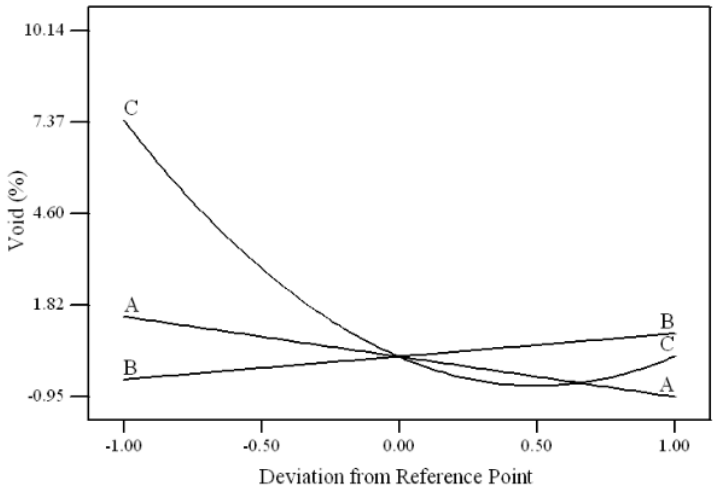

(c)Void

Figure 4.72b Perturbation plot for: (c) Void. Coded values for each factor are referring to the actual values listed in Table 3.2. (Note: *A* = inlet pressure, *B* = wire diameter, and *C* = vent height) (Continued).

The factors exhibited crucial effects on the particular responses in the PBGA encapsulation process are as mentioned above. Inlet pressure (*A*) showed a significant effect to the wire sweep, percentage of void formation and filling time. This situation may be ascribed to the EMC flow in the feeding process, whereas at high pressure, faster flow front shortens the filling time and reduces the void formation (Khor et al., 2012b). The void formation can be minimized through high pressure and low transfer speed (Liu et al, 2004a).From the perturbation graphs (Figure 4.72 (b) and (c)), the design of the vent height (*C*) crucially affected the filling time and void formation. The increased in wire diameter reduced the wire sweep and the increased vent height reduced the filling time. This may provide a challenge to the package designer when using a small wire diameter with the vent height arrangement in the moulded PBGA package. Alternatively, this problem can be overcome by increasing the number of wires in the package; meanwhile, the application of high density (number) of wires had reduced the wire sweep (Jong, 2005).

Moreover, vent height (*C*) mainly affected to the filling time and void formation as illustrated in Figure 4.72(b) and (c). Small wire diameter experienced high wire deformation in the encapsulation process. The wire experienced an interaction with continuous EMC flow and the unstable flow front induced unstable forces acted on the wires. As mentioned in sub Section 4.6.2, void formation would induce the delamination (Tay and Lin, 1999) problem in the actual size PBGA package.

Other factors such as inlet design (Lee et al., 2008a), vent arrangement (Chai and Zohar, 1999; Lee et al., 2008b) may influence the void formation in the IC encapsulation.

Figure 4.73a and 7.73b depicts the 3D surface response and contour plots of the quadratic model, which was plotted using Design Expert software to study the interactive relationship between each factor and responses. In the 3D surface response, the selection of two variables and a constant variable was determined according to the level of sensitivity towards the responses that depended on the perturbation plots in Figures 4.72.

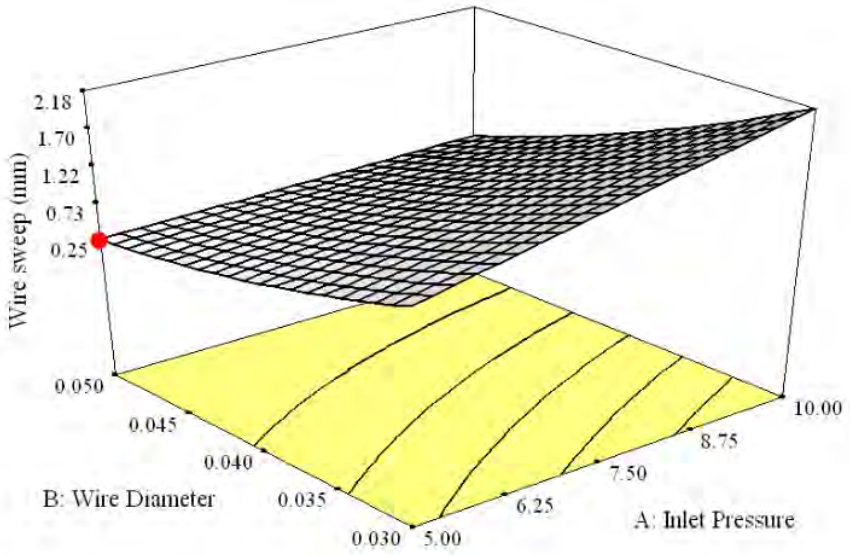

(a) Wire sweep.

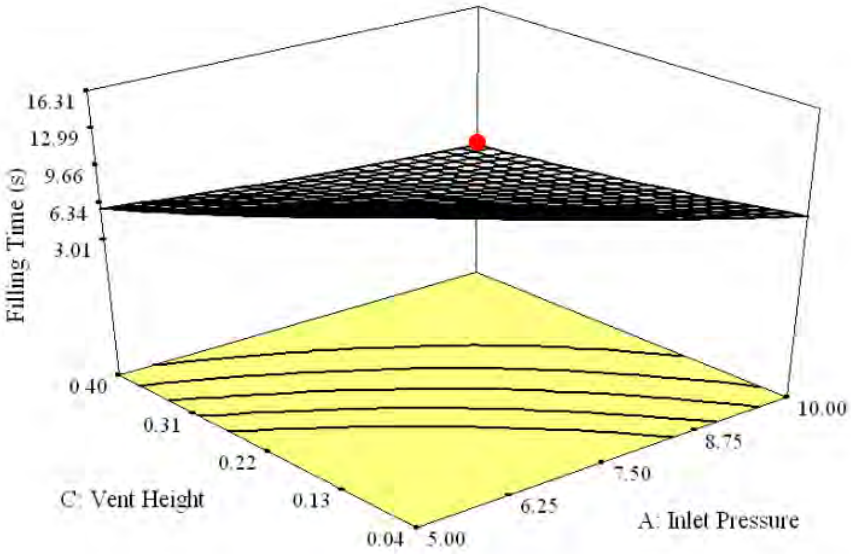

(b) Filling time.

Figure 4.73a 3D response surfaces for: (a) Wire sweep and (b) Filling time.

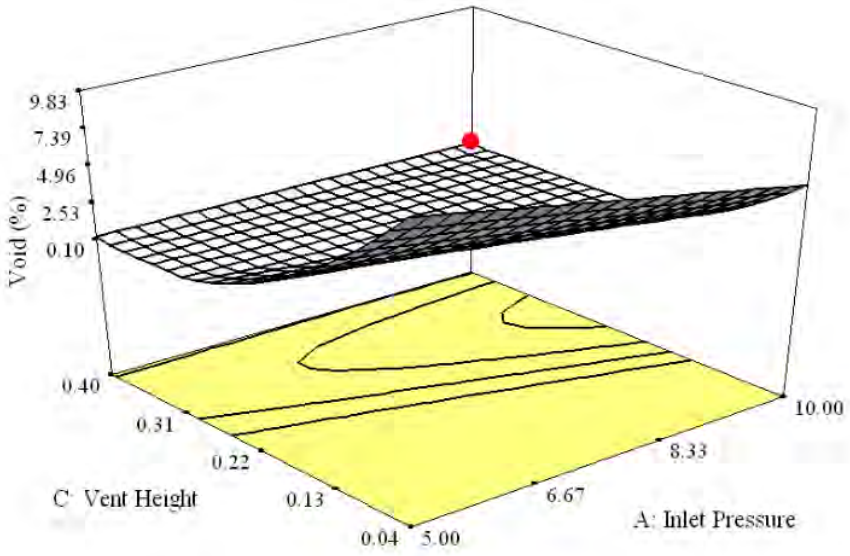

(d) Void.

Figure 4.73b 3D response surfaces for: (c) Void (continued).

The minimum wire sweep(Y_1) was identified at 0.05 mm wire diameter and 5 MPa inlet pressure (red dot). Similarly, two variables were also selected for plotting 3D surface response for responses Y_2 and Y_3. Inlet pressure and vent height were selected to vary with filling time and void formation due to their significance as shown in Figure 4.72(b) and(c). The shortest filling time was found at 0.4 mm of vent height and 10MPa of inlet pressure. However, the lower void formation was achieved also at 0.4 mm of vent height and 10MPa of inlet pressure. The minimum value of the responses (Y_1–Y_3) varied with two of the most influential factors is summarized in Table 4.10.

Table 4.11 Minimum value of the responses varied with two of the most influential factor

Response	Y_1 (mm)	Y_2 (s)	Y_3(%)
2 of the most influence factors	*A*	*A*	*A*
	B	*C*	*C*
Minimum Value	0.25	4.46	2.52

4.8.4 Optimisation of Simulation Conditions

The solution for the optimized factors in order to minimize the responses as suggested by Design Expert software was examined through the FSI simulation at A = 5.57 MPa, B = 0.05 mm and C = 0.36 mm. The comparison results between model response and simulation are listed in Table 4.11. The discrepancy in results varied within the range of 0.20–11.88%, which demonstrates that reasonable prediction can be achieved using the empirical model. The interactive relationship and optimum value of each factor were successfully determined using the response surface methodology.

The percentage of wire sweep for all wires of simulation optimization result is shown in Figure 4.74. The isometric view in detail for all wire sweeps is shown in Appendix J. It can be found that the maximum wire sweep is at wire nos. 3 and 11 with wire sweep index about 8 % and 7.5 % respectively. The trend of the wire sweep of each position was similar with previous work by Su et al. (2003) and Wu et al. (1998).

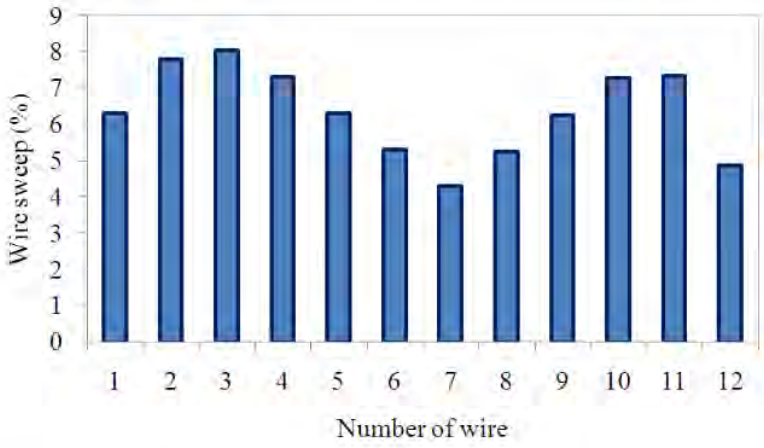

Figure 4.74 Percentage of wire sweep for all wires of simulation optimization result.

The Von Mises and Shear Stress formation for all wires of simulation optimisation result are shown in Figure 4.75 and 4.76 respectively.

Table 4.12 Validation of model response and simulation for factor a) inlet pressure (5.57 MPa), b) wire diameter (0.05 mm) and c) vent height (0.36 mm).

	Response (*Y*)		
	Wire sweep (mm)	Filling time (s)	Void (%)
Model Response	0.86	7.71	0.27
Simulation	0.98	7.70	0.24
Error (%)	11.88	0.20	11.81
Standard deviation	0.08	0.01	0.02

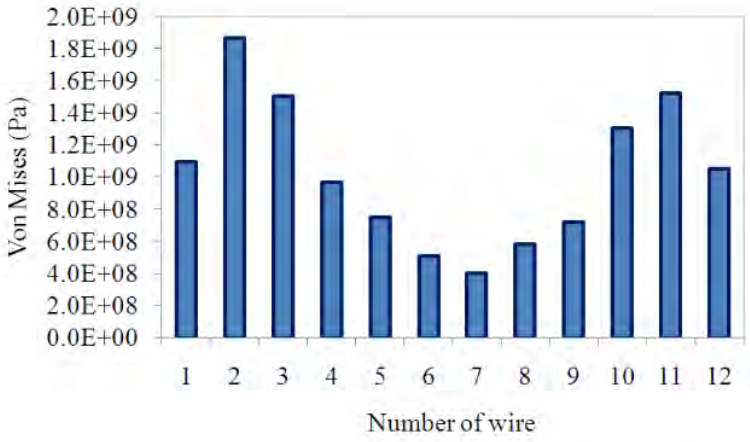

Figure 4.75 Von Mises for all wires of simulation optimization result.

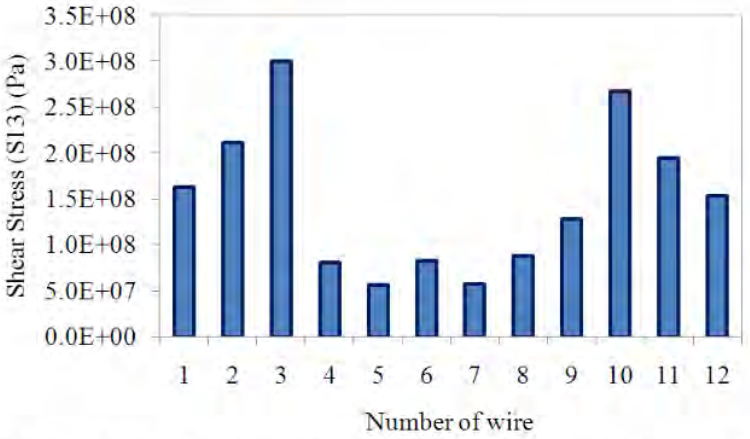

Figure 4.76 Shear Stress for all wires of simulation optimization result.

Whereas the detailed view of maximum von Mises stress and Shear stress distribution for wire 4 of simulation optimization result are shown in Figure 4.77 and 4.78 respectively, that demonstrates the highest stress around un-deformed fixed boundary, especially near to the wire bonds (isometric view of von Mises and Shear Stress in detail is shown in Appendix K). According to the simulation, stress distribution varied according to the fluid force. At 6.0s, maximum stress was concentrated at the joint between the die and the bumps or bending region (red circle). This means the sweep displacement of wire is dominated by the bending moment instead of the twisting moment (Kung et al., 2006a).

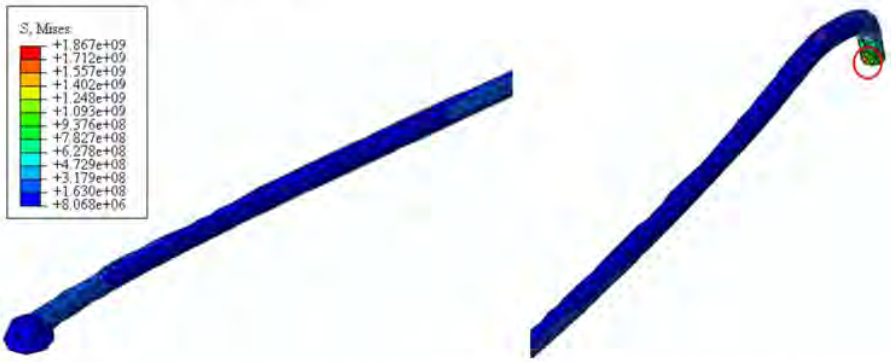

Figure 4.77 Detailed view of maximum von Mises stress distribution for Wire 4 of simulation optimization result.

Figure 4.78 Detailed view of maximum Shear stress (S13) distribution for Wire 4 of simulation optimization result.

4.9 Summary

This chapter has explained the results from the research work in the encapsulation process of both the scale-up and the actual size PBGA. This study started with the grid independent test for all cavity designs. Grid independence test is performed to obtain the optimum mesh size. Five different mesh sizes were tested, and the corresponding filling percentage were calculated for a scale-up single die with four-wire in a PBGA package, a scale-up single and stacked die with eight-wire in a PBGA package and also finally an actual size PBGA.

The experimental and model validation of fluid flow and wire deformation for scaled-up four and eight-wire PBGA and actual size PBGA encapsulation process were obtained for the validation of simulation.

Several parameters for the observation of wire sweep behaviour of scaled up and actual size PBGA such as stacking die, inlet and outlet arrangement and inlet pressure were studied. The wire sweep profiles and pressure distribution were analyzed and presented. The flow front of test fluid and EMC and wire sweep phenomenon could be simultaneously visualised through the FSI simulation and experiment.

The physical and process parameters of the PBGA package in the encapsulation process were optimized through RSM. The influence of three factors (i.e., inlet pressures (A), wire diameter (B), and vent height (C)) were modelled and optimized to minimise wire sweep (Y_1), filling time (Y_2), and void formation (Y_3).

REFERENCES

Books:

Ardebiri,H., Pecht, M. (2009)Encapsulation Technologies for Electronic Applications.Linacre House, Jordan Hill, Burlington, USA, Elsevier.

Montgomery, D.C.,(2009) Design and Analysis of Experiments, seventh ed. John Wiley&Sons, New York.

Journal:

Abdullah, I., Ahmad, I., Talib,M. Z. M., Bachok,N. N., Mokhtar, U., Said A.E.(2008a), Warpage and Wire Sweep Analysis of QFN Molded Array Strip Using Modeling and Experimental Methods.Solid State and Technology, 16(2), p. 153-163.

Abdullah, M. K., Abdullah, M. Z., Kamaruddin, S., Ariff, Z. M. (2007a) Study of Flow Visualization in Stacked-chip Scale Packages (S-CSP).International Communications in Heat and Mass Transfer. 34, p. 820-828.

Abdullah, M. K., Abdullah, M. Z., Mujeebu, M. A., Kamaruddin, S., Ariff, Z. M.(2008b)Study on the Effect of Stack Thickness during Encapsulation of Stacked-chip Scale Packages (S-CSP).Journal of International Microelectronics and Electronics Packaging 5(2),p. 62-67.

Abdullah,M. K., Abdullah,M. Z., Mujeebu,M. A., Kamaruddin, S. (2009) A Study on the Effect of Epoxy Molding Compound (EMC) Rheology during Encapsulation of Stacked-chip Scale Packages (S-CSP).Journal of Reinforced Plastics and Composites. 28(20), p. 2527-2538.

Abdullah, M. K.,Abdullah, M. Z., Mujeebu, M. A., Ariff, Z. M., Ahmad, K. A. (2010) Three-Dimensional Modeling to Study the Effect of Die-stacked Shape on Mould Filling during Encapsulation on Microelectronic Chips. IEEE Transactions on Advanced Packaging.33(2), p. 438-446.

Abdullah, S., Aziz, Z.A., Ahmad, I. I., Abdullah, M.F.(2008c) Low Looping Challenges in The QFN Wire Bonding Process. Solid State Science and Technology, 16(2), p. 25-32.

Adlan, M.N.B., Palaniandy, P., Aziz, H.A. (2011) Optimization of Coagulation and Dissolved Air Flotation (DAF) Treatment of Semi-aerobic Landfill Leachate

Using Response Surface Methodology (RSM).Journal of Desalination. 277, p. 74-82.

Brand,J.M., Ruggero,S.A., Shah,A.J. (2008) Wire Sweep Reduction via Direct Cavity Injection during Encapsulation of Stacked Chip-scale Packages.Journal of Electronics Packaging. 130, p. 011011-(1-6).

Chai, H. and Zohar, Y. (1999) Wire Sweep Due to Transfer Molding in A 160L QFP Package under Steady-State Condition. ASME Journal of Electronic Packaging. 121, p. 137-142.

Chang, R. Y., Yang, W. H., Hwang, S. J., Su, F. (2004) Three Dimensional Modeling of Mold Filling in Microelectronics Encapsulation Process. IEEE Transactions on component and Packaging Technologies. 27(1), p. 200-209.

Gokce A.and Advani, S. G. (2004)Simultaneous Gate and Vent Location Optimization in Liquid Composite Molding Processes, Composites Part A. 35,p. 1419-1432.

Han,S.J., Huh,Y.J. (2000) A Study of Wire Sweep During Encapsulation of Semiconductor Chips.Journal of the Microelectronics and Packaging Society. 7(4), p. 17-22.

Han, S., Wang, K.K. (1995a) A Study on Wire Sweep in Encapsulation of Semiconductor Chips Using Simulated Experiments. Journal of Electronics Packaging.Transaction of the ASME, 117, p.178-184.

Han, S., Wang, K.K. (1995b) Effects of Fillers on Wire Sweep inSemiconductor Chip Encapsulation. IEEE Transaction on Components, Packaging, and Manufacturing Technology-Part B, 18(4), p. 744-750.

Hassan, H., Regnier, N., Pujos, C., Defaye, G. (2008) Effect of viscous dissipation on the temperature of the polymer during injection molding filling, Polymer Engineering and Science 48,p. 1199–1206.

Ishiko,M, Usui,M, Ohuchi,T, Shirai,M. (2006) Design Concept for Wire Bonding Reliability Improvement by Optimizing Position in Power Devices.Microelectronics Journal. 37, p. 262-268.

Jong,W.R., Chen,Y.R., Kuo,T.H. (2005) Wire Density in CAE Analysis of High Pin Count IC Packages: Simulation and verification.International Communications in Heat and Mass Transfer. 32, p. 1350-1359.

Khor, C.Y., Abdullah, M.K., Abdullah, M.Z., Mujeebu, M.A., Ramdan, D., Majid, M.F.M.A., Ariff,Z.M.. (2010a) Effect of Vertical Stacking Dies on Flow

Behavior of Epoxy Molding Compound during Encapsulation of Stacked-chip Scale Packages.Heat Mass Transfer. 46, p. 1315-1325.

Khor,C.Y., Mujeebu,M.A., Abdullah,M.Z., Che Ani,F. (2010b) Finite Volume Based CFD Simulation of Pressurized Flip-chip Underfill Encapsulation Process.Journal of Microelectronics Reliability.50, p. 98-105.

Khor, C.Y., Ariff, Z.M., Che Ani, F., Mujeebu, M.A., Abdullah, M.K., Abdullah, M.Z., Joseph,M.A..(2010c) Three-dimensional Numerical and Experimental Investigations on Polymer Rheology in Meso-scale Injection Molding.International Communicationin Heat and Mass Transfer. 37, p. 131-139.

Khor, C.Y., Abdullah, M.Z., Abdullah, M.K., Mujeebu, M.A., Ramdan, D, Majid, M.F.M.A., Ariff, Z.M., Abdul Rahman, M.R. (2011) Numerical Analysis on The Effects of Different Inlet Gates and Gap Heights in TQFP Encapsulation Process.International Journal of Heat and Mass Transfer.54, p. 1861-1870.

Khor, C.Y., Abdullah, M.Z., Tan, H.J.T., Leong, W.C., Ramdan, D. (2012a) Investigation of the Fluid/Structure Interaction Phenomenon in IC Packaging.Microelectronics Reliability. 52(1), p. 241-252.

Khor, C.Y., Abdullah, M.Z. (2012a) Optimization of IC Encapsulation Considering Fluid/Structure Interaction Using Response Surface Methodology. Simulation Modelling Practice and Theory, 29, p. 109-122.

Khor, C.Y., Abdullah, M.Z. (2012b)Modeling and Analysis of the Effect of Stacking Chips withTSVS in 3D IC Package Encapsulation Process.Maejo International Journal Science Technology.2012, 6(02), 159-185.

Kim,W., Bae,J.W., Choi,I.D., Kim,Y.S. (1999) Thermally Conductive EMC (Epoxy Molding Compound)for Microelectronic Encapsulation.Polymer Engineering and Science. 39(4), p. 756-766.

Kung,H.K., Lee,J.N., Wang,C.Y. (2006a) The Wire Sweep Analysis Based on the Evaluation of the Bending and Twisting Moments for Semiconductor Packaging.Microelectronic Engineering. 83, p. 1931-1939.

Kung, H.K., Huang, B.W.(2006b) High-temperature Wire Sweep Characteristics of Semiconductor Package for Variable Loop-height WireBonding Technology.Microelectronic Engineering, 83, p. 197-205.

Kung,H.K., Sun,Y.P., Lee,J.N., Chen,H.S. (2008) A Method to Determine the Sweep Resistance of Wire Bonds for Microelectronic Packaging.Microelectronic Engineering. 85, p. 1902-1909.

Kung, H.K., Chen, H.S., Lu, M.C. (2012) TheWire Sag Problem in Wire Bonding Technology for Semiconductor Packaging. Microelectronics Reliability, http://dx.doi.org/10.1016/j.microrel.2012.08.017.

Lee, T.K., Han, S., Ko, Y. S., Kim, J.H. (2008a) Some Case Studies on Air Venting Analysis of Semiconductor Packages Using MOLFLOW. IEEE 10th Electronics Packaging Technology Conference. p. 444-449.

Liang,J.Z. (2001) Pressure Effect of Viscosity for Polymer Fluids in Die Flow.Polymer. 42, p. 3709-3712.

Lim, S. T., Lee, W. I. (2000) An Analysis of the Three-dimensional Resin Transfer Mold Filling Process. Composites Science and Technology. 60, p. 961-975.

Liu,D.S., Chao,Y.C., Wang,C.H.(2004a) Study of Wire Bonding Looping Formation in the Electronic Packaging Process Using the Three-dimensional Finite Element Method.Finite Elements in Analysis and Design. 40, p. 263-286.

Liu, S.L., Chen, G., Yong, M.S. (2004b) EMC Characterization and Process Study for Electronics Packaging.Thin Solid Films. 462-463, p. 454-458.

Mulgaonker, S. and Berg, H.M. (1996) Thermal Sensitivity Analysis for the 119 PBGA-A Framework for Rapid Prototyping.IEEETransactions on Components, Packaging, andManufacturing Technology-Part A, 19(1), March 1996, p. 66-74.

Nguyen,L., Quentin,C., Lee,W., Bayyuk,S., Bidstrup-Allen,S.A., Wang,S.T.(2000) Computational Modeling and Validation of the Encapsulation of Plastic Packages by Transfer Molding.Journal of Electronics Packaging. 122, p. 138-146.

Onodera, M., Meguro, K., Tanaka, J., Shinma, Y., Taya, K., and Kasai, J., 2007, Low-cost Vacuum Molding Process for BGA Using a Large Area Substrate,IEEE Transactions on Advanced Packaging, 30(4), November 2007, pp. 674-680.

Pei,C.C., Hwang,S.J. (2005a) Prediction of Wire Sweep during the Encapsulation of IC Packaging with Wire Density Effect.ASME Journal of Electronic Packaging. 127, p. 335-339.

Pei,C.C., Hwang,S.J. (2005b) Three-dimensional Paddle Shift Modeling for IC Packaging. Transactions of the ASME, 127, p. 324-334.

Reddy, A.M.K., Han, R., Gupta, M. (1998) Numerical and Experimental Investigation of Microchip Encapsulation.Journal of Reinforced Plastics and Composites. 17(1), p. 70-93.

Sato, M. Yokoi, H. (2000) Visualization Analysis of Melt Flow in IC Packaging Process along Thickness Direction. IEEE Transaction on Advanced Packaging. 23(4), p. 729-737.

Schreiber,A., Metsch,T., Kersken,H.P. (2005) A Problem Solving Environment for Multidisciplinary Couple Simulations in Computational Grids.Future Generation Computer System. 21, p. 942-952.

Schueller, R.D.,Plepys, A.P. (1996) Design of a Low Cost Wire BondTape Ball Grid Array Package. Circuit World, 22(3), p. 10-15.

Shojaei, A., Ghaffarian, S. R., Karimian, S. M. H. (2002) Numerical Simulation of Three-Dimensional Mold Filling Process in Resin Transfer Molding Using Quasi-steady State and Partial Saturation Formulations. Composites Science and Technology. 62, p. 861-879.

Su, J., Hwang, S.J., Su, F., Chen, S.K.(2003) An Efficient Solution for Wire Sweep Analysis in IC Packaging.ASME Journal of Electronic Packaging. 125, p. 139-143.

Tay, A.A.O., Lin, T.Y. (1999) Influence of Temperature, Humidity and Effect Location on Delamination in Plastic Packages. IEEE Transaction on Component Packaging Manufacturing Technology. Part A 22(4), p. 512-518.

Teng,S.Y., Hwang,S.J. (2008) Simulation and Experiments of Three Dimensional Paddle-shift for IC Packaging.Microelectronics Engineering. 28, p. 115-125.

Wang,H, Zhou,H, Zhang,Y, Li D. (2010) Stabilized Filling Simulation of Microchip Encapsulation Process.Microelectronics Engineering. 87, p. 2602-2609.

Wu, J.H., Tay, A.A.O., Yeo,K. S., Lim, T.B. (1998)A Three-dimensional Modeling of WireSweep Incorporating Resin Cure. IEEE Transactions on Components, Packaging, and Manufacturing Technology—Part B, 21(1), February 1998, p. 65-71.

Yang,H.Q., Mazumder,S., Lowry,S., Krishnan,A., Przekwas,A., Nguyen, L. (2001) Time Accurate, 3-D Computation of Wire Sweep during Plastic Encapsulation of Electronic Components.Journal of Pressure Vessel Technology.123, p.501-509.

Yang,S.Y., Jiang,S.C., Lu,W.S. (2000) Ribbed Package Geometry for Reducing Thermal Warpage and Wire Sweep during PBGA Encapsulation.IEEE Transactions on Components and Packaging Technologies. 23(4), p. 700-706.

Yao,F., Njoman,B., Chua,K.H., Lin, T.Y. (2005) New Encapsulation Development for Fine Pitch IC Devices.Microelectronics Reliability. 45, p. 1222-1229.

Yao,Y.F., Lin,T.Y., Chua,K.H. (2003) Improving the Deflection of Wire Bonds in Stacked Chip Scale Package (CSP).Microelectronics Reliability.43(12), p. 2039-2045.

Yigit, S., Schafer, M., Heck, M. (2008) Grid Movement Techniques and Their Influence on Laminar Fluid/Structure Interaction Computations.Journal of Fluids and structures. 24, p. 819-832.

Yong, T.P., Yoo, K.W., Joon, K.H., Kwang, Y.B. (2006) Warpage Analysis of FBGA (Fine Ball Grid Array) Package by the Altered EMC (Epoxy Molding Compound) Filler Contents, Key Engineering Material. 306-308, p.625-630.

Yoshihara, T., Yuki, M., Hayashida, T., Ohno,Y. (1999a) Factor Governing Wire Sweep in Plastic IC Encapsulation.Electronics Communication Japan.82(7), p. 59-67.

Yoshihara, T., Ohno, Y., Kusuhara, A., Fujita, H., Maeda, M. (1999b) Effects of Molding Compound on Wire Sweep in PlasticEncapsulated IC Packages. Electronics and Communications in Japan, Part 2, 82(11), p. 28-34.

Zhang, K. and Pecht, M., (2000) Effectiveness of Conformal Coatings on a PBGASubjected to Unbiased High Humidity, High Temperature Tests, MicroelectronicsInternational, vol. 17, no. 3, p. 16-20.

Proceedings/Sumposium/Conference:

Abdullah, I., Chiang, N.C., Mokhtar, U., Said, A., Talib, M.Z.M., Ahmad, I. (2007b) Warpage and Wire Sweep Analysis of QFN Molded Strip Using Experimental and Modeling Methods. In: Proceedings IEEE 9th Electronics Packaging Technology Conference, 10-12 Dec. 2007, p. 494-498.

Abdullah, S., Aziz, Z. A., Ahmad, I., Jalar, A., Abdullah, M.F. (2008d) Wire Sweep Issue in a Newly Developed Quad Flat No-lead(QFN) Semiconductor Package. In Proceedings: 7th WSEAS International Conference on Microelectronics, Nanoelectronics, Optoelectronics (MINO '08), Istanbul, Turkey, May 27-30, 2008, p. 40-44.

Bailey, J., Sett, S., Benko, R.J. (2006) A Fluid/Structure Interaction Analysis of the VernaFlo Flow Control Device, 2006 ABAQUS Users' Conference, p. 53-62.

Brunner, J., Qin, I.W., Chylak, B. (2004) Advanced Wire Bond Looping Technology for Emerging Packages. In:Proceedings IEEE International Electronics Manufacturing Technology Symposium, July 14-16, 2004, p. 85-90.

Chen, J.Y., Teng, S.Y., Hwang, S.J., Lee, H.H., Huang,D.Y., Lin, Y.J., Stoke Chen, Shen, G.S., Lily Wu (2007a) Prediction of Flow Induced Lead Deflection of Leadframe Assemblies in Plastic Encapsulation during Molding. In Proceedings: IEEE, 8th ICEP International Conference on Electronic Packaging Technology,14-17 Aug. 2007,p. 1-5.

Chou, Y.Y., Chiu, H.S., Yang, W.H. (2009) Three-dimensional CAE of Wire Sweep and Paddle Shift in Microchip Encapsulation. In Proceedings: IEEE 4thInternational Microsystems, Packaging, Assembly and Circuits Technology Conference, IMPAC 2009, 21-23 Oct. 2009, p.35-38.

Chylak, B., Levine, L., Babinetz, S., Kwon, O.D.(2006) Advanced Ultra-low-loop Wire Bonds. SEMICON China 2006, SEMI 2006.

Cohn, C.,Richman,R.M., Saxena,L.S., Shih, M.T. (1995) High I/O Plastic Ball Grid Array PackagesAT&T Microelectronics Experience. In Proceedings: IEEE Electronic Components and Technology Conference, 1995. Proceedings., 45th,21-24 May 1995, p. 10-20.

Ganesh, V.P. Sivakumar, M. (2002) Process Development for Ultra Low Loop Reverse Wire Bonding on Copper Bond Pad Metallization.In Proceedings: Electronics Packaging Technology Conference, 2002. 4th, 10-12 Dec. 2002, 356-360.

Gatzhammer,B., Mehl,M., Neckel,T. (2010) A Coupling Environment for Portioned Multiphysics Simulations Applied to Fluid/Structure Interaction Scenarios.In Proceedings: Computer Science I, p.681-689.

Han, J., Chen, H., Xue, K., Wong, F., Leung, K., Shiu, I., Wu, J. (2011a) Wire Sweep Study for SOT Package Array Matrix Molding with Simulation and Experimental Analysis. In Proceeding: IEEE International Conference on Electronic Packaging Technology & High Density Packaging, 8-11 Aug. 2011, p. 601-606.

Han, J., Chen, H., Wong, F., Leung, K., Shiu, I., Wu, J. (2011b) Effects of Package and Mold Cavity Structures on the Wire Sweep Behavior duringPackage Array

Transfer Molding. In Proceeding: IEEE International Conference on 13th Electronics Packaging Technology Conference, 7-9 Dec. 2011,p. 667-673.

JoppichW., Urschner M.K., the MpCCI team (2006), MpCCI—a tool for thesimulation of coupledapplications, CONCURRENCY AND COMPUTATION: PRACTICE AND EXPERIENCE*Concurrency Computat.: Pract. Exper.*2006; **18**:183–192

Kapoor,R, Kuan,L.B., Hao,L. (2004) Package Design Optimization and Materials Selection for Stacked Die BGA Package.In Proceedings: IEEE/CPMT/SEMI 2004 29thInternational Electronics Manufacturing Technology Symposium,San Jose, CA USA, July 14-16, 2004, p. 113-118.

Kung, H.K., Huang, C.H., Chanyshev, A.I. (2006c)On the Study of Loop Profiles in Improving the Sweep Stiffness of Wire Bond. In Proceedings: IEEE 8th Electronics Packaging Technology Conference, 2006, EPTC, 6-8 Dec. 2006, p. 472-477.

Lee,M.W., Khim,J.Y., Yoo,M., Chung,J.Y., Lee,C.H. (2006) Rheological Characterization and Full 3D Mold Flow Simulation in Multi-die Stack CSP of Chip Array Packaging.In Proceedings: IEEE,56thElectronics Components Technology Conference, San Diego, CA, p. 1029-1037.

Lee, M.W., Jung, W.K., Sohn, E.S., Lee, J.Y., Hwang, C.H., Lee, C.H. (2008a) A Study on the Rheological Characterization and Flow Modeling of Molded Underfill (MUF) for Optimized Void Elimination Design. In Proceedings: Electronic Components and Technology Conference 27-30 May, Lake Buena Vista, FL, p. 382-388.

Lee, T.K., Han, S., Ko, Y.S., Kim, J.H. (2008b) Some Case Studies on Air Venting Analysis of Semiconductor Packages using Moldflow™.In Proceedings: IEEE 10th Electronics Packaging Technology Conference. 9-12 Dec. 2008, p. 444-449.

Liu, J.M., Yao, J.Z., Wei, G., Lu, Y.S. (2007a) Wire Sweep Improvement Study for Fine Pitch Device. In Proceedings: IEEE 2007 9th Electronics Packaging Technology Conference, 10-12 Dec. 2007, p.61-65.

Liu, J.M., Lu, Y.S., Pang, X.S. (2007b) FFT (Flow Free Thin) Mold Study for 44 μm Fine Pitch Device Application, In Proceeding: CS MANTECH Conference, 14-17 May 2007, p. 25-28.

Lu, X., Xu, L., Lai, H., Du, X., Liu, J., Cheng, Z. (2009) Studies on Microstructure of Epoxy Molding Compound (EMC)-Leadframe Interfaceafter Environmental

Aging.In Proceedings: IEEE 2009 International Conference on Electronic Packaging Technology & High Density Packaging (ICEPT-HDP), 10-13 Aug. 2009,p. 1051-1053.

Muniandy, K., Ruzaini, I., Wei, S.K. (2006) Top-gate Molding Process Deveopment of Cavity Down TBGA for High Density Wire Bonding and Low K Dielectric Wafer Technology Application. In Proceedings: International Electronic Manufacturing Technology, IEMT, Putrajaya, Malaysia, p. 390-395.

Nguyen, L.T. and Lim, F.J.(1990) Wire Sweep during Molding of Integrated Circuits. In Proceedings: IEEE Conference, 40th Electronic Components and Technology Conference, 1990, 20-23 May 1990, p. 777-785.

Nguyen, L., Jackson, J., Teo, C.H., Chillara, S., Asanasavest, C., Ho, D., Rauhut, H (1997) Wire Sweep Control with Mold Compound Formulations.In: Proceedings., 47thElectronic Components and Technology Conference. 18-21 May 1997, p. 60-71.

Nguyen, L.T., Quentin, C.G., Lee, W.W. (1999) Flow Modeling and Visualization of the Transfer Molding of Plastic Ball Grid Array Packages.In: IEEE 1999 Proceedings. 49thElectronic Components and Technology Conference, p. 177-184.

Qin, H.B., Li, X.P., Zhang, X.P. (2012) Solder Volume Effects on Fatigue Life of BGA Structure Cu/Sn-3.0Ag-0.5Cu/Cu Interconnects. In Proceedings: EMAP 2012, The 14th International Conference on Electronic Materials and Packaging, December 2012, Citygate, Lantau Island, Hong Kong, p. 360-366.

Schueller, R.D., Aeschliman, D., Han, C.T. (1997) Performance and Reliability of a Cavity DownTape BGA Package. In: IEEE EPTC ConferenceProceedings of the 1997 1stElectronic Packaging Technology Conference,8-10 Oct 1997, p. 151-162.

Shu, W.K. (1996) PBGA Wire Bonding Development. In: IEEE Proceedings., 46thElectronic Components and Technology Conference, 28-31 May 1996, p. 219-225.

Sze, H.M.W., Papageorge, M. (1998) Encapsulation Selection, Characterization and Reliability for Fine Pitch BGA (fpBGA™), ASAT, LTD, Hongkong, p.1-7.

Wintergerste, T. (2002) Computational of Fluid-Structure Interaction in a Static Mixer Using MpCCI. In Proceedings: ASME Pressure Vessels and Piping Conference (PVP2002) 5-9August, 2002, Vancouver, BC, Canada, p. 57-65.

Yang,W.H., Hsu,D.C., Yang,V, Chang,R.Y., Su,F, Huang,S.J. (2004) Three Dimensional CAE of Wire-sweep in Microchip Encapsulation.In Proceedings: Soc.PlasticsEngineering, Technical Conference-ANTEC, Conference Proceeding, Brookfield, IL, 2, p.1679-1683.

Tay,A.A.O., Lee, W.H. (2002) Transient Three Dimensional Simulation of Mold Filling and Wire Sweep in an Over Mold BGA Package.In Proceedings:IEEE 2002, 52nd Electronics Component Technology Conference, San Diego, CA, 2002, p. 897-904.

Thesis:

Chen,Y.R. (1990) Mold Flow Simulation and Wire Sweep in IC Encapsulation, M.S. Thesis, Mech. Eng., Christian Univ. of Chun Yuan, Taiwan.

Pei, C.C. (2004) Wire Sweep and Paddle Shift Modeling of IC Packages During Encapsulation Process, M.S. Thesis, Mech. Eng., National Cheng Kung Univ., Tainan, Taiwan.

Others:

MpCCI 3.1.0-1 Documentation Part I Overview, Fraunhofer Institute for Algorithms and Scientific Computing SCIA, Germany, January 2009.

Mawer A. (1996) Plastic Ball Grid Array (PBGA). Motorola Semiconductor Technical Data.Motorola Fast Sram, P. 1-27.

Michael, S., Halger, L., Markus, H. (2005) Implicit Partitioned FSI Coupling. Resumepoerle 1er Colloqkie du GDR Interaction Fluid-Structure, 26-27 Sept 2005.

National Semiconductor Corporation (2000),Semiconductor Packaging Assembly Technology. www.national.com.

Plastic Ball Grid Array (PBGA), Application Report, Texas Instruments, Submit Documentation Feedback. SSZA002–August 2009, p. 1-17.

Prior, B. Low Cost, Small Form Factor Packaging.BiTS Workshop 2010 Archive, Comprise the Proceedings of the 2010 BiTS Workshop, p. 1-8.

Wolf, K. (2007) MpCCI the General Code Coupling Interface. Dynamore GmbH, LS-Dyna Anwenderforum. p. 1-8.

Internet Source:

Fraunhofer Institute for Algorithms and Scientific Computing SCIA.(2009, Jan.).MpCCI 3.1.0-1 Documentation Part I Overview, SanktAugustin, Germany [Online]. Available: http://www.scai.fraunhofer.de/mpcci

Thirifay,F., Geuzaine,P. (2008)Numerical simulations of fluid-structure interaction problem using MpCCI [Online].Available: http://mecanique.in2p3.fr/JU-samtech/ proceedings/03_16_CENAERO_Delanaye/ 03_16_CENAERO_Delanaye.pdf

Buku

ORIGINALITY REPORT

71%	48%	45%	%
SIMILARITY INDEX	INTERNET SOURCES	PUBLICATIONS	STUDENT PAPERS

PRIMARY SOURCES

1	eprints.usm.my Internet Source	28%
2	D. Ramdan, M. Z. Abdullah, ChuYee Khor, Wei Chiat Leong, Wei Keat Loh, Chun Keang Ooi, Renn Chan Ooi. "Fluid/Structure Interaction Investigation in PBGA Packaging", IEEE Transactions on Components, Packaging and Manufacturing Technology, 2012 Publication	9%
3	Dadan Ramdan, Zulkifly Mohd Abdullah, Muhammad Abdul Mujeebu, Wei Keat Loh, Chun Keang Ooi, Renn Chan Ooi. "FSI Simulation of Wire Sweep PBGA Encapsulation Process Considering Rheology Effect", IEEE Transactions on Components, Packaging and Manufacturing Technology, 2012 Publication	7%
4	Dadan Ramdan, Darianto, C. Y. Khor. "Optimization of PBGA encapsulation considering fluid/structure interaction using response surface methodology", 2016 2nd	6%

International Conference of Industrial, Mechanical, Electrical, and Chemical Engineering (ICIMECE), 2016
Publication

5	core.ac.uk Internet Source	3%
6	eprints.undip.ac.id Internet Source	3%
7	C.Y. Khor, M.Z. Abdullah. "Optimization of IC encapsulation considering fluid/structure interaction using response surface methodology", Simulation Modelling Practice and Theory, 2012 Publication	2%
8	Dadan Ramdan, Usman Harahap, Mohd. Zulkifli Abdillah. "Fluid structure interaction simulation in IC encapsulation process", 2013 International Conference on QiR, 2013 Publication	1%
9	Huang-Kuang Kung, Jeng-Nan Lee, Chin-Yu Wang. "The wire sweep analysis based on the evaluation of the bending and twisting moments for semiconductor packaging", Microelectronic Engineering, 2006 Publication	1%
10	Khor, C.Y.. "Investigation of the fluid/structure interaction phenomenon in IC packaging",	1%

Microelectronics Reliability, 201201
Publication

11 A.A.O. Tay, W.H. Lee. "Transient three dimensional simulation of mold filling and wire sweep in an overmold BGA package", 52nd Electronic Components and Technology Conference 2002. (Cat. No.02CH37345), 2002 — 1%
Publication

12 Ramdan, D.. "Effects of outlet vent arrangement on air traps in stacked-chip scale package encapsulation", International Communications in Heat and Mass Transfer, 201203 — <1%
Publication

13 Khor, C.Y., and M.Z. Abdullah. "Optimization of IC encapsulation considering fluid/structure interaction using response surface methodology", Simulation Modelling Practice and Theory, 2012. — <1%
Publication

14 Jiale Han, Haibin Chen, Fei Wong, Karina Leung, Ivan Shiu, Jingshen Wu. "Effects of package and mold cavity structures on the wire sweep behavior during package array transfer molding", 2011 IEEE 13th Electronics Packaging Technology Conference, 2011 — <1%
Publication

Internet Source

<1%

16 H ARDEBILI. "Encapsulation Process Technology", Encapsulation Technologies for Electronic Applications, 1994
Publication

<1%

17 doaj.org
Internet Source

<1%

18 H. Chai, Y. Zohar. "Wire Sweep Due to Transfer Molding in a 160L QFP Package Under Steady-State Conditions", Journal of Electronic Packaging, 1999
Publication

<1%

19 C.Y. Khor, M.Z. Abdullah, M.K. Abdullah, M.A. Mujeebu, D. Ramdan, M.F.M.A. Majid, Z.M. Ariff, M.R. Abdul Rahman. "Numerical analysis on the effects of different inlet gates and gap heights in TQFP encapsulation process", International Journal of Heat and Mass Transfer, 2011
Publication

<1%

20 Soldering & Surface Mount Technology, Volume 26, Issue 3 (2014-09-16)
Publication

<1%

21 W.R. Jong, Y.R. Chen, T.H. Kuo. "Wire density in CAE analysis of high pin-count IC packages: Simulation and verification", International

<1%

Communications in Heat and Mass Transfer, 2005
Publication

22 www.ukm.my
Internet Source
<1%

23 Huang-Kuang Kung, Hung-Shyong Chen, Ming-Cheng Lu. "The wire sag problem in wire bonding technology for semiconductor packaging", Microelectronics Reliability, 2013
Publication
<1%

24 M. K. Abdullah. "A Study on the Effect of Epoxy Molding Compound (EMC) Rheology During Encapsulation of Stacked-CHIP Scale Packages (S-CSP)", Journal of Reinforced Plastics and Composites, 10/01/2009
Publication
<1%

25 link.springer.com
Internet Source
<1%

26 Jiale Han, Haibin Chen, Ke Xue, Fei Wong, Karina Leung, Ivan Shiu, Jingshen Wu. "Wire sweep study for SOT package array matrix molding with simulation and experimental analysis", 2011 12th International Conference on Electronic Packaging Technology and High Density Packaging, 2011
Publication
<1%

27 opensiuc.lib.siu.edu
Internet Source

		<1%
28	C. Y. Khor, M. K. Abdullah, M. Z. Abdullah, M. Abdul Mujeebu, D. Ramdan, M. F. M. A. Majid, Z. M. Ariff. "Effect of vertical stacking dies on flow behavior of epoxy molding compound during encapsulation of stacked-chip scale packages", Heat and Mass Transfer, 2010 Publication	<1%
29	Sejin Han, K. K. Wang. "A Study on Wire Sweep in Encapsulation of Semiconductor Chips Using Simulated Experiments", Journal of Electronic Packaging, 1995 Publication	<1%
30	tfhrc.gov Internet Source	<1%
31	svn.drone.codehaus.org Internet Source	<1%
32	dspace.lib.cranfield.ac.uk Internet Source	<1%
33	Microelectronics International, Volume 26, Issue 2 (2009-05-03) Publication	<1%
34	Kung, H.K.. "High-temperature wire sweep characteristics of semiconductor package for	<1%

variable loop-height wirebonding technology", Microelectronic Engineering, 200602
Publication

35 M. S. Abdul Aziz, M. Z. Abdullah, C. Y. Khor, Z. M. Fairuz, A. M. Iqbal, M. Mazlan, Mohd Sukhairi Mat Rasat. "Thermal Fluid-Structure Interaction in the Effects of Pin-Through-Hole Diameter during Wave Soldering", Advances in Mechanical Engineering, 2015 <1%
Publication

36 technav.ieee.org <1%
Internet Source

37 C.Y. Khor, M.Z. Abdullah, Chun-Sean Lau, I.A. Azid. "Recent fluid–structure interaction modeling challenges in IC encapsulation – A review", Microelectronics Reliability, 2014 <1%
Publication

38 www.me.ncku.edu.tw <1%
Internet Source

39 Shim Kar Wei. "Top-Gate Molding Process Development of Cavity Down TBGA for High Density Wire Bonding and Low K Dielectric Wafer Technology Application", 2006 Thirty-First IEEE/CPMT International Electronics Manufacturing Technology Symposium, 11/2006 <1%
Publication

40	mdpi.com Internet Source	<1 %
41	Yejun Zhu, Habin Chen, Jingshen Wu, Ke Xue, Fei Wong, Paul Tsang. "Three dimensional flow analysis for incomplete fill failure during matrix array transfer molding of small QFN packages", 2013 14th International Conference on Electronic Packaging Technology, 2013 Publication	<1 %
42	fedetd.mis.nsysu.edu.tw Internet Source	<1 %
43	www.chemweb.com Internet Source	<1 %
44	Huang-Kuang Kung, Chi-Lung Hsieh. "Effects of Stacked Layers and Stacked Configurations on Wire Sweep and Wire Sag of Advanced Overhang/Pyramid Stacked Packages", Journal of Electronic Packaging, 2017 Publication	<1 %
45	Jason M. Brand, Salvatore A. Ruggero, Amip J. Shah. "Wiresweep Reduction via Direct Cavity Injection During Encapsulation of Stacked Chip-Scale Packages", ASME 2007 InterPACK Conference, Volume 1, 2007 Publication	<1 %

46	Mior Firdaus Mior Abd Majid, Mohamad Sabri Mohamad Sidik, Muhamad Husaini Abu Bakar, Khairul Shahril Shafee et al. "Chapter 1 Three Dimensional Simulation of Filling Process for Stacked-Chip Scale Packages", Springer Science and Business Media LLC, 2019 Publication	<1 %
47	www.coursehero.com Internet Source	<1 %
48	Chien-Chang Pei, Sheng-Jye Hwang. "Prediction of Wire Sweep During the Encapsulation of IC Packaging With Wire Density Effect", Journal of Electronic Packaging, 2005 Publication	<1 %
49	Adlan, M.N.. "Optimization of coagulation and dissolved air flotation (DAF) treatment of semi-aerobic landfill leachate using response surface methodology (RSM)", Desalination, 20110815 Publication	<1 %
50	Microelectronics International, Volume 24, Issue 3 (2007-07-29) Publication	<1 %
51	Kung, H.K.. "A method to determine the sweep resistance of wire bonds for	<1 %

Document Accepted 1/7/21

microelectronic packaging", Microelectronic Engineering, 200809
Publication

52	ndltd.ncl.edu.tw Internet Source	<1%
53	M. K. Abdullah, M. Z. Abdullah, M. A. Mujeebu, Horizon Gitano, Z. M. Ariff, R. Razali, K. A. Ahmad. "Three-Dimensional Modeling of Mold Filling in Microchip Encapsulation Process With a Matrix-Array Arrangement", Journal of Electronic Packaging, 2010 Publication	<1%
54	id.scribd.com Internet Source	<1%
55	www.cad-journal.net Internet Source	<1%
56	D. Ramdan, M.Z. Abdullah, N.M. Yusop. "Effects of outlet vent arrangement on air traps in stacked-chip scale package encapsulation", International Communications in Heat and Mass Transfer, 2012 Publication	<1%
57	H ARDEBILI. "Encapsulation Defects and Failures", Encapsulation Technologies for Electronic Applications, 2009 Publication	<1%

58	Internet Source	<1%
59	www.eng.nus.edu.sg Internet Source	<1%
60	www.fose1.plymouth.ac.uk Internet Source	<1%
61	www.ismans.fr Internet Source	<1%
62	Chu Yee Khor, Mohd Zulkifly Abdullah, Wei Chiat Leong. "Fluid/Structure Interaction Analysis of the Effects of Solder Bump Shapes and Input/Output Counts on Moulded Packaging", IEEE Transactions on Components, Packaging and Manufacturing Technology, 2012 Publication	<1%
63	dbicorporation.com Internet Source	<1%
64	Khor, C.Y.. "Study on the fluid/structure interaction at different inlet pressures in molded packaging", Microelectronic Engineering, 201110 Publication	<1%
65	Soldering & Surface Mount Technology, Volume 21, Issue 4 (2009-10-02) Publication	<1%

Document Accepted 1/7/21

66	botany.cs.tamu.edu Internet Source	<1%
67	www.hpl.hp.com Internet Source	<1%
68	www.scilit.net Internet Source	<1%
69	Yun Chen, Fuliang Wang. "Comparison of Fundamental Frequency and Sweep Resistance of Different Wire Loops Using Finite Element Model", International Journal of Structural Stability and Dynamics, 2015 Publication	<1%
70	hybrid-analysis.com Internet Source	<1%
71	leva.leeds.ac.uk Internet Source	<1%
72	publications.lib.chalmers.se Internet Source	<1%
73	www.inderscience.com Internet Source	<1%
74	Chien-Chang Pei, Sheng-Jye Hwang. "Three-Dimensional Paddle Shift Modeling for IC Packaging", Journal of Electronic Packaging, 2005 Publication	<1%

Document Accepted 1/7/21

75	eptc.elite.sg Internet Source	<1 %
76	onlinelibrary.wiley.com Internet Source	<1 %
77	researchoutput.ncku.edu.tw Internet Source	<1 %
78	www.eurojournals.com Internet Source	<1 %
79	International Journal of Numerical Methods for Heat & Fluid Flow, Volume 15, Issue 7 (2006-09-19) Publication	<1 %
80	dblp.dagstuhl.de Internet Source	<1 %
81	www.deepdyve.com Internet Source	<1 %
82	Khor, C.Y., M.Z. Abdullah, Chun-Sean Lau, and I.A. Azid. "Recent fluid–structure interaction modeling challenges in IC encapsulation – A review", Microelectronics Reliability, 2014. Publication	<1 %
83	Ya-Yuen Chou, Hsien-Sen Chiu, Jyh-Jer Jwo. "A numerical prediction of wire crossover applying to microchip encapsulation", 2011 6th International Microsystems, Packaging,	<1 %

Assembly and Circuits Technology Conference (IMPACT), 2011
Publication

84 doktori.uni-sopron.hu
Internet Source
<1%

85 Abdullah, M.K.. "Study of flow visualization in stacked-Chip Scale Packages (S-CSP)", International Communications in Heat and Mass Transfer, 200708
Publication
<1%

86 C.Y. Khor, M.Z. Abdullah, H.J. Tony Tan, W.C. Leong, D. Ramdan. "Investigation of the fluid/structure interaction phenomenon in IC packaging", Microelectronics Reliability, 2012
Publication
<1%

87 www.mdpi.com
Internet Source
<1%

88 Jason M. Brand, Salvatore A. Ruggero, Amip J. Shah. "Wiresweep Reduction via Direct Cavity Injection During Encapsulation of Stacked Chip-Scale Packages", Journal of Electronic Packaging, 2008
Publication
<1%

89 www.gaas.org
Internet Source
<1%

90 H.K. Kung, C.H. Huang, A.I. Chanyshev. "On the study of loop profiles in improving the
<1%

sweep stiffness of wire bond", 2006 8th Electronics Packaging Technology Conference, 2006
Publication

91	Khor, C.Y.. "Effect of stacking chips and inlet positions on void formation in the encapsulation of 3D stacked flip-chip package", International Communications in Heat and Mass Transfer, 201205 Publication	<1 %
92	M.S. Abdul Aziz, M.Z. Abdullah, C.Y. Khor. "Thermal fluid-structure interaction of PCB configurations during the wave soldering process", Soldering & Surface Mount Technology, 2015 Publication	<1 %
93	C.Y. Khor, M.Z. Abdullah. "Analysis of fluid/structure interaction: Influence of silicon chip thickness in moulded packaging", Microelectronics Reliability, 2013 Publication	<1 %
94	oh-mylove.x-y.net Internet Source	<1 %
95	ssh.ele.tut.fi Internet Source	<1 %
96	link.lib.umanitoba.ca Internet Source	<1 %

97	www.tandfonline.com Internet Source	<1%
98	dspace.lboro.ac.uk Internet Source	<1%
99	J. Akiyama, M. Naeshiro, M. Amagai. "A Study of Hot Spot in Silicon Device for Stacked Die Packages", 2005 International Symposium on Electronics Materials and Packaging, 2005 Publication	<1%
100	hdl.handle.net Internet Source	<1%
101	www.ijert.org Internet Source	<1%
102	Microelectronics International, Volume 16, Issue 3 (2007-06-27) Publication	<1%
103	kurskservice.ru Internet Source	<1%
104	www.emeraldinsight.com Internet Source	<1%
105	www.mfg.mtu.edu Internet Source	<1%
106	zidapps.boku.ac.at Internet Source	<1%

107	H. Chai, Y. Zohar. "Unsteady Wire Sweep Due to Transfer Molding in a 160L QFP Package", Journal of Electronic Packaging, 1999 Publication	<1 %
108	Khor, Chu Yee, Mohd Zulkifly Abdullah, and Wei Chiat Leong. "Visualization of Fluid/Structure Interaction in IC Encapsulation", IEEE Transactions on Components Packaging and Manufacturing Technology, 2012. Publication	<1 %
109	www.informs-cs.org Internet Source	<1 %
110	Ong, Ernest E.S., M.Z. Abdullah, W.K. Loh, C.K. Ooi, and R. Chan. "FSI implications of EMC rheological properties to 3D IC with TSV structures during plastic encapsulation process", Microelectronics Reliability, 2012. Publication	<1 %
111	asmedigitalcollection.asme.org Internet Source	<1 %
112	www.engineous.com Internet Source	<1 %
113	M. H. H. Ishak, M. Z. Abdullah, M. S. Abdul Aziz, A. A. Saad, M. K. Abdullah, W. K. Loh, R. C. Ooi, C. K. Ooi. "Study on the Fluid–Structure Interaction at Different Layout of Stacked	<1 %

Chip in Molded Packaging", Arabian Journal for Science and Engineering, 2017
Publication

114	ir.library.osaka-u.ac.jp Internet Source	<1%
115	m.scirp.org Internet Source	<1%
116	"Arbitrary Lagrangian-Eulerian and Fluid-Structure Interaction", Wiley, 2013 Publication	<1%
117	Siddiqi, Muftooh Ur Rehman, Corney, Jonathan R., Sivaswamy, Giribaskar, Amir, Muhammad, Bhattacharya, Rahul. "Design and validation of a fixture for positive incremental sheet forming", 'SAGE Publications', 2018 Internet Source	<1%
118	Wen-Shu Lu, Shin-Chang Jiang, Sen-Yeu Yang. "Ribbed package geometry for reducing thermal warpage and wire sweep during PBGA encapsulation", IEEE Transactions on Components and Packaging Technologies, 2000 Publication	<1%
119	epdf.tips Internet Source	<1%

120	Internet Source	<1%
121	www.icfdpegypt.org Internet Source	<1%
122	www.matec-conferences.org Internet Source	<1%
123	Chi Hoe Liew, Foo Wei Lee, Yee Ling Lee, Ming Han Lim. "Behavioural Study of Concrete Surface Crack Filling Conditions on Surface Rayleigh Wave", MATEC Web of Conferences, 2019 Publication	<1%
124	Huang-Kuang Kung, Chi-Lung Hsieh. "A theoretical study to improve wire sag of ultra-long wire bond loops for 3D/MCM packaging", Microelectronics Reliability, 2017 Publication	<1%
125	Soldering & Surface Mount Technology, Volume 24, Issue 3 (2012-06-30) Publication	<1%
126	Soldering & Surface Mount Technology, Volume 25, Issue 2 (2013-05-27) Publication	<1%
127	bura.brunel.ac.uk Internet Source	<1%
128	repository.dl.itc.u-tokyo.ac.jp Internet Source	

		<1%
129	www.scribd.com Internet Source	<1%
130	www.semanticscholar.org Internet Source	<1%
131	W. C. Wong, C. Y. Khor, O. Ernest, M. Z. Abdullah, A. A. Saad, N. Md. Yusop, W. K. Loh, C. K. Ooi, R. C. Ooi. "Effect of stacking chips and fluid/structure interaction simulation in 3D stacked flip-chip encapsulation process", 2012 7th International Microsystems, Packaging, Assembly and Circuits Technology Conference (IMPACT), 2012 Publication	<1%
132	www.dbicorporation.com Internet Source	<1%
133	"Fluid-Structure Interaction", Springer Science and Business Media LLC, 2006 Publication	<1%
134	repozitorij.fsb.unizg.hr Internet Source	<1%

Exclude quotes Off
Exclude bibliography Off
Exclude matches Off

Document Accepted 1/7/21